2020-09-11

Effects of Surface Live Loads on the Behaviour of Decommissioned Pipelines: Numerical Modelling and Analysis

Walsh, Coltin

UNIVERSITY OF CALGARY

Effects of Surface Live Loads on the Behaviour of Decommissioned Pipelines: Numerical Modelling and Analysis

by

Coltin Walsh

A THESIS

SUBMITTED TO THE FACULTY OF GRADUATE STUDIES

IN PARTIAL FULFILMENT OF THE REQUIREMENTS FOR THE

DEGREE OF MASTER OF ENGINEERING

GRADUATE PROGRAM IN CIVIL ENGINEERING

CALGARY, ALBERTA

SEPTEMBER, 2020

Abstract

Steel pipelines are used throughout the energy industry as the primary means of transporting natural gas, crude oil, and petroleum-related products and chemicals. When a pipeline permanently ceases operation, it is decommissioned and may be abandoned and left in place underground. Over time, the pipeline will degrade due to environmental and in-*situ* conditions. Corrosion is the principal mechanism for the degradation of decommissioned pipelines. Corrosion and degradation reduce the material strength and stiffness of the pipe section. Degraded pipes may no longer be capable of bearing the loads imposed by groundcover and surface vehicles. Potential collapse of decommissioned pipelines poses a risk to both the public and the environment. The static structural response of buried decommissioned pipelines subjected to surface live load was analyzed using the finite element analysis software ABAQUS. The buried pipeline was modelled within a uniform soil block, eliminating the effects of boundary conditions. Soil-pipe interaction was considered assuming a frictional slippage contact definition. The pipe was subjected to both overburden dead load and surface live load. Surface live load was taken as the maximum axle load of a CL-800 truck using an appropriate dynamic loading factor. The effects of various in-*situ* parameters including the burial depth, pipe diameter, and wall thickness were investigated. The investigation further expanded to analyze the effects of surface loading magnitude, geometry and direction of travel, along with performing an ultimate limit states analysis. The primary results indicate that for reasonable burial depths, soil stiffness, pipe diameter, and wall thickness, the maximum stresses lie below the elastic limit. However, for shallow burial depths, local deformations and stresses become significant and increase rapidly.

Acknowledgements

I would first like to express my sincerest gratitude and acknowledgement to Dr. Mamdouh El-Badry for his continual patience, support, guidance, technical and personal advice, and overall expertise. Over the course of this project, Dr. El-Badry devoted his time to provide me with the best of his many decades of knowledge and guided me in every step of the way. He made every effort to maintain my motivation and focus when I encountered challenges and always sought to expose my full potential.

I would also like to acknowledge Mr. Mark Laybolt (Engineer, Major Projects – Mainline Projects) of Enbridge for his valuable input and feedback. The investigation reported within this thesis was financially supported by a research contract from Enbridge Pipelines Inc. and a Collaborative Research and Development (CRD) grant from Natural Sciences and Engineering Research Council of Canada (NSERC).

Finally, and most importantly, I would like to thank my wife, Rory, for her unwavering support through the many moments of success, failure, frustration, sleepless nights, and general challenges. Through this entire process, she continually provided words of encouragement and showed exemplary patience and understanding and I worked to complete this project and final thesis. By far she was my biggest source of motivation and deserves all the thanks I can give.

Table of Contents

List of Tables

List of Figures

List of Symbols

Chapter 2

A	=	Cross-sectional area of pipe, modelled as a prism (m^2)
A_0	=	Area bounded by circumference of pipe (m^2)
B'	=	Empirical coefficient for elastic support
C	=	Depth of soil cover (m)
D	=	Actual outside diameter of steel pipeline (m)
D_E	=	Depth of soil cover as per AASHTO (1998) (ft)
E	=	Young' s modulus of pipeline steel (MPa)
E'	=	Young' s modulus of soil (MPa)
$(EI)_{eq}$	=	Equivalent stiffness of pipe wall per unit length (Nm)
F'	=	Impact factor
FS	=	Factor of safety (2.5 if $C/D \geq 2$, 3.0 if $C/D < 2$)
I	=	Second moment of area of pipeline steel per unit length (m^4/m)
IM	=	Dynamic allowance factor as per AASHTO (1998)
K	=	Relative axial stiffness coefficient
K'	=	Bedding constant (~0.1)
K_f	=	Relative flexural stiffness of pipelines
L	=	Lag factor (~1.0 to 1.5)
L_p	=	Length of pipe (m)
P	=	Surface point load (N)
$P_{cap,elastic}$	=	Elastic load bearing capacity (N)
$P_{cap,plastic}$	=	Plastic load bearing capacity (N)
P_{live}	=	Live point load at soil surface (N)
P_{pipe}	=	Uniform pressure exerted on pipe surface (Pa)
P_{soil}	=	Soil pressure acting on pipe surface (Pa)
R	=	Actual outside radius of steel pipeline (m)
R'	=	Length of vector from surface point load to soil element of interest (m)
R_w	=	Water buoyancy factor
d	=	Horizontal offset distance from pipe centerline to surface point load (m)
h_w	=	Height of water table measured from pipe crown (m)
t	=	Wall thickness of steel pipeline (m)
z	=	Depth of soil element of interest (m)
σ_{yield}	=	Yield stress (MPa)
σ_{zz}	=	Vertical stress tensor (Pa)

Chapter 3

A	=	Cross-sectional area (m^2)
DLA	=	Dynamic load allowance factor as per CSA S6 (2014)
D_E	=	Depth of soil cover as per CSA S6 (2014) (m)
E	=	Young' s modulus of pipeline steel (MPa)
E'	=	Young' s modulus of soil (MPa)

F	=	Applied load (N)
c	=	Cohesion stress (MPa)
f	=	Surface coating dependent factor
l	=	Actual specimen length (m)
l_0	=	Original specimen length (m)
n	=	Ramberg-Osgood exponential coefficient
$\boldsymbol{n}$	=	Unit normal vector
$n_i\boldsymbol{e_i}$	=	Unit orthogonal basis vector in direction i
p	=	Contact pressure (MPa)
α	=	Yield offset strain
γ	=	Soil unit density (kg/m^3)
ε	=	Strain (m/m)
ε_{nom}	=	Nominal strain (m/m)
ε_p	=	Logarithmic plastic strain (m/m)
ε_T	=	True strain (m/m)
μ	=	Coulomb static friction coefficient
ν	=	Poisson's ratio
ρ_s	=	Unit density of steel (kg/m^3)
σ	=	Applied stress (MPa)
σ_i	=	Principal stress in direction i (MPa)
σ_{nom}	=	Nominal stress (MPa)
σ_T	=	True stress (MPa)
σ_{yield}	=	Yield stress (MPa)
τ	=	Shear stress (MPa)
τ_{crit}	=	Critical frictional shear stress (MPa)
φ	=	Internal friction angle (^{o})
ψ	=	Dilation angle (^{o})

Chapter 4

DL	=	Dead load (MPa)
DLA	=	Dynamic load allowance factor as per CSA S6 (2014)
LL	=	Live load (MPa)
ULS	=	Ultimate Limit States load combinations as per CSA S6 (2014)
σ_{VM}	=	Von Mises stress (MPa)
σ_{ii}	=	Normal stress acting in direction *i* (MPa)
σ_{ij}	=	Shear stress acting in direction *ij* (MPa)

Chapter 1

Introduction

1.1 General

Steel pipelines are used by the energy-related industry in North America as the primary means of transporting crude oil, natural gas, and petroleum related products. Pipelines are often considered one of the most economical methods of transporting energy-related products over vast distances from the often remote areas of production. In Canada alone, the energy pipelines extend along more than 700,000 km (Nazemi & Das, 2010). The production facilities within Canada are often located within landlocked provinces, requiring distant transportation reach ports, destined for the global markets. The main pipeline network in North America is shown in Figure 1-1 (Canadian Association of Petroleum Producers, 2019). The majority of these pipelines run underground, as to both protect the pipeline itself from damage and sabotage, and the public and environment.

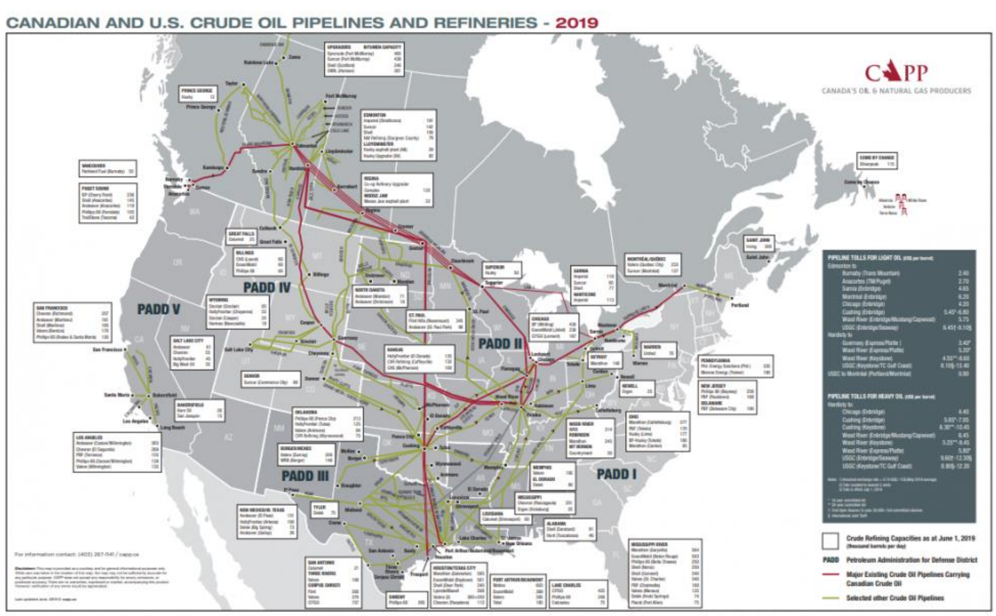

Figure 1-1: Major petroleum pipelines throughout North America (Canadian Association of Petroleum Producers, 2019)

When a pipeline permanently ceases operation, it is decommissioned and may be left in place and abandoned underground. Leaving a decommissioned pipeline in place underground is an economical resolution that further acts to prevent disruption to the environment, community, and soil stability. Over time, the pipe will begin to degrade due to environmental and in-*situ* conditions. Corrosion is the principal mechanism for degradation of decommissioned pipelines (Cheng, 2013). Degradation reduces the material strength and stiffness of the pipe section, and the pipe may no longer be capable of bearing the imposed loads due to groundcover and surface vehicles – particularly heavy equipment. Collapse of decommissioned pipelines poses a risk to both the public and the environment. Collapse may lead to release of contaminants and to excessive soil subsidence. Therefore, understanding the structural integrity of degraded decommissioned pipelines is critical for anticipating and assessing the risks of pipeline collapse.

The initial step in determining the structural integrity of decommissioned pipelines is assessing the static response of a pipeline when subjected to loading immediately after decommissioning and as the pipe section begins to corrode. Pipelines can be subjected to a variety of mechanical and environmental loading, the most significant of which is surface live load. Surface live load applied directly above a pipeline will be resisted by the immediate groundcover, the surrounding soil, and the pipeline itself. The static response of a pipeline when subjected to surface live load is dependent on a variety of factors including load geometry and location, soil stiffness, pipe section properties, and depth of soil cover. The depth of soil cover, or burial depth, is a primary factor influencing the load path distribution and determines the portion of the total load resisted by the pipeline. The burial depth of a pipeline can vary significantly depending on environmental conditions, soil conditions, and pipeline design requirements.

With multiple variable loading and geometric conditions influencing the static response and resulting stresses and strains within a decommissioned pipeline, it is imperative to conduct a parametric investigation to determine the influence of each variable. Through gaining an understanding of the influence of each parameter, the critical case can be defined for a pipeline section. The designer is then able to evaluate the in-*situ* pipeline conditions against the critical case and perform an assessment on the pipeline safety and remaining life.

1.2 Objectives and Scope

The primary objective of the presented research is to determine the static response of decommissioned pipelines subjected to surface live loading. The static response of the pipe section is heavily reliant on, and influenced by, a number of parameters including burial depth; pipe wall thickness; soil stiffness; pipe diameter and diameter-to-thickness ratio; surface load magnitude, geometry and orientation; and loading and material limit state factors. The primary results of interest include the maximum principal stresses and the pipe section ovalization.

In order to investigate the influence of various parameters on the structural response of buried decommissioned pipelines, a numerical parametric analysis was performed using the finite element software ABAQUS. As will be described, the static behavior of buried pipelines subjected to surface live loads is heavily dependent on the burial depth. Soil arching effects describe the process of surface loading being transferred through a soil matrix to an adjacent stable section and or structure. In the scenario considered regarding buried pipelines, the relative stiffness of the pipeline is much higher than the surrounding soil. As a result, the pipeline is considered much more stable and therefore attracts a large portion of the surface load (Terzaghi, 1943).

As the burial depth is reduced, the path from the surface load to the stiff pipe section becomes shorter and more direct. Since the pipe section is much stiffer than the surrounding soil, the load attracted by the pipe section is expected to increase. Based on this fundamental observation, the initial analysis consists of investigating the effects of depth of soil cover on the resulting stresses and deformations of the pipe section. A reasonable critical depth is then selected to investigate the effects of wall thickness and subsequently, soil stiffness. Investigating variable wall thickness serves two-fold in determining the initial response of variable section thickness that may be used and investigating the long-term effects of global corrosion. Global corrosion is considered as pitting corrosion extending over a large section of pipeline, idealized in this thesis as the uniform wall thinning of the pipe section.

In addition to the above, other loading geometries were considered including heavy construction equipment, surface load travelling parallel to the pipe axis, and multiple surface loads travelling perpendicular to the pipe axis. Finally, the stresses resulting from ultimate limit state load commination factors were observed. Within all analyses conducted, four separate pipe sections are used, enabling the effect of pipe diameter to be observed simultaneously. Pipe diameters 20", 24", 28", and 34" were used for all analyses. Pipe wall thickness was taken as the standard wall thickness of 3/8".

1.3 Research Significance

The primary purpose of this research was to determine the static response of decommissioned pipelines subjected to surface live loads and to understand the influence of various parameters on the resulting behavior. Through this research, the criticality of decommissioned pipelines can be determined and the risk of failure can be assessed. Based on an individual pipe's in-*situ* conditions and environment, an economic and risk assessment can be performed on a case by case basis to determine the remaining life of a decommissioned pipeline and when or if it should be ultimately removed. However, through this research it was determined that under typical loading and geometric conditions, decommissioned pipelines pose little risk of catastrophic collapse when subjected to standard surface loadings. The results can be used to gain greater confidence of both the immediate stakeholders and the general public regarding the overall safety of pipelines, post-decommissioning. It can be shown that generally, leaving pipelines in the ground after decommissioning is economical while still holding paramount the safety of the public and the environment.

1.4 Thesis Organization

The thesis is organized into five separate chapters. Chapter 2 explores the relevant research reported in the literature and applies the findings to the current scope of research. The literature in analyzed to identify gaps within the recent research and seeks to determine areas where further investigation is required. The literature review is subdivided into four categories exploring the research focusing on general pipeline and pipe section static analysis; the process, types, and effects of pipeline corrosion; the specific topic of buried pipelines subjected to various loading conditions and the influence of soil-structure interaction; and the use and applicability of finite element analysis and numerical modelling as applied to pipeline analysis and design. Chapter 3 focuses on the development of the finite element models used for all subsequent analyses, defining all primary parameters including element selection, geometric size and boundary conditions, mesh convergence, material properties of both soil and pipe sections, contact definition between the soil and pipeline, load definition, and analysis steps. A brief summary of the conducted parametric investigations is also provided. Chapter 4 describes each of the parametric investigations in detail and presents the results for discussion. The finite element modelling methodology described is adapted and applied to the various parametric investigations. The primary results from each of the investigations are presented and discussed, describing the effect and influence of each parameter. Finally, the concluding Chapter 5 summarizes the key results and implications and provides recommendations for scope expansion and future work.

Chapter 2

Background and Literature Review

2.1 General Overview

With the increasingly common use of pipelines throughout various industries, there continues to be expansive research on the performance and integrity of pipelines. Pipelines pose high economic and public safety consequences should a pipeline failure occur while in operation and even after decommissioning. Therefore, it is vital that a comprehensive understanding of pipeline behavior be known to reduce the risk tolerance of pipeline usage. Extensive research has been carried out over the last several years to study the behavior of pipelines subjected to a variety of different loading types, geometric arrangements, and in-*situ* conditions. In this chapter, a review of the current literature was conducted to investigate the learnings of recent studies and examine how these findings can be applied to decommissioned pipelines. This review has been categorized into research focusing on pipeline analysis in general, the causes, processes and influence of pipeline corrosion, investigations of buried pipelines subjected to surface loading, and the use of the finite element method for structural analysis of pipeline systems. In addition, the necessity and effect of incorporating accurate soil-structure interaction on the resulting pipeline behavior was reviewed. This review allows for understanding of the typical experimental techniques used, fundamental conclusions regarding pipeline sections subjected to various loadings, general corrosion processes and impacts, and describes the methodology and validity of using finite element analysis for the research scope.

2.2 Pipeline Analysis

Numerous studies have been conducted examining the structural response, integrity, and capacity of pipeline sections. Sections of buried pipelines have been tested under a variety of loadings. These sections are typically tested in laboratory settings using equipment and machinery inducing pressures and loading applied directly to the pipe surface. The learnings from these investigations can be used to determine ultimate capacities and failure modes of pipelines in operation from a purely mechanical and structural perspective, ignoring the influence of soil-pipe interaction. Primary results from these investigations are used to define the governing physical properties of the pipe section and the influence of various parameters and imperfections.

Ozkan and Mohareb (2009) investigated steel pipelines subjected to a static load combination including bending, tension, and internal pressure. The pipelines investigated were elevated pipelines, commonly used within petrochemical facilities and refineries, supported on steel or concrete structures. These pipelines are subjected to bending moment due to gravity, axial tension due to thermal expansion, and internal pressure based on operating conditions. Pipe sections with thick walls have the ability to deform into the plastic range, while still maintaining structural integrity. However, these stocky sections are expensive and thinner walled sections are commonly used. The researchers sought to determine if the presence of internal pressure and axial tension would allow thin-walled pipe sections to achieve plastic moment prior to buckling. To determine the peak plastic moment and mode of failure for the thin-walled sections, six 508 mm diameter pipe sections with an average wall thickness of 6.26 mm (D/t ratio = 81.2) were experimentally subjected to various magnitudes of axial tension and internal pressure. An externally applied bending moment was then monotonically increased until section failure. It was found that the presence of internal pressure and axial tension acted to stabilize the buckling mode of failure. Increasing the internal pressure enhanced the peak moment capacity of the pipe section. The presence of internal pressure further altered the mode of buckling. Pipe sections without internal pressure experienced inward diamond shaped buckling while pipe sections with high internal pressure experienced outward bulging buckling. The experimental results were compared with numerical models developed in ABAQUS. The plastic moment capacity and buckling behavior of the numerically modelled pipelines correlated closely with the experimental results. It was observed that the resulting plastic moments and deformed behavior obtained from the finite element models were directly proportional to the size and quality of the finite element mesh. The models utilizing a very fine mesh resulted in reliable predictions of the plastic moment and post-peak behavior. This research indicates that even the relatively thin-walled pipe sections used throughout the industry have the ability to reach plastic moments depending on the sequence of load combinations applied. Therefore, when defining material properties, it is important to model an accurate representation of the plastic range and post-peak material behavior.

The influence of various surface damages including wrinkling and denting on the fracture life and operational capacity of pipeline sections was researched by Das et al. (2007). Pipe wall wrinkling can occur due to axial forces or movement of the pipe section. Axial forces can result from thermal loading, soil moment, seismic events, and operation upset conditions such as slug loading. Local deformation from compressive axial forces results in local buckling at the damaged locations and the number of wrinkles rapidly increases. There exists limited safety codes available to assess the risk associated with wrinkled pipelines. The objective of the research by Das et al. (2007) was to assess the strain reversal behavior and fracture of a wrinkled pipe section subjected to low cycle fatigue. The authors conducted an experimental investigation, subjecting wrinkled coupons of pipeline steel to monotonic axial loading followed by low cycle fatigue loading. Strips of pipeline steel were cut and monolithically bent at 45° to represent a wrinkle. The bent strip was then subjected to low cycle loading, with the machine actuator opening and closing the bend in the strip. This compressive and tensile loading induced a bending moment with the crest of the bend acting as a hinge. In general, a wrinkled pipeline subjected to monotonic axial loading does not rupture. The pipe section will buckle and develop wrinkles, but exhibits adequate ductility to avoid fracture. Under increasing axial load, the section will continue to bend, reducing the half wavelength of the wrinkle until the wrinkle ultimately closes. The axial load then bypasses the damaged location. Fracture in the damaged pipelines occurred as a result of plastic strain reversals at the wrinkle location. The wrinkled location experienced the largest stress concentrations and intuitively the largest strain reversals. Through this research, it was determined that under static, monotonic loading, the wrinkled section poses little risk of rupture. If it is expected that the pipeline will not sustain strain reversals, even under upset conditions, repair of the section may be able to be postponed.

Das et al. (2010) further modeled their abovementioned experimental investigations in the finite element software ABAQUS and conducted a numerical analysis. The motivation behind this additional investigation was the recovery of a wrinkled pipe section that fractured in the field, whose load history did not indicate strain reversal. To verify the field observations and gain understanding of the unexpected fracture mechanism, a finite element model was developed. ABAQUS was used as it is capable of non-linear material modelling and analysis, particularly post-buckling behavior of the pipe, isotropic material hardening, and complex contact simulations. The pipe section was modelled using S4R shell elements which can account for plate thinning as the section deforms. Seven sections through the thickness of the element were selected to adequately model the plasticity due to the large displacements. The element selection and nodal configuration is shown in Figure 2-1 (Das et al., 2007).

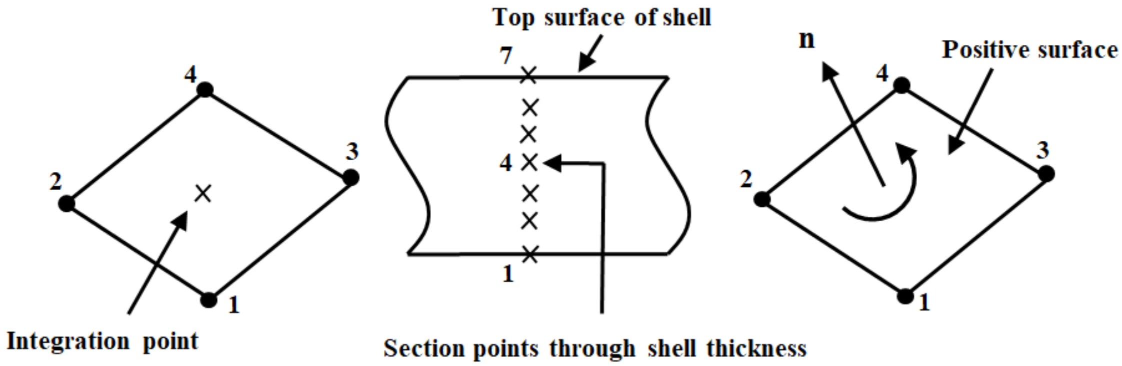

Figure 2-1: S4R element configuration for pipe section (Das et al., 2007)

The pipe ends at the boundary locations were modelled with a thicker pipe wall thickness to avoid local buckling due to the finite element discontinuities. As a crucial step to properly capture the unexpected failure mechanism, an initial imperfection model was incorporated into the finite element analysis. A “ring” type imperfection was assumed, representing an outward bulge with a 4% amplitude (relative to the wall thickness) around the circumference of the pipe, as shown in Figure 2-2 (Das et al., 2007). This imperfection acted to initiate and accentuate the resulting wrinkle.

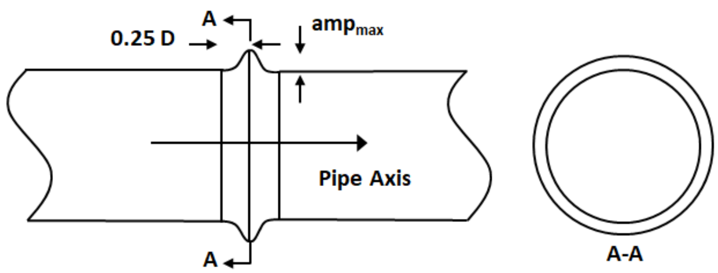

Figure 2-2: Initial "ring" imperfection considered around the pipe section (Das et al., 2007)

The field pipe underwent non-axisymmetric telescoping deformation, indicative of an eccentric compressive axial load. This eccentricity induced an additional bending moment on the pipe section. A non-linear analysis was performed to account for the large plastic strains and contact at the wrinkled location. The stresses, strains, and deformed shapes obtained from the numerical models correlated well with the experimental observations. Through the numerical analysis, it was found that even under monotonic loading, although non-axisymmetric, the location of the pipe wrinkle experienced strain reversals on the compression side. Therefore, the previous conclusions by Das et al. (2007) were amended, stating that rupture and tearing fracture at the wrinkle location can occur under monotonic loading or after a small number of loading cycles. This correlated well with fractures found in the field under few loading cycles and extended beyond the findings from the previous limited experimental investigation.

Limam et al. (2012) further investigated the influence of the presence of initial imperfections on the behavior of pipe sections subjected to internal pressure and bending moment. The researchers looked at the effect of localized dents on the bending capacity of small bore-pressurized piping. Dents can be present on pipe surfaces due to a variety of reasons including improper handling of material and impact with excavation equipment during installation or other adjacent activities. In an experimental investigation, small bore pipes of 38 mm diameter were initially dented, pressurized to 40% of the yield pressure, and then subjected to pure bending moment until failure. The transverse dents were formed on the crown of the pipe using a smooth steel bar and a hydraulic press. The pipe was confined in wax during the denting procedure to limit global ovalization of the section. The depth of denting was varied between 20 specimens from 0 to 1.7 times the wall thickness. It was found that for the dent geometry considered, the presence of the dents had minimal effect on the elastic behavior of the pipe section. However, the dents significantly affected the post-yield behavior and reduced the collapse capacity of the section. This reduction was up to 50% for the deepest dent geometry. This experiment was further modelled and verified using the finite element analysis software ABAQUS. The resulting analysis closely matched the experimental observations. It was determined that in order to accurately analyze the pipe behavior numerically, the dents and curvature must be accurately modelled, the material model must represent the true plastic behavior, and the local wall thickness variations should be included. The conclusions showed that the presence of dents reduces the ultimate bending capacity of the section and can be extended to include other initial imperfections such as girth welds and local corrosion.

Ghazijahani and Showkati (2013) investigated the behavior of thin-walled cylindrical shells subjected to pure bending and external pressure. Six 2.8 m long small bore specimens with an outer diameter of 127 mm and wall thickness of 0.5 mm were tested. The pipelines were subjected to constant bending moment resulting from two concentrated loads. External pressure was simulated by inducing vacuum pressure on the interior of the pipe section. The section free body diagram is shown in Figure 2-3 (Ghazijahani & Showkati, 2013). The bending moment was initially applied, varying between the specimens, and the external pressure subsequently increased until buckling failure.

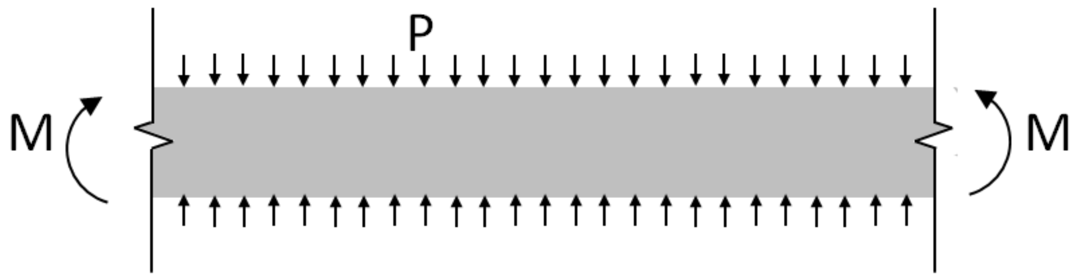

Figure 2-3: Cylindrical shell under pure bending and external pressure (Ghazijahani & Showkati, 2013)

The resulting bending moment capacity and mode of failure were observed. Due to the very thin walls of the pipe sections examined, the influence of discontinuities due to the load application apparatus and boundary condition collars was significant and difficult to eliminate. Great care was taken to ensure that stress concentrations were not developed at the boundary conditions in order to obtain an accurate representation of the bending behavior and capacities. The primary mode of failure under the loading conditions was buckling initiated within the maximum compression zone. As the external pressure was increased (internal pressure decreased), the bending moment capacity of the pipe section decreased. The external pressure acted to accentuate the ovalization and curvature caused by the initial bending moment. The experimental results were further validated by finite element models developed with ABAQUS.

The application of the cylindrical shell investigations by Ghazijahani and Showkati (2013) is representative of numerous pipeline systems such as underground drainage systems and low-pressure fluid transportation. The pipelines used in the petrochemical industry are generally much stiffer and have diameter-to-thickness ratios less than the cylinders; with thicker wall thicknesses than those considered in the analyses. However, as global corrosion occurs, the effective pipe wall thickness is reduced and the diameter-to-thickness ratio increases to that within the range discussed in the research by Ghazijahani and Showkati (2013). Therefore, the key conclusions from their research are also applicable for discussion within the scope of the research reported in this thesis. Primary conclusions included the significant influence of stress concentrations at the boundary locations, ovalization of the pipe section as the external pressure increased, and additional bulging witnessed at the maximum bending moment locations. However, Ghazijahani and Showkati (2013) did not consider soil-structure interaction. Attempting to directly apply the results to the current study ignores the confining effects of the surrounding soil matrix on the behavior of the buried pipeline. In their experiment, the external pressure acted to increase ovalization and curvature since the pressure was applied as an internal vacuum pressure, allowing free deformation of the section. However, the presence of a confining medium would certainly limit and restrict this deformation. Therefore, the resulting ovalization, stresses, and strains are exaggerated when compared with a buried section. An additional key observation was that the finite element models appeared to over-estimate the bending capacities compared with the experimental results. This is a direct result of inherent pipeline imperfections present in the experiments and excluded from the finite element models.

2.3 Pipeline Corrosion

Buried pipelines are often subjected to highly corrosive environments both internally and externally. Pipelines within the petrochemical industry carry corrosive products, while the surrounding soils can have high concentrations of dissolved minerals and salts that increase the corrosive potential. Pipelines are typically protected from corrosion by coatings or cathodic protection. However, these protections are not infallible and pipelines tend to corrode throughout their lifespan. Corrosion acts to degrade the material properties and overall strength and stiffness of a pipe section, causing it to be more prone to failure. Corrosion is the primary cause of the majority of pipeline failures within Alberta (Alberta Energy Regulator, 2013). Once decommissioned and abandoned, the corrosion protection systems are no longer maintained or present, allowing corrosion to increase unmonitored. Therefore, it is essential to examine the effects of corrosion on pipeline integrity both during operation and after decommissioning and abandonment in the soil.

There are two primary types of corrosion: global corrosion and local corrosion. Global corrosion refers to the uniform wall thinning of a large section of pipe while local corrosion refers to the extensive thinning of the wall thickness over a very small localized area. The research reported in the literature primarily focuses on the effects of local corrosion as this is most common in pipes during operation. Local debonding of corrosion protection coatings generally leads to the onset of local corrosion. Global corrosion exists as either the proliferation of local pitting along a large section of the pipeline or occurs when cathodic protection is removed from otherwise unprotected sections. Corrosion of pipelines can occur as either internal or external corrosion, or both. External corrosion of buried pipelines is a result of the pipeline being in direct contact with the corrosive soil environment. All soils can be considered as a corrosive environment to some extent, and nearly half of all pipeline failures in Canada are a result of external corrosion (Jeglic, 2004). External corrosion is caused by the failure or removal of the various corrosion protection systems – coatings, cathodic protection, or the like. By comparison, internal corrosion is a result of the contents being transported in the pipeline. The presence of water, dissolved gasses, salts, and chlorides all pose the potential to cause a corrosive interior environment (Dewanbabee, 2009). Internal corrosion is more difficult to quantify as there are many parameters that can make an identical fluid corrosive in one pipe and noncorrosive in another. These parameters include temperature, pressure, velocity, etc. In both cases, corrosion acts to reduce the effective wall thickness, resulting in a structurally weaker section having the potential to cause failure.

Xu and Cheng (2012) closely examined the effects of stress and load history on the corrosion rates of pipelines. In their experimental investigation, the researchers subjected high strength X100 pipeline steel coupons to a corrosive environment with a neutral pH level. The test solution was considered representative of the corrosive environment under debonded pipeline coatings. An elastic axial stress was applied to the coupons and the resulting stress and strain, corrosion potential, and surface morphology of the corrosion scale formed was observed. It was determined that the tensile stress acted to increase the porosity and subsequent corrosion potential, while compressive stresses acted to decrease the porosity and corrosion potential. This increase in corrosion potential was transient only and was subsequently offset by the formation of the corrosion scale. There was no significant change to the steady state corrosion potential under constant tensile or compressive stress. When a tensile stress was applied after corrosion took place, the surface scale became damaged, allowing the depth of corrosion to increase. This effect is critical when considering dynamic and fatigue loading. Cyclic loading results in continual damage to the surface scale, allowing the corrosion to penetrate further into the pipe more quickly. Cyclic loading greatly increases the corrosion potential and corresponding rate of corrosion. Under surface loading, pipelines experience tensile stresses and stress reversals. Therefore, it is expected that the presence of vehicular traffic loading will accelerate the corrosion rate of the pipe section compared to one with no loading present.

Liu and Cheng (2020) investigated the rate of corrosion and the factors influencing the corrosion potential of abandoned pipeline steel containing pre-existing corrosion pits. Corrosion of pipelines can be initiated by numerous environmental causes, one of which is microbiologically influenced corrosion (MIC). External corrosion occurs beneath debonded coatings, where water and dissolved gasses generate corrosive electrolytes. When sulfate-reducing bacteria are present in the solution, the rate of corrosion can increase significantly. These bacteria are common in soils with high organic material including oil fields. To understand the effects of the presence of these bacteria around corrosive pits, the researchers developed four artificial pits in a coupon of X52 pipeline steel. The pits had varying depths and the coupon was placed in a simulated soil solution containing sulfate-reducing bacteria. The presence of the live bacteria and corresponding corrosion potential was observed. It was found that in pipelines with preexisting corrosive pits, the bacteria tend to gather on the steel surface outside the pits. There were very little live bacteria within the pits themselves. The presence of bacteria outside the pits provided a galvanic effect with the interior of the pit acting as a cathode and the pipe surface as an anode. This galvanic reaction greatly increased the rate of corrosion on the pipe surface. It was found that the presence of sulfate-reducing bacterial can accelerate pipeline corrosion by a factor of 10. The researchers were able to demonstrate that the rate of corrosion can accelerate post-abandonment and the extent of this corrosion often goes unnoticed and unmonitored.

Dewanbabee (2009) examined the effects of axial load and internal pressure on pipeline behavior, focusing on corroded pipelines. This dissertation had the objective of determining the load deformation behavior of corroded pipelines subjected to internal pressure and axial compression, up to the point of rupture. The researcher selected small bore pipe sections, 6 inches in diameter, with a low diameter to thickness ratio, D/t = 34. A square local corrosion shape was selected, with the circumferential dimension increased and the longitudinal dimension remaining constant between specimens, as shown in Figure 2-4 (Dewanbabee, 2009). A total of ten different specimens were analyzed, each with varying circumferential extents and depth of corrosion patch.

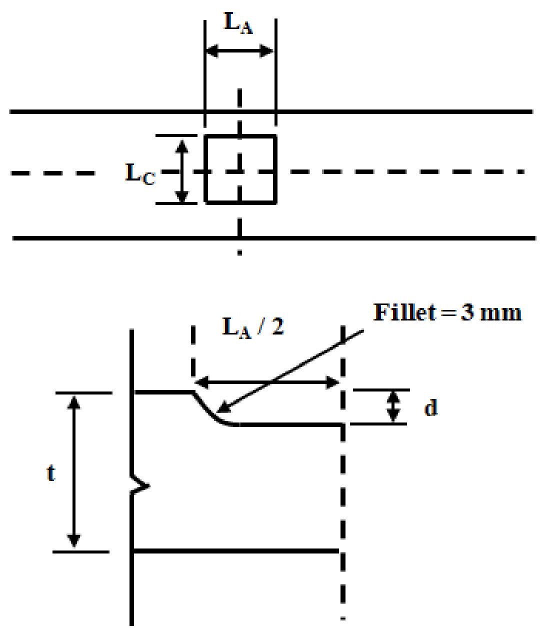

Figure 2-4: Details of corrosion patch considered by Dewanbabee (2009)

The pipe sections were placed between two loading plates and rigid collars were attached to the pipe ends. The intent of using the collars was to ensure that local buckling at the boundary conditions would not occur. The specimens were subjected to constant internal water pressure and then monotonically increasing axial compression until failure. Two different internal pressures were assumed, 0.2 and 0.4 times the pipe yield pressure. The load displacement curves were obtained until the point of buckling and/or rupture. It was found that a higher internal pressure reduced the axial compression capacity while increasing the deformability. A higher internal pressure tends to develop a bulge at the corrosion location, resulting in earlier onset of buckling and wrinkle formation. An increase in the depth and dimension of corrosion reduced both the compression capacity and deformability. An increase in the circumferential dimension of the corrosion acted to reduce the axial capacity and the deformability. It was found that due to the high ductility of the pipeline steel, the pipeline never ruptured during the full-scale experimental tests, with all failures caused by buckling only. This observation corresponds well with the previously discussed literature, finding that rupture of pipe sections in the field under monotonic loading is rare. However, rupture was able to be initiated in the finite element analysis by locally modifying the extent of corrosion, generating greater stress concentrations. Both the experimental and finite element analyses did not incorporate soil-pipe interaction and subsequent confining effects. It is apparent that since the experimental pipelines did not rupture without the presence of surrounding soil, rupture would not occur if these effects were included. The same cannot be said for the excessive local corrosion finite element analyses and further investigation is warranted.

Grigory and Smith (1996) performed 13 full scale tests of locally corroded 48 inch diameter X65 steel pipe sections subjected to the combination of internal pressure, axial bending, and axial tension. The goal of that research was to develop an extensive experimental baseline for development and verification of subsequent numerical and analytical models. Test specimens of 3.7 m long, 48-inch pipe sections were machined with uniform depth corrosion patches. The initial sections had symmetrical patches machined on the tension and compression sides; however, it was determined that rupture typically occurred on the compression side so symmetrical patch machining was discontinued. The extents of the patches were varied between specimens, varying dimensions in the circumferential and longitudinal dimensions. The pipes were subjected to internal water pressure and four-point bending, with eight of the pipes subjected to an additional initial axial compression. An internal pressure of 6.7 MPa was applied, four-point bending was applied to a specified deflection, and the internal pressure was once again increased until failure. When subjected to axial compression, the compression force was applied as the initial load. Through the experimental investigation, it was found that the pipes experienced one of three failure modes: an axial direction rupture resulting from internal pressure hoop stress, a circumferential direction rupture resulting on the tensile side of the pipe, and bending buckling initiated at the corroded section. Applied to the current research, this experimental investigation showcases that the primary mode of failure occurs on the compression side of the pipe section and the section failure becomes more critical as the effective wall thickness is reduced. Therefore, for pipelines subjected to bending resulting from surface loading, failure would be expected to occur at the pipe crown; at the location of maximum bending moment.

Finally, Scott (2015) prepared a report for the Det Norske Veritas (DNV) Materials & Corrosion Technology Centre regarding the process and effects of corrosion on abandoned pipelines. Utilizing typical equations found in pipeline design codes and guidelines, the elastic and plastic collapse pressures were calculated for buried pipelines subjected to point surface live loads, as shown in Figure 2-5 (Scott, 2015). The surface point load was assumed to be transferred as distributed load acting on the pipe surface.

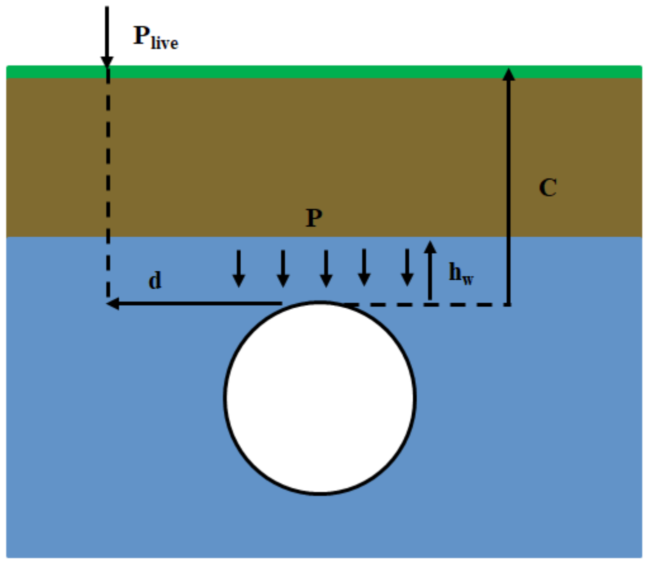

Figure 2-5: Schematic of buried pipeline showing transfer of surface live load to pipe crown (Scott, 2015)

Analytical models were developed for the applied loading and the elastic and plastic collapse mechanism of the pipe crown. The pipe was assumed to be subjected to soil overburden, water table gravity loading and buoyancy forces, and surface live load. The load due to soil and water gravity was calculated using the burial depth and the respective mass density. The live load pressure transferred to the pipe crown was determined as:

$$P_{pipe} = \frac{3 \cdot P_{live} \cdot F'}{2 \cdot \pi \cdot C^2 \cdot \left[1 + \left(\frac{d}{C}\right)^2\right]^{5/2}} \tag{2-1}$$

The live load, P_{live}, applied at the soil surface was assumed to be a point load, in Newton. In Equation (2-1), P_{pipe} is the uniform pressure exerted on the pipe surface, in Pa; F' is an impact factor; C is the depth of soil cover, in m; and d is the horizontal offset distance, in m, measured from the pipe centerline to the surface point load. The plastic collapse mechanism was calculated based on the bending stress acting on the pipe crown. It was assumed that plastic collapse would occur when the pipe stress reaches the yield stress, thus:

$$P_{cap.\,plastic} = \frac{2 \cdot \pi \cdot C^2}{3 \cdot F'} \cdot \left[\left(\frac{\sigma_{yield}}{4 \cdot E} \right) \cdot \left(\frac{D}{t} \right) \cdot \frac{(EI)_{eq} + 0.06 \cdot E' \cdot R^3}{L \cdot K' \cdot R^3} - P_{soil} \right] \tag{2-2}$$

where $P_{cap,plastic}$ is the plastic collapse load bearing capacity of the pipe section, in Newton; σ_{yield} is the pipeline steel yield strength, in MPa; D is the pipe outer diameter, in m; E is the Young's modulus of the pipeline steel, in MPa; $(EI)_{eq}$ is the equivalent stiffness of the pipe wall per unit length, in N.m; E' is the Young's modulus of the soil, in MPa; L is a lag factor; K' is the bedding constant; R is the pipe outer radius, in m; and P_{soil} is the soil overburden pressure acting at the pipe crown, in Pa. Equation (2-2) indicates that, as the wall thickness is reduced, the inertial stiffness of the section decreases, but so does the bending stress. Therefore, it is not intuitive that the bending capacity of the section is proportional to the wall thickness as the wall thickness affects both the attracted load and the section resistance. The second mode of failure assumed was an elastic collapse mechanism, commonly referred to as buckling prior to yield. The elastic collapse pressure was defined as:

$$P_{cap.\,elastic} = \frac{2 \cdot \pi \cdot C^2}{3 \cdot F'} \cdot \left[\frac{1}{FS} \sqrt{32 \cdot R_w \cdot B' \cdot E' \cdot \frac{(EI)_{eq}}{D^3}} - P_{soil} \right] \tag{2-3}$$

where $P_{cap,elastic}$ is the elastic buckling load bearing capacity of the pipe section, in Newton; FS is an applied safety factor; R_w is the water buoyancy factor; and B' is an empirical coefficient for elastic support. The collapse pressures were then compared with the live load pressure to determine the potential for collapse and critical surface live load pressures. A simplified parametric study was conducted looking at three different pipe diameters, burial depths, and soil stiffness. The study showed that the load bearing capacity of the pipe sections decreased with the increase in pipe diameter and decrease in burial depth, soil stiffness and effective wall thickness.

Through the analytical model developed, it was determined that a typical buried pipeline would be able to adequately support a surface load for 9 000 years before potential collapse. At the most extreme critical case of the largest diameter pipe at the shallowest burial depth, the pipe would still be able to support surface loading for over 100 years. Based on the prismatic nature of soil subsidence, the maximum extent of soil subsidence was predicted to be only 40 cm, with the average being less than 10 cm. The analysis considered bare sections, while most pipelines have external coatings which would act to significantly extend the lifespan of abandoned pipelines. Therefore, there appears to be minimal risk of immediate collapse of abandoned pipelines.

However, as the author noted, this report is a high-level analytical application of code equations and corrosion rates to assess the life of abandoned pipelines. Further, the pipeline was subjected to pedestrian traffic live load at a burial depth of 1.2 m. The surface load was applied as a uniformly distributed load at the pipe crown and the three-dimensional stress state was largely ignored. As the pipe deformed, redistribution of the stresses was not considered. As will be discussed in detail below, as the depth of cover is reduced, the three-dimensional distribution of the load is significantly impacted and the assumption of a uniformly distributed load is no longer valid. As a result, although this report provided a high-level guidance for corrosion of abandoned pipelines, a more in-depth and thorough analysis of the various influencing parameters is warranted and necessary. The author further stated such in their concluding remarks, specifying finite element modelling is recommended for the development of more accurate models.

2.4 Buried Pipelines Subjected to Surface Loading

Throughout the literature, it is common for researchers to perform analyses on pipeline sections above grade, testing directly in the test apparatus. The investigations described above typically involve the pipe section fixed between two or more support points and the internal pressure and external forces are directly applied. Although these experiments allow for understanding the influence of various loading parameters and can be used to determine properties such as moment capacities and deformations of the isolated section, these experimental investigations deviate from actual in-*situ* buried pipeline conditions. The presence of a soil matrix influences both the load path of surface applied loads and the response of the pipe section due to soil-structure interaction effects.

Brachman et al. (2000) designed a proposed laboratory facility to be used for testing and evaluating the response of buried pipelines. Large-scale facilities for testing buried pipelines are valuable in evaluating the structural response of pipelines; however, few such facilities are readily available. The facilities that do exist have various limitations that cause the results to differ from the in-*situ* conditions experienced in the field. Such limitations include: no elimination of or consideration for friction between the soil and test facility walls, earth pressures on the pipe section are considered as uniform radial pressures, and an inaccurate representation of the biaxial soil pressure response observed in the field. Therefore, the results obtained experimentally in these facilities still are not true representations of the field conditions; with the previous isolated pipe experiments differing even more significantly. When designing the proposed test facility, finite element analysis was used to determine the influence of boundary friction, lateral boundary stiffness, and test cell dimensions. A buried pipe section was modelled and the parameters were varied in an attempt to determine the optimal values. As the friction between the soil and side walls was reduced, the resulting vertical stresses in the pipe section increased. The soil was able to translate freely from the wall, increasing the imposed load on the pipe section. An optimal solution was determined to have side wall friction < 5°. With a side wall friction of 35°, only one third of the surface pressure reached the base of the wall with the remainder taken up through interface friction. Further, as the lateral stiffness of the test walls decreased, the resulting vertical deformations and bending stresses of the pipe section increased due to the reduced confining pressure. Finally, as the dimensions of the test cell increased relative to the pipe section, the pipe stresses also increased. The researchers demonstrated that the presence and accurate representation of the soil matrix was critical in determining the structural response of buried pipelines subjected to surface loading. Great effort must be made to limit the influence due to the proximity and stiffness of the soil block boundary conditions.

2.4.1 Influence of Soil-Structure Interaction

The effects of soil-pipe interaction between the buried pipeline and the surrounding soil matrix were investigated by Noor and Dhar (2003). The researchers examined the response of buried concrete pipelines subjected to surface vehicle loads at shallow burial depths using the finite element analysis software ANSYS. The concrete pipeline was modelled within a uniform soil matrix and a unit live load was applied to the surface of the soil block. At deep burial depths, it is reasonable to assume a uniformly distributed load at the level of the pipe due to a surface applied load. However, this assumption is not valid for shallow burial depths and a three-dimensional analysis is required. The researchers conducted a linear analysis for 0.5 m, 1.0 m, and 1.5 m burial depth and the resulting stress distributions were obtained and compared to design code equations. It was determined that for depths greater than 1.5 times the pipe diameter, classical soil mechanics can be applied to determine the stress distribution. However, at a burial depth 0.5

times the diameter, soil-pipe interaction must be considered to accurately determine the stress distribution, and the resulting stresses exceeded the design codes. In addition, the maximum stresses were found at the pipe crown in all cases.

Kabir (2006) further investigated the influence of soil-structure interaction on the resulting stresses of buried pipelines subjected to surface live loads. The author again focused his research on the behavior of rigid pipelines subjected to surface live loads utilizing finite element analysis software ANSYS. Rigid concrete pipelines were modelled within a uniform soil matrix, a surface live load was applied, and the burial depth was incrementally decreased. The resulting load transferred to the surface of the pipeline was determined. Current pipeline design methods typically assume that a surface applied live load is transferred to the pipe section as a uniformly distributed load, added to the overburden earth pressure. The classical Boussinesq's theory uses the theory of elasticity to calculate the stress distribution and load transfer of a surface applied load through an infinite, uniform medium; see Figure 2-6 (Verruijt, 2018).

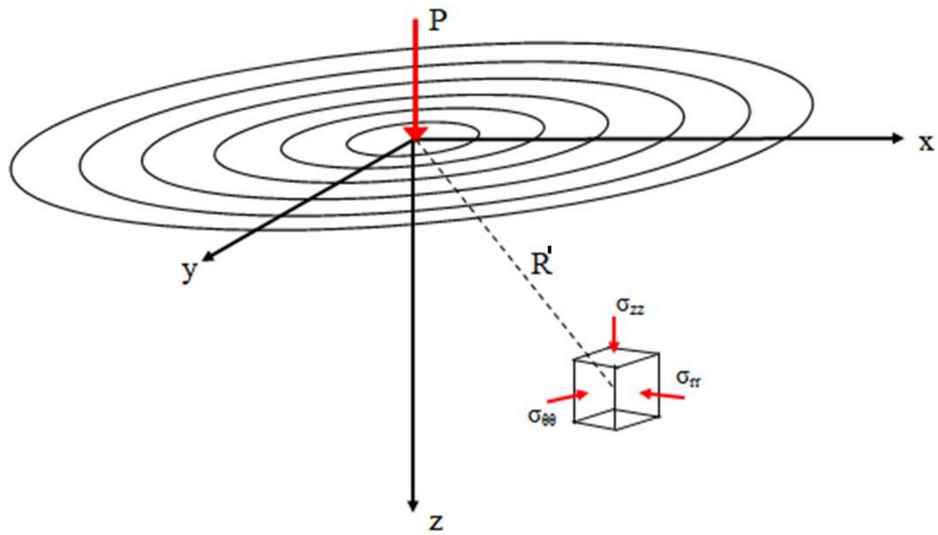

Figure 2-6: Surface Load Acting on Medium (Verruijt, 2018)

Figure 2-6 showcases the transfer of a surface applied point load to a selected soil element of interest. The three dimension distance from the soil element to the surface load greatly influences the resulting stresses acting on the element. The vertical stress tensor acting on the soil element is described as:

$$\sigma_{zz} = \frac{3P}{2\pi}\frac{z^3}{R'^5} \tag{2-4}$$

where, σ_{zz} is the vertical stress tensor, in Pa; P is the surface applied load, in Newton; z is the depth of the soil element of interest, in m; and R' is the direct radial distance from the surface applied load to the soil element of interest, in m. Within the geotechnical engineering field, it is generally accepted that a surface applied load has a zone of influence with a slope of 2:1.

Utilizing Boussinesq's theory, the stresses acting on the surface of a pipeline can be easily calculated. However, this theory has the fundamental assumption of a homogenous isotropic soil medium. This assumption is generally acceptable for deeply buried pipelines in which the volume of overburden soil is sufficient to achieve this idealized distribution. As the load is transferred through the soil, it can be sufficiently described as a uniform stress at the elevation of the pipeline. However, as the burial depth decreases, the assumption of a homogenous material is no longer valid due to the presence of a much stiffer pipeline section. With a shallow overburden cover, the relative stiffness between the two media – the soil matrix and the pipeline cross section – is substantial and must be considered.

At shallow burial depths, the pipeline tends to attract a larger portion of the load due to its higher relative stiffness through a mechanism known as *soil arching*. Soil arching describes the process through which an unstable soil mass (due to translation or yielding) transfers stress to an adjacent rigid body. In a soil block, this rigid body may be adjacent stable soil or an adjacent rigid pipeline. This phenomenon was further shown by Kabir (2006) using two extremes: soil with a buried pipe present versus soil with an open hole and no pipe present. It was shown that with the pipe present, the adjacent soil stresses were lower than that compared to when no pipe is present. This suggests that the pipeline attracted a significant portion of the load due to its inherently higher stiffness. Therefore, soil-pipe interaction must be accounted for in pipeline analysis. The author further confirmed the critical stress distributions around the circumference of the pipe section. The maximum stresses were observed at the pipe crown (the 12 o'clock position), followed by the pipe springlines (the 3 o'clock and 3 o'clock positions), with minimum stresses at the pipe invert (the 6 o'clock position). Although at shallow burial depths, the three-dimensional stress state must be considered, it was determined that classical Boussinesq's theory can be applied when the burial depth is greater than three times the pipe diameter with high accuracy.

Trickey and Moore (2007) examined the complementary stiffness extreme compared with the rigid concrete pipes, focusing on the response of flexible pipelines subjected to surface loading. A finite element model was developed in ANSYS to determine the maximum deflections and central moment while modifying the burial depth and pipe stiffness. The results of the parametric study were compared to results from Poulos (1974) who used the fundamental theory of elasticity to model the pipe using a relative flexural flexibility and axial stiffness factor. The soil medium was modelled using an elastic isotropic continuum, while the pipe was modelled as a horizontal strip with stiffness *EI*. The factors describing the pipe stiffness relative to the surrounding soil are defined as:

$$\text{Flexural Stiffness} = K_f = \frac{EI}{E'L_p^4} \tag{2-5}$$

$$\text{Axial Stiffness} = K = \frac{EA}{E'A_0} \tag{2-6}$$

where K_f and K are the dimensionless flexural stiffness and axial stiffness factors, respectively; E is the pipe section Young's modulus, in MPa; E' is the soil Young's modulus, in MPa; I is the pipe section second moment of area, in m^4; L_p is the length of pipe section, in m; A is the pipe section cross-sectional area, in m^2; and A_0 is the area bounded by the outer circumference of the pipe section, in m^2. A buried pipe section was subjected to a circular surface applied load. A significant mesh simplifying assumption was made, considering the pipe section as a solid rectangular section. Through the parametric study, it was found that the maximum central deflections and moments occurred in the pipe having the shallowest burial depth. For flexible pipes, the observed deflections and central moments were found to be underestimated by analysis of Poulos (1974). As the pipe stiffness increased, Poulos' analysis tended to overestimate the resulting deformations and moments. It was clearly shown that accurate representation of the soil-pipe relative stiffness and soil-pipe interaction properties significantly influenced the resulting three-dimensional response of the buried pipe sections.

The findings from the above investigations suggest that soil-pipe interaction is critical in determining the three-dimensional stress state of shallow buried pipelines. However, the papers focused on rigid concrete pipelines or highly flexible pipelines. Within the energy and chemicals industry, steel pipelines are more commonly used and are more susceptible to corrosive environments and long-term deterioration. Steel sections can be classified as semi-rigid when compared with concrete sections. The same principals and fundamental methodology of these analyses should be considered and applied to understand the three-dimensional stress state of buried steel pipelines subjected to surface live loads.

Neya et al. (2017) further looked specifically at the static response of buried steel pipelines subjected to moving surface live loads. Using the finite element analysis software ABAQUS, the authors performed a numerical analysis of a buried pipeline within a uniform soil block, subjected to moving pedestrian traffic loads. The surface loading was applied both parallel and perpendicular to the pipeline axis. The key results of interest included maximum stresses in relation to the direction of vehicle motion, the velocity of vehicles, diameter of pipe, burial depths, and soil type. The pipe and the soil were modelled using solid continuum elements and linear elastic material properties. Soil-structure interaction was considered through a frictional contact definition and the pipeline was subjected to a combination of internal pressure, soil overburden, and surface pressure load. Through the parametric study, it was found that maximum principal stresses became significant at depths of soil cover less than one meter, maximum stresses were experienced with vehicles travelling perpendicular with the pipe axis (for large bore pipes), the stresses increased with decreasing pipe diameter, and the stresses decreased with increasing soil stiffness.

The premise of the research by Neya et al. (2017) is similar to the research presented within this thesis hereafter. However, the pipelines used in the analysis by Neya et al. (2017) were also subjected to internal pressure, were fully intact and corrosion was not considered, and the loading considered was residential as opposed to commercial and industrial equipment. Internal pressure has the tendency to reduce the net external pressure caused by the surface loading, corrosion will act to decrease the wall thickness and resulting stiffness of the pipeline section, and industrial vehicles and equipment have much higher and more critical loads than those considered. Therefore, there is significant room to expand upon this research and to focus on more critical geometric and loading parameters.

Finally, Arockiasamy et al. (2006) conducted full-scale experimental field tests on buried flexible corrugated pipes subjected to surface live loading. The researchers considered four commonly used buried pipe materials including high-density polyethylene (HDPE), polyvinyl chloride (PVC), steel, and aluminum. A total of 36 different pipes were buried at varying depths of 0.5D, 1D, and 2D, where the diameter, D, was considered to be 900 mm and 1200 mm pipes. Figure 2-7 outlines the buried pipe geometry for each burial depth and the location of pressure cells (Arockiasamy et al., 2006). The pipe sections were buried and adequately backfilled using well-graded sand/silty soil compacted to 95% Standard Proctor maximum dry density. The buried pipes were subjected to an axle load of 141 kN, modified with the appropriate dynamic load allowance factor, *IM*, given by Equation (2-7) as per AASHTO (1998), based on the depth of soil cover, D_E.

$$IM = 33\% \cdot (1.0 - 0.125 D_E) \tag{2-7}$$

Applying the load factor, the maximum axle load applied was 181 kN.

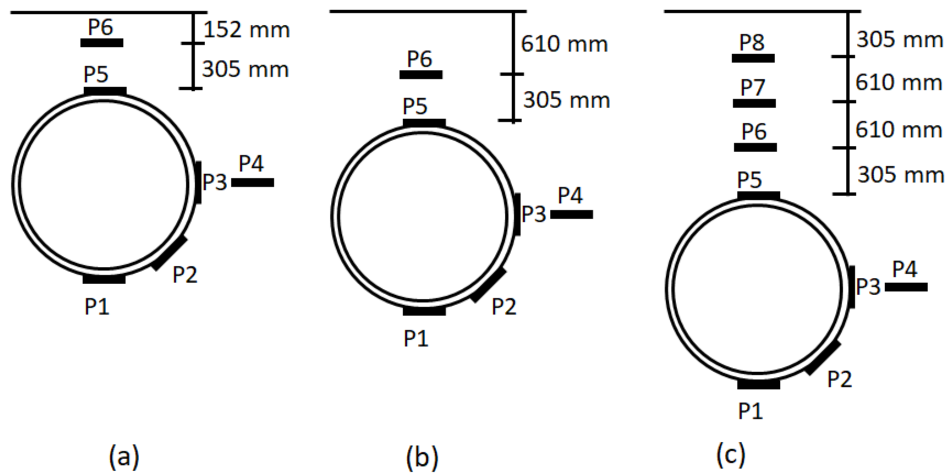

Figure 2-7: Buried 900 mm pipe - showing location of pressure cells for a) 0.5D, b) 1.0D, and c) 2.0D depth of soil cover (Arockiasamy, Chaallal, & Limpeteeprakarn, 2006)

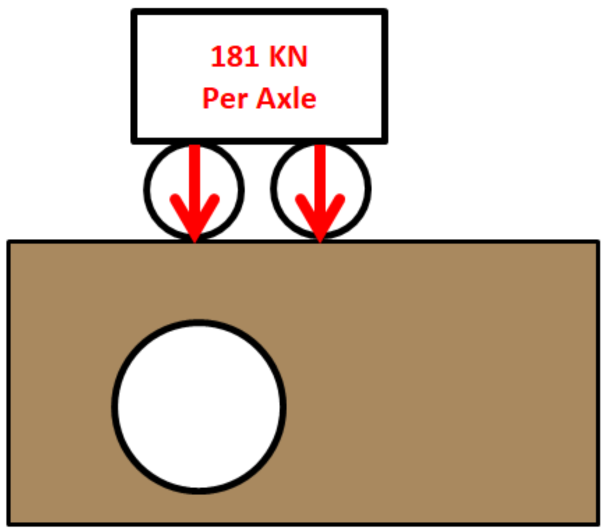

Figure 2-8: Schematic of the full-scale field test of 900 mm pipe at 0.5D depth of soil cover (Arockiasamy, Chaallal, & Limpeteeprakarn, 2006)

The surface loading was applied as shown in Figure 2-8 with two adjacent axle loads; one applied centered over the pipe cross-section (Arockiasamy et al., 2006). The resulting pipe surface soil pressures, strains, and deformations were obtained. The problem was further modelled using finite element analysis software ANSYS. The finite element analysis corresponded well with the results obtained from the field experiments. It was observed that the pipes did not fail during the tests and experienced limited deflection, with the HDPE pipe experiencing only 5 mm, or 0.6%, deflection when considering the minimum soil cover. This value lies well within the 5% limits specified by AASHTO (1998). It was also found that the maximum soil pressures and strains are located at the pipe crown. The pressures at the spring line were only 50% compared with the pipe crown; while the pipe base and haunch (below 135°) experienced pressures only 15-35% of those at the pipe crown. Therefore, it was concluded that the soil provided adequate confining pressure and base support, and that the pipe crown was the critical stress location.

2.5 Use of Finite Element Analysis for Pipeline Investigation

As noted in many of the investigations described above, the static and dynamic response of buried pipelines subjected to a variety of geometry and loading conditions are commonly modelled and analyzed using finite element software. Finite element analysis (FEA) is commonly used throughout the pipeline industry to investigate the complex response of pipelines and allow the researchers to quickly analyze a variety of parameters and determine critical cases. Many of the researchers have corroborated the finite element results with experimental and/or theoretical results, validating the accuracy of the models. Although there are numerous different finite element analysis software available for use, it has been found that ABAQUS is most commonly used throughout the literature.

ABAQUS is seen as an ideal finite element analysis software for modelling pipeline behavior as it has the following capabilities and features, as summarized by Mohareb et al. (2001), with additional capabilities listed:

i. shell (S4, S4R) elements with the ability to accurately model large displacements and rotations;

ii. elastoplastic isotropic hardening material models for accurate representation of pipeline steel materials;

iii. Mohr-Coulomb material models for accurate representation of soil matrix materials;

iv. non-linear modeling of material, geometries, deformations, and analysis;

v. post-processing features allowing the user to visualize results, easily extract data, and develop plots relating to variables of interest;

vi. and a variety of contact definitions between two deforming bodies, ranging from rigid contact to pressure and friction defined contact simulations.

Mohareb et al. (2001) performed both experimental and finite element analyses of pipe sections subjected to internal pressure, axial loading, and bending. In the experimental tests, the pipe section was capped at both ends and an internal pressure was introduced. The pipe was subjected to an eccentric axial compressive load, inducing an additional bending moment. The axial force was increased until buckling failure of the section occurred. It was found that the presence of internal pressure greatly enhanced the bending moment capacity of the pipe section. All of the specimens exhibited ductile behavior – yielding and then buckling. Post-buckling, wrinkles developed and the resistance curve softened. The experimental test was then replicated in finite element software ABAQUS. The objective of the finite element analysis was to verify the experimental observations and establish that numerical models are capable of predicting pipe moment capacity, curvature, and wrinkling deformations. During the formation of the wrinkles, the section underwent large deformations. To capture these displacements, the pipe was modelled using S4R shell elements. To ensure that buckling occurred away from the boundary conditions, the pipe section near the boundary was modelled with an ideal elastic material, preventing plastic deformations. The loading was applied with the axial compression load first, followed by the internal pressure, and then the moment was applied as end rotations as measured during the experimental investigation. Through the analyses, it was found that the moment-curvature relationship can be used to validate finite element models. However, since moment-curvature is based on pipeline length, it cannot be considered a pipeline section property. The finite element model was able to predict accurate buckling forces and modes of failure as compared with the experimental observations.

Soil-pipe interaction of a pipeline subjected to lateral ground movement was investigated by Roy et al. (2016) using the finite element analysis software ABAQUS. Buried pipelines can be subjected to lateral ground displacements due to soil subsidence, slope movement, and earthquakes. Relative displacement between the soil and pipeline impart frictional forces to the pipe surface in a variety of directions. To study the load-displacement curves of a buried pipeline in a sand matrix, a two-dimensional finite element model was developed. The soil was modelled using the Mohr-Coulomb material model. In addition, the researchers also used a modified Mohr-Coulomb model, incorporating the effects of dense sand properties including non-linear pre-peak and post-peak variant in the friction and dilation angles. Contact between the soil and pipe surface was defined as a frictional contact, variable with the soil friction angle. The pipe was subjected to displacement-controlled loading, with the pipe being laterally translated a pre-defined amount. A parametric study was conducted examining the effects of pipe diameter, soil properties, and burial depth. It was found that the modified Mohr-Coulomb soil model generated more accurate load-displacement curves and corresponded well with the previously obtained experimental data. The mobilized friction and dilation angles varied significantly in value and slope compared to the peak and pre-peak values. The larger pipe diameters experienced the largest peak stress values and as the burial depth increased the peak stress and required mobilization forces also increased. ABAQUS material models were able to provide a realistic representation of the soil behavior and soil-pipe interaction.

Finally, the influence of local corrosion on the resulting burst pressure of pipelines was investigated by Yeom et al. (2015). As pipelines in operation begin to corrode, large local corrosion pockets can form beneath the surface coating. The local reduction in wall thickness has the tendency to reduce the burst pressure of the pipe section. Local corrosion patches result in large stress concentrations and tend to experience outward bulging due to internal pressure. Using experimental tests and finite element analysis, the researchers examined the influence of local corrosion depth, length, and width on the ultimate burst pressure. A parametric analysis of these variables was performed using ABAQUS. The pipe section was modelled using C3D8 solid continuum elements. The solid elements allowed for a high degree of accuracy in modelling the dimensions of the corrosion patch. The resulting burst pressure, deformation, and failure mechanism of the finite element models correlated closely with the full-scale experimental tests. It was determined that the burst pressure was proportional to the wall thickness and as the depth of the local corrosion increased, the corresponding burst pressure decreased rapidly. Stress concentrations were observed at the edges of the corrosion patch and bulging and increased deformation occurred.

These three studies were selected as they showcase the applicability of ABAQUS for the analysis of pipe behavior, soil behavior, and corroded pipe sections using a variety of different element types and analysis methodology. However, there are numerous other studies utilizing ABAQUS, and finite element analysis in general, found throughout the literature; some of which have been covered through this review. Based on the studies described above, it is apparent that ABAQUS is capable of accurately modelling and analyzing pipeline structural behavior, buried pipeline behavior, soil behavior, and soil-pipe interaction under a variety of applied loads.

2.6 Summary of Literature

The majority of the studies within the literature focused on the effects of loading and corrosion on pipeline behavior during operation. While in operation, pipelines are typically under high internal pressure and rupture can be catastrophic. Therefore, the focus on pipelines in operation is warranted. However, when the pipeline reaches the end of its useful life and is decommissioned, the resulting abandoned pipelines still pose a major risk to both the public and the environment. The presence of internal pressure in operation reduces the net pressure differential of pipelines subjected to surface applied external loading. Depending on the depth of soil cover and the effective corroded wall thickness, many pipelines can experience their critical stresses long after decommissioning. In addition, a majority of the research examined investigated pipeline behavior without considering soil-structure interaction. As noted above, the literature has shown that at shallow burial depths, soil-pipe interaction is highly influential on the resulting stress distribution due to soil arching effects and there exists limited theoretical solutions to describe this complex behavior. As a result, a comprehensive three-dimensional analysis must be performed.

There is limited literature regarding the specific topic of long-term structural integrity of decommissioned and abandoned pipelines. Prewitt et al. (2017) performed a technical case study assessing the residual strength of abandoned pipelines subjected to a high degree of corrosion. Finite element models of a pipeline section were developed. Extensive perforated corrosion was modelled at the springline of the pipe section and a uniform vertical load was applied to the top hemisphere of the pipe section. Soil confining pressure was simulated through modelling a larger rigid cylinder around the pipe section and defining a contact pressure between the two, representative of the soil stiffness. Through this analysis, it was determined that even with 75% perforation at the springline, the section is still capable of sustaining highway traffic loading. However, the analysis conducted in this investigation was overly simplified. The analysis did not comprehensively incorporate soil-pipe interaction, primarily soil slippage around the pipe; pipelines may be subjected to much higher surface loading than the highway traffic considered; and pipelines are commonly placed at very shallow burial depths, much shallower than the 1.3 m considered. Therefore, there is significant room to improve and expand on the fundamental concepts of the research and to develop more robust and comprehensive models to investigate the structural response of abandoned decommissioned pipelines.

Chapter 3

Finite Element Model

To achieve the above mentioned objectives and investigate the research motivations, finite element models were developed using the commercial software ABAQUS. As seen throughout the literature, ABAQUS is commonly used and accepted in the pipeline industry for finite element analysis of buried pipelines subjected to a variety of loads including surface live load, soil movement, internal and external pressure, bending moments, and axial forces. Results from these finite element analyses have been validated and corroborated with their respective experimental data. Further, ABAQUS possesses the capabilities of performing non-linear analysis and modelling non-linear material properties and geometries (Dassault Systemes, 2014). As the pipeline models are expected to undergo significant local non-linear deformations under the effects of surface loading, non-linear analysis capabilities are essential. Finally, ABAQUS has the capability of modelling contact constraints with strict slave and master element algorithms, enabling accurate representation of the contact between the pipe and surrounding soil.

In this thesis, over 100 models were developed to investigate the influence of various parameters on the structural response of decommissioned pipelines including burial depth, pipe section wall thickness, pipe diameter, diameter-to-thickness ratio, soil stiffness, surface live load magnitude and geometry, and ultimate limit state factors. Additional preliminary models were developed for the geometric optimization and mesh convergence analyses. Each of the models developed consisted of a buried pipeline section within a uniform soil block. The initial analysis conducted was to determine the optimized geometric dimensions of the model. Subsequently, a mesh convergence study was performed. Once the optimized model was developed, the primary parametric analysis conducted examined the influence of burial depth on the resulting static behaviour. Pipelines can be buried at a variety of depths depending on a multitude of conditions including severity of pipeline failure, depth of frost penetration, and any superficial features such as roadways and rivers. Therefore, prior to investigating the influence of the previously noted parameters, it was imperative to determine a critical depth of soil cover on which all analyses will be based. This critical depth of soil cover was defined as the reasonable depth at which the stresses in the pipe section became significant and began to increase rapidly. The initial models developed consisted of a single pipeline with standard wall thickness, buried directly beneath the surface load. The depth of soil cover was varied between 3.0 m to 0.25 m in 0.5 m decrements, with a final decrement of 0.25 m, as shown in Figure 3-1. For each burial depth, four separate pipe diameters were examined - 34”, 30”, 24”, and 20” nominal pipe diameter. These pipe diameters were chosen as they are commonly used throughout the downstream transmission pipeline industry and are readily available for experimental investigations to be completed by another researcher in a future separate investigation. Further, smaller pipe diameters would be less critical in terms of soil subsidence resulting from a potential collapse. Through analyzing multiple diameters, the effects of pipe diameter on the resulting stress state were obtained simultaneously. The effects of soil-structure interaction were included in the analysis through the use of a contact definition between the pipe section and surrounding soil. A frictional slip contact definition was modelled, allowing the soil to deform across the surface of the pipe should the frictional resistance be overcome.

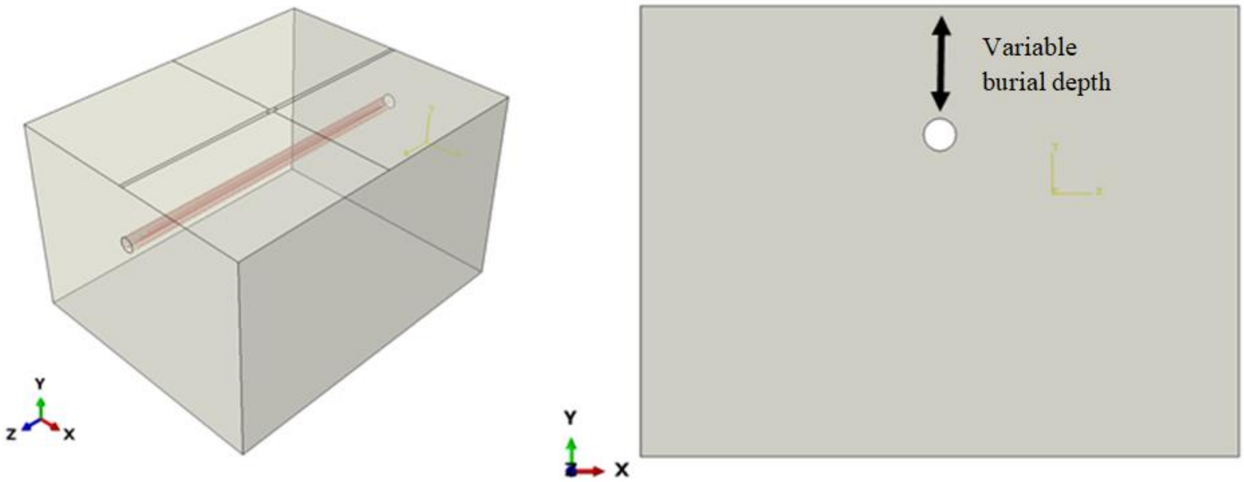

Figure 3-1: Finite element representation of buried pipeline

3.1 Element Selection

One of the most important modelling selections to ensure accuracy of the model is the selection of the actual finite element types used. The element types are responsible for the system's overall stiffness and resulting stresses and strains. Element selection is based on a number of factors including type of loading, expected structural behaviour, desired output, system geometry, and computational capacity. ABAQUS offers many different elements in the standard element library including solid, shell, wire, and membrane elements. The structural system under consideration contained two distinct parts, each with their own unique element selection criteria. The elements of particular use in this analysis include solid and shell elements. As shown throughout the literature review, it is common practice for the pipe sections to be modelled using shell elements. Shell elements are capable of capturing the large in-plane strains as the pipe deforms and are computationally much more efficient for this application as compared with solid elements. The soil matrix itself was modelled using solid elements for obvious reasons, including the overall gross volume and the requirement for accurate three-dimensional stress transfer of the surface loading to the pipe section.

3.1.1 Pipe Section Elements

Pipe sections are commonly modelled using shell elements due to the relatively large diameter-to-thickness ratios and local deformations (Sadowski, 2013). A large diameter-to-thickness ratio corresponds to a pipe section with a large diameter and standard or relatively thin wall thickness. Further, as the wall thickness decreases due to corrosion, the diameter-to-thickness ratio will continue to increase. Buried pipelines within the petrochemical industry are mostly classified with large diameter-to-thickness ratios as the thin wall sections are economically efficient, the surrounding soil provides adequate confining pressures, and these sections are less susceptible to large thermal stresses as compared with thicker walled sections. There are two common shell elements within the ABAQUS element library: S4 and S8 elements, consisting of four and eight nodes, respectively (Dassault Systemes, 2014). Both S4 and S8 elements offer reduced integration variations (S4R and S8R). Reduced integration is most commonly used with the S8 elements in an attempt to reduce the computational requirements of using an element with a higher number of nodes. S4 elements are four-node, first-order, general purpose shell elements with 6 degrees of freedom for each node. The geometry of the S4 element is shown in Figure 3-2 (Massachussets Institute of Techonology, 2017). These elements are capable of capturing arbitrary large rotations and finite membrane strain. These elements can be used for both thin-shell and thick-shell applications and in situations with large strains. Since S4 elements have an inherent assumed large-strain formulation, they are applicable for in-plane bending problems and are not significantly sensitive to element distortion. These elements do not have hourglass modes of deformation in either membrane or bending applications; therefore, hourglass control is not required. S8R elements are eight-node, second-order, thick-shell elements and include finite rotations in addition to translations. These elements are able to describe the shear flexibility deformations, enabling a smooth displacement field. However, these elements tend to converge poorly due to shear locking and only permit small strains, ignoring changes in element thickness as the elements deform. Therefore the S8R elements are recommended for thick-shell applications only.

The ABAQUS user guide provides a recommended thickness ratio of greater than 1/15 compared to a characteristic length to differentiate between a thin-shell and thick-shell application (Dassault Systemes, 2014). With a higher thickness ratio, a greater number of thick-shell S8R elements are required through the thickness of the section to accurately capture the through-thickness bending behavior. For pipelines, the characteristic length of interest was chosen as the pipe diameter. The smallest diameter-to-thickness ratio, D/t, was 53.3 for the 20” pipe section with a standard 3/8” wall thickness. The largest 34” diameter pipe section had a D/t value of 90, with a standard 3/8” wall thickness. Therefore, it was concluded that the models developed constitute a thin-shell application and the use of S4 elements was appropriate. In addition, it was expected that at shallow burial depths, local deformations become significant and result in large strains. Again, first-order S4 elements are recommended for this application. To account for the greater rotational stiffness of the S4 elements compared to the S8R elements, an appropriate mesh refinement was performed.

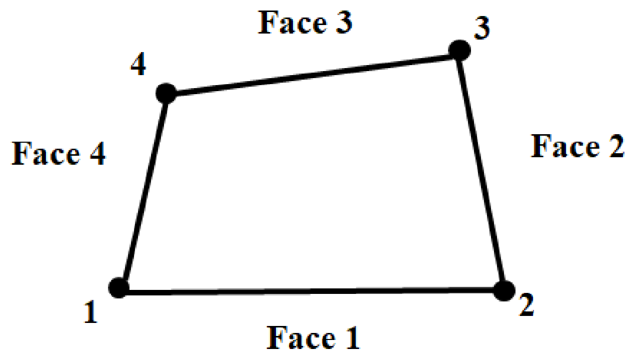

Figure 3-2: S4 shell element (Massachussets Institute of Techonology, 2017)

First-order shell elements also offer the option of using reduced integration during analysis. Reduced integration uses a lower order constraint condition (only one integration point) to generate the element stiffness. Using reduced integration significantly reduces the computational demand required to perform the analysis while still providing accurate results (Dassault Systemes, 2014). However, reduced integration should not be used in applications where in-plane bending is expected to occur. Reduced integration introduces the possibility of element hourglassing occurring, resulting in zero energy modes and excessive distortion. Again, it was expected that with shallow burial depths, local deformations become significant resulting in in-plane bending of the pipe wall. In all of these applications it was determined that S4 elements would outperform S4R elements and generate more accurate results. Hence, full integration elements were used. Due to the computational cost of using S4 elements, it is recommended by ABAQUS that these elements be used in highly sensitive regions of concern, while S4R elements can be used elsewhere. However, the computational cost of modelling S4 elements for the entire length of the pipe section was deemed acceptable.

In addition to shell elements, solid elements can also be used for pipeline applications. However, it is generally recommended to maintain an element aspect ratio as close to 1.0 as possible and to model a minimum of two elements through the thickness of the cross section in order to capture the through-thickness bending (Sadowski, 2013). An aspect ratio equal to 1.0 requires all dimensions of the element be equal, resulting in isotropic stiffness of the element. Implementing these two recommendations would have required an enormous number of additional elements and a prohibitively increased computational demand. Solid elements would not be efficient or accurate in the pipeline modelling application considered. In general, it is seen as uneconomical to use solid elements when the thickness ratio of the cylindrical shell exceeds 25. Therefore, the pipeline was modelled using S4 shell elements for all models discussed here within. A total of five section points were defined through the thickness of the element. The number of section points represents the number of integration points through the thickness. Increasing the number of section points allows for increased accuracy of modelling plastic deformation. However, as will be shown, the models remained in the elastic range for all analyses. Therefore, five sections were deemed acceptable while still allowing for the ability to capture any potential plastic deformation. If excessive plastic deformation occurred, the analysis would be re-analyzed using a greater number of section points and results compared.

3.1.2 Soil Block Elements

The soil block consisted of an expansive uniform material matrix and was modelled using three-dimensional stress, solid continuum elements. Solid continuum elements are the standard volume elements within ABAQUS, used in structures with analytically significant geometric volume. ABAQUS offers three primary solid element geometries including hexahedral, tetrahedral, and triangular prism shapes. Elements for the soil block were chosen to be second order, ten-node tetrahedron, C3D10 elements. The geometry of the C3D10 element is shown in Figure 3-3 (Massachussets Institute of Technology, 2017). The primary factor influencing the choice of solid elements was the ability to obtain a high-quality mesh with complex geometry. Due to the transition from the rectangular geometry of the soil block to the circular geometry around the pipe section, tetrahedral elements proved best to model a uniform and well distributed mesh. Tetrahedral elements are far more versatile when meshing complex geometries and are less sensitive to distortion and original element shape (Dassault Systemes, 2014). Hexahedral elements should be modelled as close as possible to rectangular in shape for accurate performance and accuracy decreases significantly if the elements become distorted. The soil experienced relatively large deformations at the point of load application due to the concentrated nature of the forces applied. Therefore, there was an increased possibility of element distortion, potentially reducing the accuracy of hexahedral elements.

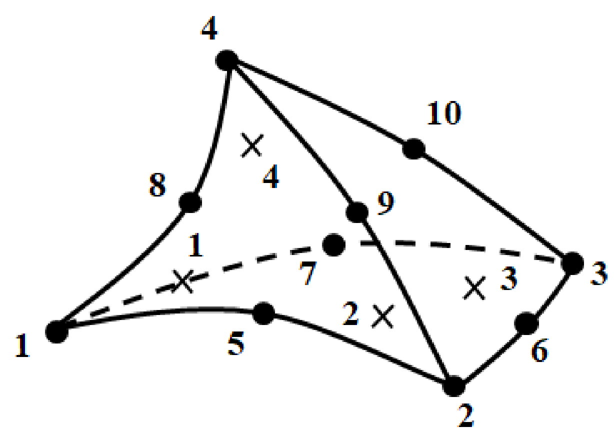

Figure 3-3: C3D10 solid element (Massachussets Institute of Technology, 2017)

It is also noted that hexahedral elements are more commonly used when the stress state of the element is of highest interest, such as in a structural beam bending. These elements tend to provide the most efficient balance between model accuracy and computational cost and, when initially undistorted, produce accurate three-dimensional stress states. However, in the parametric investigation conducted, the stress state of the pipe itself was of highest importance and the stress state of the soil was minimally considered. The soil acted as a medium through which the surface load was transferred to the pipe section. Therefore, an efficient mesh that limited element distortion and provided an accurate representation of the contract interface was of most importance. The C3D10 elements allowed for both of these objectives to be achieved.

3.2 Boundary Conditions and Model Size

In the finite element models developed, two distinct boundary conditions were considered to ensure stability of the model: the bottom surface and the four side surfaces. The four side surfaces were assumed to be roller supported, preventing movement normal to the surface while allowing all other translations and rotations. This boundary condition was acceptable as the pipe should ideally exist within an infinite soil medium. In an infinite soil block, only the vertical translation needs to be considered and the normal translation is assumed fixed at a suitable distance from the point of load application. The base of the soil block was assumed to be pin-connected, with zero translation in any direction. Again, within an infinite soil block, at a suitable distance from the point of load application, the soil at the base is assumed to be fixed. No boundary conditions were applied to the top surface of the soil block. Therefore, the interior elements of the surface were free to translate in all directions, with the edges fixed in the normal horizontal directions. Using these boundary conditions in combination, the soil block was able to deflect in the vertical direction only, with zero translation in either horizontal direction. The boundary conditions were applied to the surfaces of the soil model, as opposed to the boundary nodes. Applying these conditions to the surface inherently prevented the global rotation of the entire face, eliminating the requirement to use fixed-rotation boundary conditions which have a higher computational cost. Boundary conditions are shown schematically in Figure 3-4 (Lee, 2010).

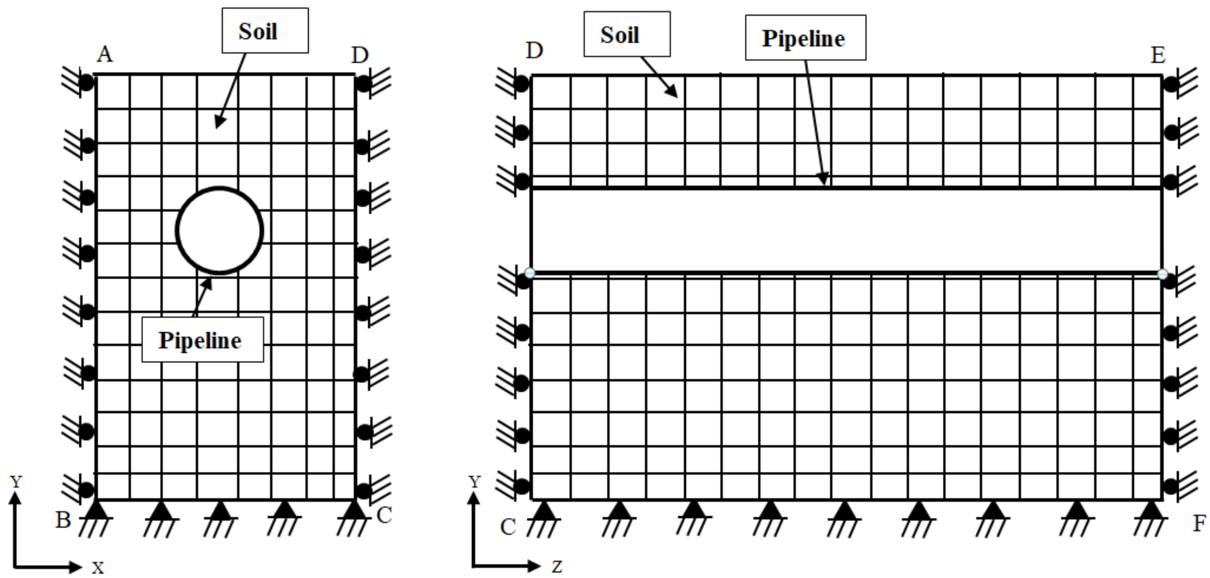

Figure 3-4: Model boundary conditions: Transverse section (left) and longitudinal section (right) (Lee, 2010)

The model size was optimized to reduce the influence of the proximity of the boundary conditions. The proposed experimental test facility developed by Brachman et al. (2000) was previously discussed, concluding that the effects of boundary conditions significantly influenced the resulting system behavior. Both the boundary stiffness and the frictional slippage greatly influenced the resulting stress state of the pipe and the load path of the surface applied loading. In reality, an in-*situ* pipeline can be idealized as existing within an infinite soil medium. However, an infinite soil space is not practical in both experimental terms and in the finite element analysis models. Therefore, to reduce the influence due to the proximity of the boundary conditions, the soil block length, width, and height were increased such that the pipe stresses under a unit surface load converged. A total of three parametric studies were performed, one for each dimension.

For the convergence analysis, a preliminary model was developed consisting of a 34” diameter pipe with standard 3/8” wall thickness, buried at a depth of 2.5 m soil cover within a soil cube with length x width x height (L x W x H) equal to 5 m x 5 m x 5 m. A mesh with an element size of 0.2 m was assumed and a unit surface pressure load was applied over the contact area of a wheel, described in subsequent sections. The result of interest for this convergence analysis was the maximum von Mises pipe stress. Using the preliminary model, the length was increased while maintaining W x H equal to 5 m x 5 m. The resulting maximum stresses were obtained and plotted against the variable dimension. An optimal model dimension was determined to be the point at which convergence of the results was achieved. The analysis was then performed again for both the width and the height of the soil block while keeping the other two dimensions constant. The plots of each dimensional study are shown below in Figure 3-5, Figure 3-6 and Figure 3-7:

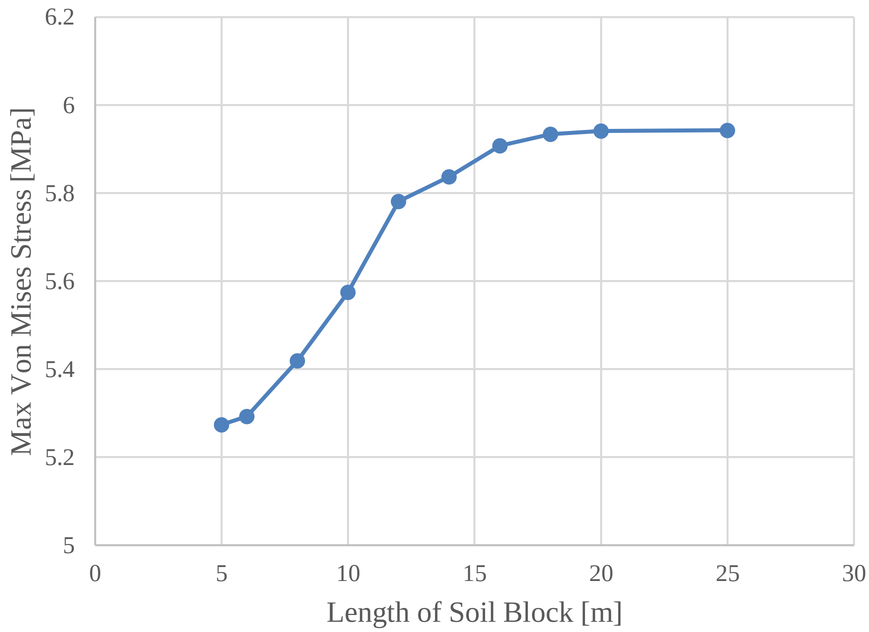

Figure 3-5: Length of soil block convergence

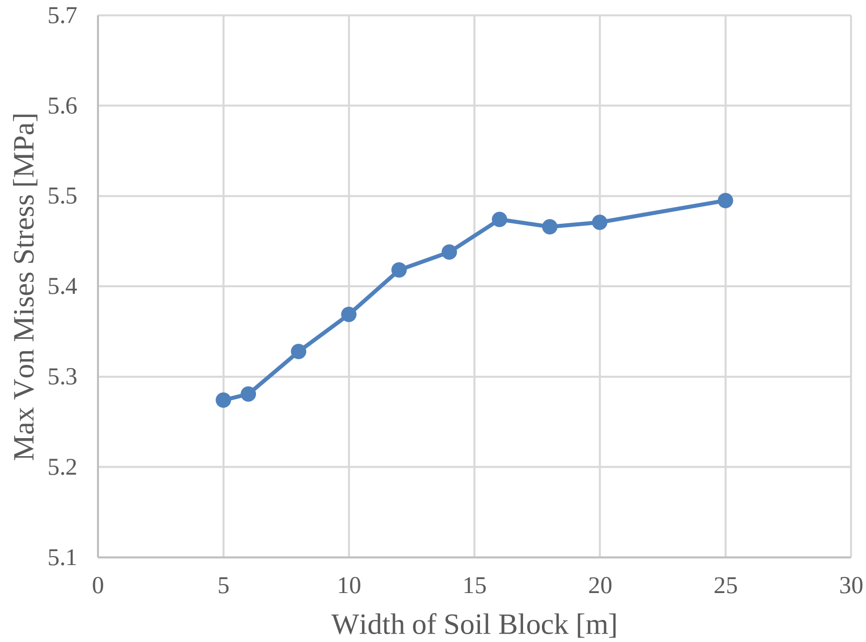

Figure 3-6: Width of soil block convergence

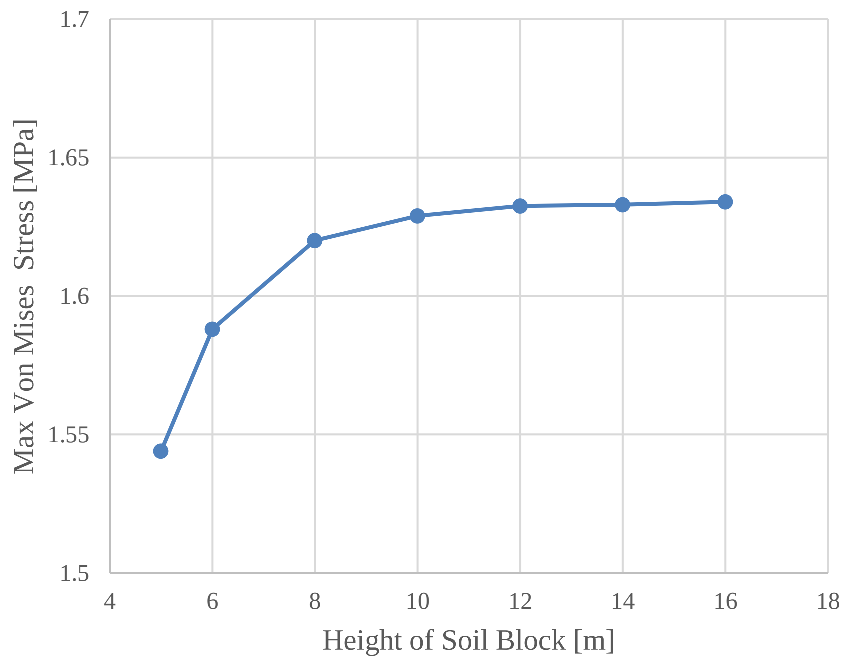

Figure 3-7: Height of soil block convergence

Based on the convergence analysis and resulting graphs, an optimal model size of L x W x H equal to 20 m x 16 m x 12 m was determined. These values aligned similarly to other values used throughout the literature (Neya et al., 2017). The actual parametric study used the full truck length consisting of five separate axles. The axles located further from the pipe section are less influential and thus, their proximity to the boundary is less critical. As will be discussed in Subsection 3.7.2, the surface live load used in this study is the Alberta Highway truck load CL-800. To accommodate the 18 m length between the front and the rear axles of this truck when placed to produce the maximum effects when travelling parallel or perpendicular to the pipe longitudinal axis, the width of the soil block was increased to 28 m, as shown in Figure 3-8. The same convergence analysis was performed to determine this value. Using these dimensions for the soil block, it was deemed reasonable to neglect the influence due to the boundary conditions and the models were considered representative of the in-*situ* infinite soil block.

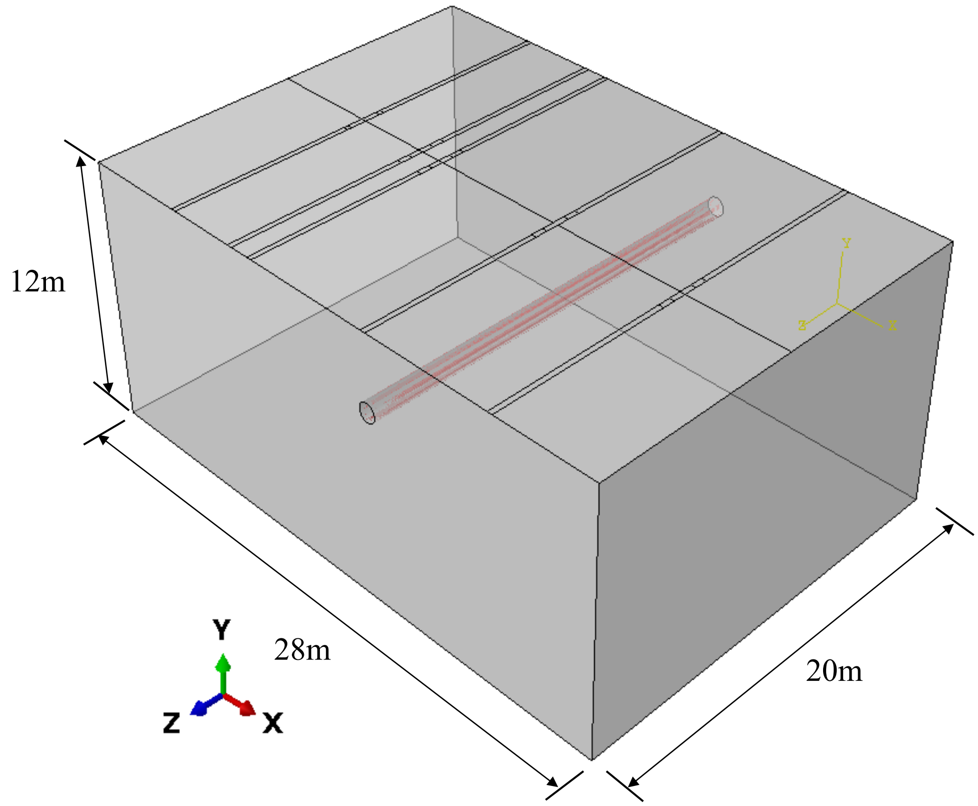

Figure 3-8: Finite element model dimensions

3.3 Mesh Refinement and Convergence

The accuracy obtained from a finite element model is directly related to the finite element mesh being used. Due to the inherent numerical integration associated with the finite element method, all results are approximated. With a coarse mesh, the number of degrees of freedom is low; increasing the significance of approximation required to converge to a solution and reducing the overall accuracy of the final solution. Further, as the elements become larger, they are inherently stiffer and unable to deform to match the curvature of the actual system deformation. Under large in-plane deformation, a coarse mesh tends to result in an overly stiff model and lower resulting stresses. For this reason, a finite element model will tend to converge to the true theoretical result from a "bottom-up" approach. As the finite element mesh is refined (size of elements reduced and number of degrees of freedom increased), the results tend to increase in accuracy and converge towards the true solution. Mesh refinement is a key component of validating any finite element model. For the buried pipe models under investigation, two mesh refinement studies were performed.

The first mesh refinement study was performed on the pipeline section. To refine the mesh of the pipe, an isolated 3 m long 34” pipe model was developed. The pipe was modelled with fixed-fixed end conditions and subjected to a uniformly distributed dead load. The resulting stresses were then compared to theoretical stresses obtained using Timoshenko beam theory. The stresses were plotted against the number of elements around the circumference of the pipe section. The mesh began as a course mesh, with very few elements around the circumference and the number of elements was subsequently increased. Increasing the number of elements around the pipe served to both increase the total degrees of freedom and to more accurately model the curved surface. Elements were maintained with the ideal 1:1 aspect ratio to ensure high accuracy of results.

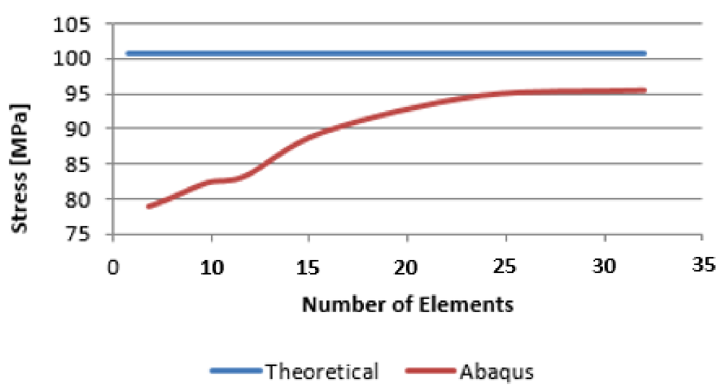

Figure 3-9: Pipe section mesh convergence for fixed-fixed beam

As can be seen in Figure 3-9, mesh convergence began to occur at approximately 20-25 elements around the circumference of the pipe section. A noticeable plateau occurred after 25 elements. Therefore, 30 elements around the circumference of the section was determined as the optimized value. Modelling more than 30 elements significantly increased the computational cost for little analytical benefit. Since the convergence analysis was performed for the largest pipe section considered, using the same number of elements around the circumference of the cross-section for the smaller diameter pipes resulted in smaller element size and more elements along the length of the pipeline, maintaining the accuracy of the model. Therefore, all pipe diameters were meshed with 30 S4 shell elements around the circumference of the section. The resulting maximum stress in this analysis differed from the theoretical stress by only 4%. The theoretical calculations are idealized and do not consider additional non-linear deformations which are included in the finite element analysis, such as wall thinning as the section deforms. As a result, the small deviation in resulting stresses was considered minimal and the pipe section finite element model was deemed acceptable.

The second mesh convergence analysis was performed on the soil block. The convergence analysis was performed using the previously optimized model size and pipe section mesh. The contact between the pipe and soil was assumed to be perfectly bonded using tied constraints to reduce the computational time of the convergence study. As described in the ABAQUS user guide, surface-based tie constraints can be useful for mesh refinement purposes for three-dimensional analysis (Dassault Systemes, 2014). Tie constrains can be used for rapid refinement of two dissimilar meshes due to the reduced computational time required to define the contact. As both penalty contact and tie constraints make use of surface-surface contact definition, the mesh refinement using tie constraints could be adopted for use with the finalized penalty contact, as is described in later sections.

The soil block was meshed using a biased mesh, in which the number of elements linearly increased or decreased from a predefined boundary point. A biased mesh was used to allow for increased local refinement over the pipeline and at the point of load application while having a coarse mesh at the boundary conditions. It was intuitive that a finer mesh was required at the point of load application as this is where the maximum stress concentrations occur in both the soil and the pipe. Therefore, it was necessary to ensure a high quality mesh at these locations to increase the overall accuracy of the structural system. The degree of bias was increased such that a finer mesh was achieved directly over the pipe, while the element size at the boundary remained constant. The finer mesh at the pipe was chosen to be 35 elements around the circumference of the pipe section. For the contact definition considered, the master surface (soil block) must be finer than the slave surface (pipe section) to ensure accuracy and convergence of results. A coarser mesh can be tolerated at the soil boundary surfaces because the model size was optimized such that the proximity of the boundary surfaces did not influence the resulting pipe stresses. Using the biased mesh approach allowed for an optimal number of elements and significantly reduced the computational time. The resulting maximum von Mises pipe stress was plotted against the number of elements in the soil block in Figure 3-10. The final three models (where convergence is realized) were re-run using the frictional contact definition described in further sections below to validate the assumption that tied constraints can be used for mesh convergence.

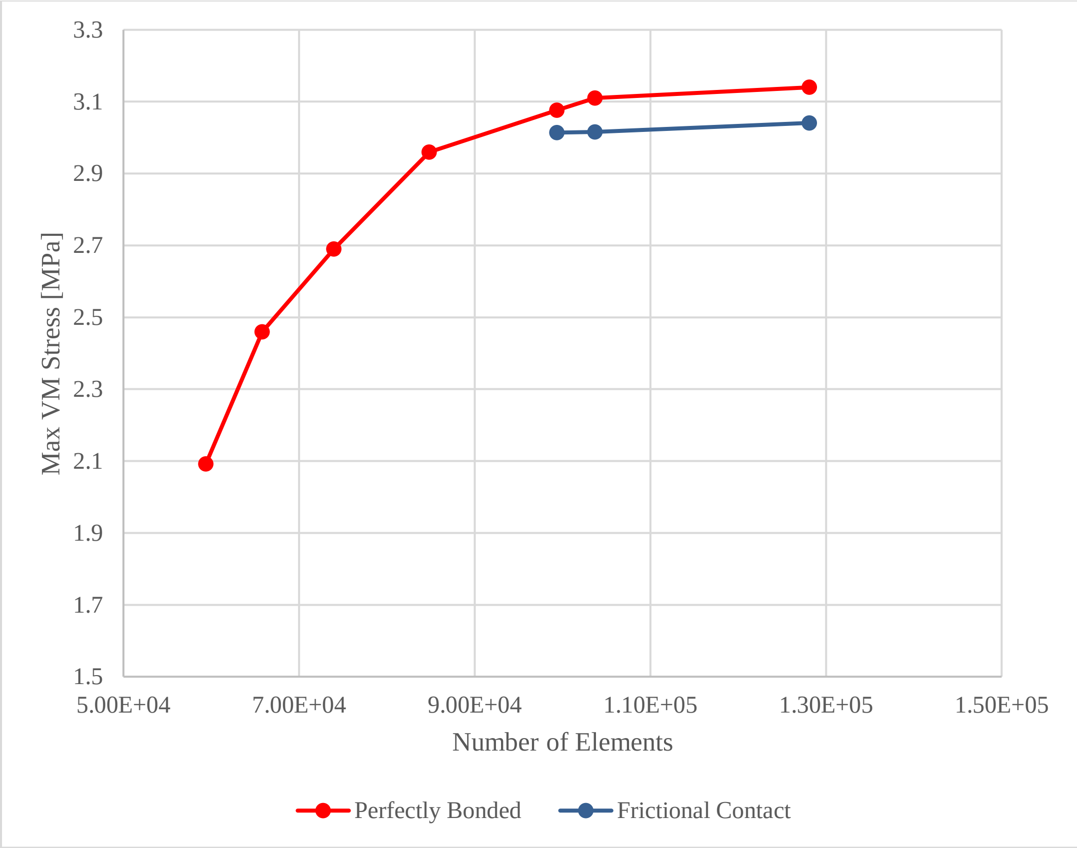

Figure 3-10: Mesh convergence of soil block

As can be seen, clear convergence was achieved at approximately 100 000 elements. After this point, the stresses plateaued and there was limited increase in accuracy compared with the increase in computational time. The same biased mesh was used for all pipe sizes. Through maintaining 35 elements around the soil pipe opening, the models using smaller diameter pipes again resulted in a reduction in element size and increase in the number of elements. Therefore, the initially accepted accuracy of the models was maintained as the diameter of the pipe decreased. To verify the above assumption of ignoring the effects of the boundary conditions, an additional analysis was run refining the boundary layer element size. The element size was substantially reduced, significantly increasing the number of elements. However, there was no significant impact on the resulting pipe stresses. This is again due to the fact that the model size was already increased such that the influence due to the proximity of the boundary conditions was negligible. As a result, even a highly refined mesh at the boundary location did not produce increased accuracy when compared to a more coarse mesh. The finalized meshing pattern for the 34” pipe section is shown in Figure 3-11. Note that the pipe is not centered in the soil block, as the pipe was positioned beneath the maximum axle load. This is explained further in subsequent sections.

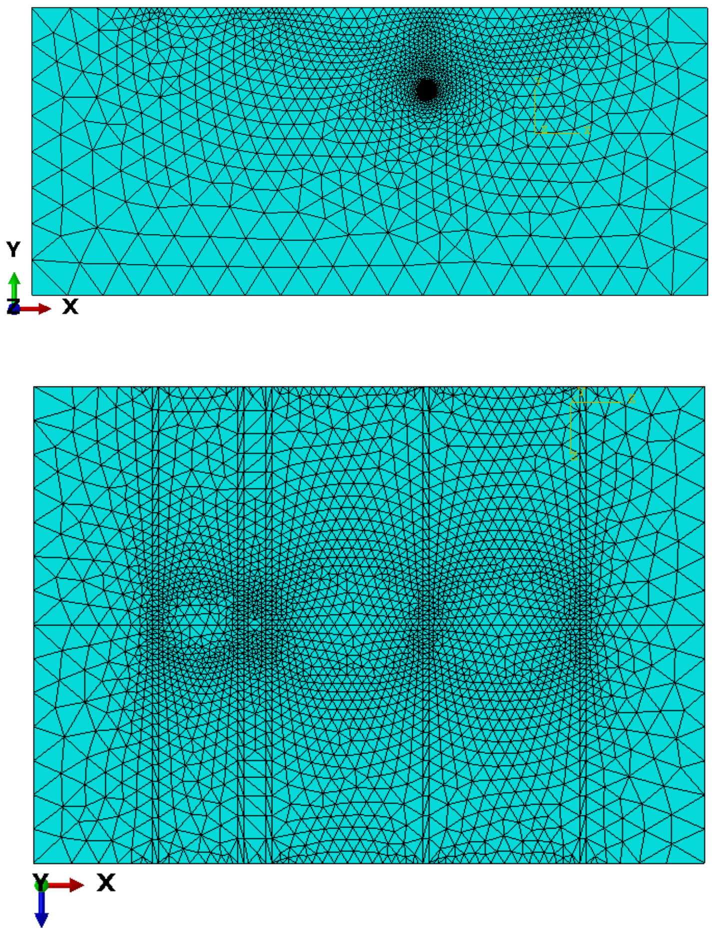

Figure 3-11: Soil block mesh: Sectional elevation (top) and top plan view (bottom)

3.4 Material Properties

Material properties define how each section of the model will respond to the applied loading. The ABAQUS material property library allows for extensive definition of material properties including general properties, elastic, inelastic, thermal acoustic, and numerous others parameters. In general, the material properties considered consist of general material properties such as mass density, along with both elastic and inelastic stress-strain behaviour. The models under consideration utilized two separate materials: the pipeline steel and the surrounding soil block.

3.4.1 Pipe Section

Pipelines can be composed of various materials depending on the contents to be transported, soil conditions, and stress requirements. For the purpose of the present analyses the pipeline steel material was assumed to be uncoated API 5L X60 steel. This steel specification is commonly used for transporting water, oil, gas, and petroleum related products in the petroleum industry (PM Internation Suppliers, 2017). The steel was assumed to be uncoated, or with corrosion protection no longer effective. The pipeline steel was modelled as a homogenous elastic material. Material plasticity beyond the yield stress was modelled assuming a Ramberg-Osgood material relation between stress and strain given as:

$$\varepsilon = \frac{\sigma}{E} + \alpha \left[\frac{\sigma}{\sigma_{yield}}\right]^n \tag{3-1}$$

where ε is the strain, in m/m. The Ramberg-Osgood relationship is used to describe the non-linear behavior between stress and strain, primarily at and post-yielding. The equation represents the hardening behavior of ductile steels. As the steel approaches yield, the material tends to harden with further plastic deformation through a process known as work hardening. The relationship assumes that even at low level of stress, plastic strain still occurs albeit negligible compared with the elastic strain. Therefore, the entire curve is considered non-linear. Using the Ramberg-Osgood relations, the nominal engineering stress-strain curve was developed with density, ρ_s = 7850 kg/m^3; Young's Modulus, E = 206 GPa; Poisson ratio, v = 0.3; and yield stress, σ_{yield} = 415 MPa. Parameter α represents the yield offset strain, assumed to be 0.2% for ductile steels. The material model was developed with comparison to literature curves (Trifonov, 2015). The exponential value of n was modified such that the resulting curve follows the literature values. The nominal stress and strain were then converted to true stress and logarithmic plastic strain through Equations (3-2) to (3-4) given below, to be used in ABAQUS (Dewanbabee, 2009). Typical stress strain curves provide the engineering stress and strain, relating to the originally undeformed cross-section. The true stress describes the actual stress calculated using the deformed geometrical properties of the specimen. When subjected to a tensile stress, the specimen will tend to elongate and the cross-sectional area will decrease due to the Poisson effect. The true stress, σ_T; true strain, ε_T; and logarithmic plastic strain, ε_p, respectively, are calculated as follows:

$$\sigma_T = \frac{F}{A} = \sigma_{nom} \cdot \frac{l}{l_0} = \sigma_{nom} \cdot (1 + \varepsilon_{nom}) \tag{3-2}$$

$$\varepsilon_T = \ln\left(\frac{l}{l_0}\right) = \ln(1 + \varepsilon_{nom}) \tag{3-3}$$

$$\varepsilon_p = \varepsilon_T - \left(\frac{\sigma_T}{E}\right) \tag{3-4}$$

where F is the force applied, in Newton; A is the undeformed cross-sectional area, in m^2; l is the deformed length, in m; l_0 is the original undeformed length, in m; σ_{nom} is the nominal stress, in MPa; ε_{nom} is the nominal strain, in m/m; and E is the Young's modulus, in MPa. Based on Equations (3-2), (3-3), and (3-4), the following material model was developed, as shown in Table 3-1.

Table 3-1: API 5L X60 steel stress-strain data

Nominal		True		
Stress, σ_{nom} [MPa]	Strain, ε_{nom}	Stress, σ_T [MPa]	Strain, ε_T	Plastic Strain, ε_p
0	0.0000	0.00	0.0000	0.00
25	0.0001	25.00	0.0001	0.00
50	0.0002	50.01	0.0002	0.00
75	0.0004	75.03	0.0004	0.00
100	0.0005	100.05	0.0005	0.00
125	0.0006	125.08	0.0006	0.00
150	0.0007	150.11	0.0007	0.00
175	0.0008	175.15	0.0008	0.00
200	0.0010	200.19	0.0010	0.00
225	0.0011	225.25	0.0011	0.00
250	0.0012	250.30	0.0012	0.00
275	0.0013	275.37	0.0013	0.00
300	0.0015	300.44	0.0015	0.00
325	0.0016	325.52	0.0016	0.00
350	0.0018	350.62	0.0018	0.0001
375	0.0021	375.78	0.0021	0.0003
400	0.0029	401.16	0.0029	0.0009
415	0.0040	416.67	0.0040	0.0020
425	0.0053	427.25	0.0053	0.0032
435	0.0072	438.15	0.0072	0.0051
445	0.0102	449.56	0.0102	0.0080
455	0.0148	461.74	0.0147	0.0125
465	0.0217	475.10	0.0215	0.0192
475	0.0321	490.24	0.0316	0.0292
485	0.0475	508.05	0.0464	0.0440
495	0.0704	529.82	0.0680	0.0654
505	0.1038	557.43	0.0988	0.0961
515	0.1525	593.56	0.1420	0.1391

The stress-strain curve was plotted for the assumed material model. As can be seen in Figure 3-12, there was close correlation between the assumed material model and the literature values developed with experimental results (Trifonov, 2015). Therefore, the material model was considered adequate. The values presented in Table 3-1 were manually input in ABAQUS. A large number of stress values were input to limit the error in the automatic interpolation performed. When a variable list of material properties is entered into ABAQUS, the software linearly interpolates between two adjacent values. As the Ramberg-Osgood relation is clearly non-linear, limiting the amount of linear interpolation was essential.

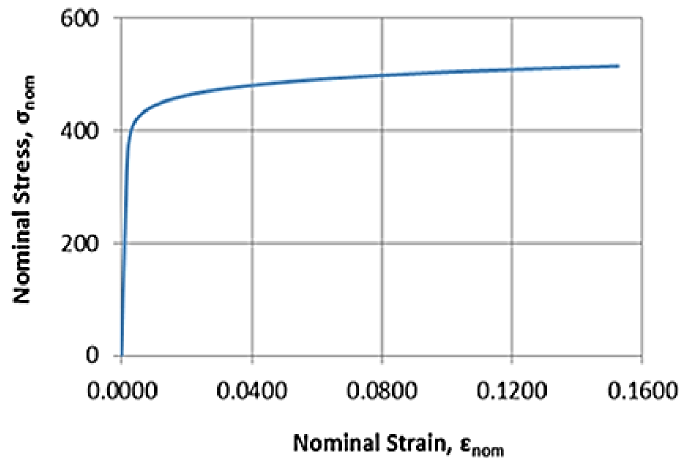

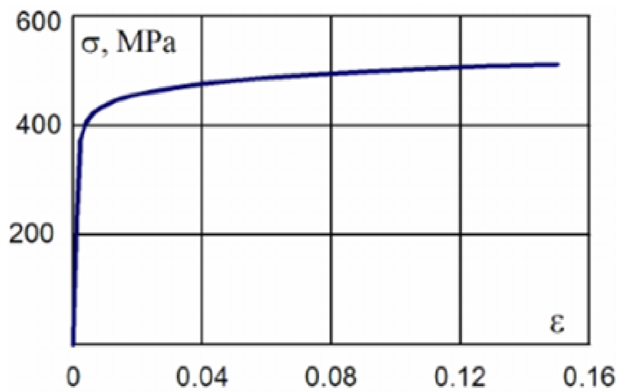

Figure 3-12: Nominal stress-strain curve used in X60 steel material model (top) compared to literature values (bottom) (Trifonov, 2015)

The yield surfaces of interest were the principal normal stresses in the longitudinal and circumferential directions. At shallow burial depths, the pipeline experienced stresses due to global bending, ovalization, and local bending of the wall section. As such, significant normal stresses developed in both the longitudinal and circumferential directions, the critical of which was determined through the analysis and described in further sections.

3.4.2 Soil Medium

It is common for multiple soil layers to be present in the overburden above a buried pipeline. An in-*situ* borehole sample can be extracted to determine the actual sedimentation overlaying a buried pipeline. However, due to the relatively shallow depths analyzed (< 3.0 m), it was deemed reasonable to assume that the overburden consisted of a single homogenous soil layer. Therefore, the soil block was modelled as a homogenous layer with uniform material properties. The soil was modelled assuming an elastic-perfectly plastic Mohr-Coulomb plasticity model. The Mohr-Coulomb model has been used extensively in finite element modelling of soil-pipe interaction analysis (Roy et al, 2016). Further, ABAQUS recommends the Mohr-Coulomb model for use in geotechnical engineering applications to study material response under monotonic loading (Dassault Systemes, 2014).

The Mohr-Coulomb model assumes that failure is controlled by the maximum shear stress. The failure criterion is written as a set of linear equations describing the failure line within principal stress space. The failure criterion typically ignores the intermediate principal stress, σ_2, and is written in terms of maximum and minimum principal stresses, σ_1 and σ_3. Mohr's circle can be plotted in terms of these maximum and minimum principle stresses as shown in Figure 3-13. The failure line is considered as the best fitting straight line which lies tangent to both of these circles. Only the top hemisphere of the circles is shown below, although the diagram is symmetrical about the zero shear line. The failure shear can be idealized as an absolute magnitude, encompassing both the positive and negative values.

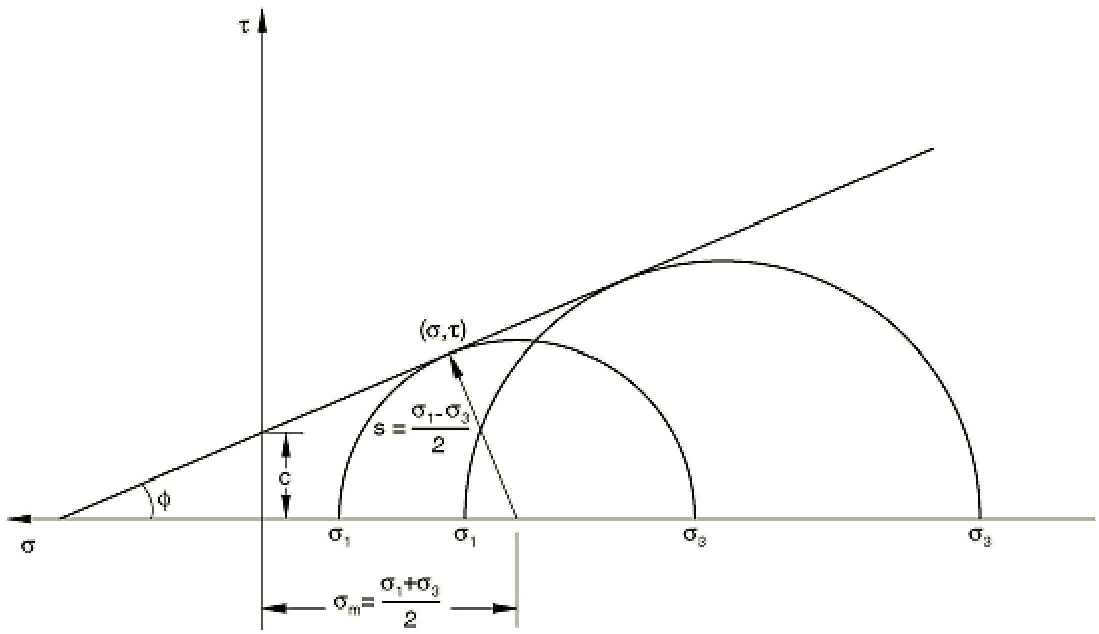

Figure 3-13: Mohr circle - soil model (Dassault Systemes, 2014)

Mohr-Coulomb shear failure stress criteria is then expressed as (Dassault Systemes, 2014):

$$\tau = c - \sigma \tan\varphi \tag{3-5}$$

$$\tau = \frac{\sigma_1 - \sigma_3}{2}\cos\varphi \tag{3-6}$$

$$\sigma = \frac{\sigma_1 + \sigma_3}{2} + \frac{\sigma_1 - \sigma_3}{2}\sin\varphi \tag{3-7}$$

where τ is the critical shear stress, in MPa; σ is the applied stress, in MPa; σ_i is the normal principal stress, in MPa; φ is the interior friction angle, in degrees; and c is the cohesive strength, in MPa. The slope of the failure line is the material internal friction angle, while the y-intercept is the cohesive strength. It can be seen that as the mean stress, σ_m, increases, so does the failure shear stress. This model was used in combination with the linear elastic material model, defining

Young's Modulus and Poisson ratio. It is noted that the Mohr-Coulomb model has limitations and can be replaced with a modified Mohr-Coulomb model to account for changes in friction and dilation angles with high plastic strains. However, the peak force imparted to the pipe can be matched using the fundamental Mohr-Coulomb model (Roy et al., 2016). Since only the stress state of the pipe itself was of interest, the standard Mohr-Coulomb model was deemed adequate.

The idealized two-dimensional Mohr-Coulomb failure envelope shown above can be further expanded into three dimensions. In three-dimensional space, the failure surface takes the shape of a cone with a hexagonal cross-section, as shown in Figure 3-14 (Kelly, 2015).

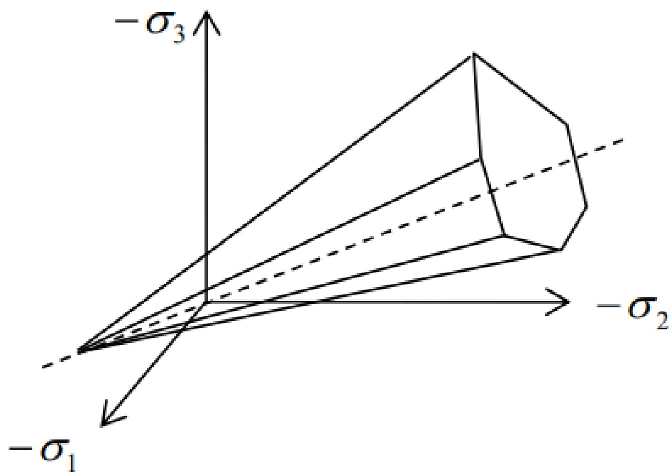

Figure 3-14: Mohr-Coulomb failure surface in three-dimensional space (Kelly, 2015)

The shear stress failure points are defined as:

$$\left\{ \begin{array}{l} \pm\dfrac{\sigma_1 - \sigma_3}{2} = \dfrac{\sigma_1 + \sigma_2}{2}\sin\varphi + c\cdot\cos\varphi \\ \pm\dfrac{\sigma_2 - \sigma_3}{2} = \dfrac{\sigma_2 + \sigma_3}{2}\sin\varphi + c\cdot\cos\varphi \\ \pm\dfrac{\sigma_3 - \sigma_1}{2} = \dfrac{\sigma_3 + \sigma_1}{2}\sin\varphi + c\cdot\cos\varphi \end{array} \right\} \tag{3-8}$$

Defining a unit normal vector, $\boldsymbol{n}$, as the sum of the orthogonal basis vectors of the principal stress planes, $n_i\boldsymbol{e}_i$, the above equations can be simplified and written in the same form as Equation (3-6):

$$\mathbf{n} = n_1\mathbf{e_1} + n_2\mathbf{e_2} + n_3\mathbf{e_3} \tag{3-9}$$

$$\sigma = n_1^2\sigma_1 + n_2^2\sigma_2 + n_3^2\sigma_3 \tag{3-10}$$

$$\tau = \sqrt{n_1^2n_2^2(\sigma_1 - \sigma_2)^2 + n_2^2n_3^2(\sigma_2 - \sigma_3)^2 + n_3^2n_1^2(\sigma_3 - \sigma_1)^2} \tag{3-11}$$

The soil parameters used to define the Mohr-Coulomb model were obtained from the soil report provided by Enbridge Pipelines Inc. regarding typical soil conditions experienced on the proposed L3R pipeline routing (BGC Engineering Inc., 2017). The report provided recommended soil spring constants to be used for pipeline analysis. However, the current structural models developed in ABAQUS did not utilize discretized spring supports or spring constants for the soil material. The report did provide some specific soil parameters which were used in the material model, but many parameters were not provided. Thus, extrapolation beyond the report was required.

Two primary soil types were specified in the report: soft clay and till/silty sand/silt/sand. It was assumed that the most critical soil influencing the pipe response was soft clay as it had a lower effective stiffness and friction angle. The lower stiffness resulted in the pipe section having a higher relative stiffness. Due to soil arching effects, a higher relative stiffness led to the pipeline attracting a higher percentage of the surface load, increasing the resulting stresses. Therefore, a homogenous soft clay soil block was used for the analyses. Parameters not specified within the report and shown in Table 3-2 were based on: Design of Steel Structures: Appendix C – Properties of Soils and the thesis Finite Element Analysis of a Buried Pipeline, 2010 (Subramanian, 2010) (Lee, 2010):

Table 3-2: Soil material properties (Lee, 2010) (BGC Engineering Inc., 2017) (Subramanian, 2010).

Parameter	Enbridge Report	Appendix C	FEA of a Buried Pipeline	Values Used in Analysis
Mass Density; γ [kg/m^3]	18	17.5	17-20	18
Young's Modulus; E' [MPa]	-	5-50	19-48	25
Poisson's Ratio; ν	-	0.3	0.25-0.45	0.3
Friction Angle; φ [°]	28	24	20-29	25
Dilation Angle; ψ [°]	-	2	2	2
Cohesion Strength; [kPa]	-	0-200	17-252	100

3.5 Section Geometry

The pipe section geometry was selected based on industry standard pipe schedule tables, as shown Table 3-3. Within the pipeline industry, pipe schedule tables are developed according to ASME/ANSI B36.10/19, with pipe classification based on both pipe diameter and wall thickness (Lawrence Berkley National Laboratory, 2017). Wall thickness can vary significantly depending on the stress requirements; however, standard wall thickness (STD) was used for the baseline analysis.

Table 3-3: Standard pipe schedule (Lawrence Berkley National Laboratory, 2017)

Pipe Size (inches)	Outside Diameter (inches)	Identification			Wall Thickness – t (inches)	Inside Diameter – d (inches)
		Steel		Stainless Steel Schedule No.		
		Iron Pipe Size	Schedule No.			
20	20.00	-	-	5S	0.188	19.624
		-	-	10S	0.218	19.564
		-	10	-	0.250	19.500
		STD	20	-	**0.375**	19.250
		XS	30	-	0.500	19.000
		-	40	-	0.594	18.812
		-	60	-	0.812	18.376
24	24.00	-	-	5S	0.218	23.564
		-	10	10S	0.250	23.500
		STD	20	-	**0.375**	23.250
		XS	-	-	0.500	23.000
		-	30	-	0.562	22.876
		-	40	-	0.688	22.624
		-	60	-	0.969	22.062
30	30.00	-	-	5S	0.250	29.500
		-	10	10S	0.312	29.376
		STD	-	-	**0.375**	29.250
		XS	20	-	0.500	29.000
		-	30	-	0.625	28.750
34	34.00	-	10	-	0.344	33.312
		STD	-	-	**0.375**	33.250
		XS	20	-	0.500	33.000
		-	30	-	0.625	32.750
		-	40	-	0.688	32.624

Based on the standard schedule, the pipe wall thickness was selected as 3/8”, or 9.525 mm, for all pipe diameters used in the baseline analysis. As previously stated, four pipe diameters were analyzed: 34”, 28”, 24”, and 20” or 836.6 mm, 711.2 mm, 609.6 mm, and 508 mm, respectively. It is noted that since the wall thickness remained the same for all diameters, the diameter-to-thickness ratios of the pipes were reduced as the pipe diameter was reduced, resulting in an increased local stiffness of the pipe section. For the diameter-to-thickness ratios to remain unchanged, non-standard wall thicknesses would be required, which was not practical. Therefore, when analyzing the effects of pipe diameter on the resulting stress state and structure behavior, the influence of the increased local wall stiffness must also be considered. This phenomenon is explained more thoroughly in Chapter 4.

3.6 Soil-Pipe Interaction

The stress state of a pipeline when subjected to surface live load is highly dependent on the applicable load path. The load path from the surface load to the pipe section is dependent on a variety of variables including, but not limited to: soil-pipe relative stiffness ratio, load offset location, burial depth, and soil-pipe interaction properties. A significant factor among these is the soil-pipe interaction properties. It is typical for the pipe section to be much stiffer than the surrounding soil. As such, as the bond between the pipe and soil increases, the pipe will attract more load as compared to the soil through a process known as soil arching. Soil arching describes the scenario were a soil mass becomes unstable due to translation or yield and transfers stress to an adjacent rigid body (Terzaghi, 1943). In a soil block, this rigid body may be adjacent stable soil or an adjacent rigid pipeline. This phenomenon has been further shown using two extremes: soil with a buried pipe present versus soil with an open hole and no pipe present (Kabir, 2006). As summarized in the literature review, it was shown that with the pipe present, the adjacent soil stresses were lower than that compared to when no pipe was present. This indicated that the pipe section attracted the surface loading and the surrounding soil experienced lower stresses. Therefore, soil-pipe interaction must be accounted for in the analysis.

The simplified approach for soil-pipe interaction would be to assume perfect bond between the pipe section and surrounding soil. However, this simplification is not realistic as thermal expansion and contraction, pipeline corrosion, soil shrinkage, and formation of drainage channels would surely reduce the bond between the soil and pipeline. As time wears on and the decommissioned pipeline further corrodes, the less valid the assumption of a perfect bond becomes. It is therefore more realistic to employ a frictional slippage model between the pipe surface and surrounding soil. This contact definition allows for finite soil slippage should the frictional resistance be overcome. This slippage acts to transfer additional load to the rigid pipe section, as well as impart an additional circumferential hoop stress on the surface of the section.

Frictional soil-structure interaction was modelled in ABAQUS using a surface-to-surface contact formulation and employing the penalty enforcement method. Penalty enforcement is a method which allows for a variety of contact slip formations including friction, shear stress, and elastic slip (Dassault Systemes, 2014). For the purposes of this analysis, slip was defined using a specified coefficient of static friction. Static friction was defined using the classical Coulomb friction model, where slip resistance is based on the critical shear stress. Critical shear stress, τ_{crit}, is related to the contact pressure, p, with the coefficient of static friction, μ:

$$\tau_{crit} = \mu p \tag{3-12}$$

The coefficient of friction between the clay soil and pipeline steel was calculated using the ASCE ALA Guidelines for Design of Buried Steel Pipe, Section B.1 (American Lifelines Alliance, 2001):

$$\mu = \tan(f\varphi) \tag{3-13}$$

where *f* is a coating dependent factor adjusting the interface friction angle based on the surface condition of the pipe section. For the purposes of this analysis, the pipe coating was assumed to be 'rough steel' (corroded section), resulting in a factor of 0.8. In all cases, this coating resistance factor is less than one, representing less than a perfect bond. As the steel becomes smoother the coating factor decreases, reducing the critical shear stress. It may be intuitive to assume that as the pipeline corrodes, the surface becomes more and more rough, increasing interfacial friction. However, the surface iron oxide scale is weak in shear and will most certainly separate from the pipe surface under any significant shear loading. Therefore only the pitted pipe surface can be considered effective, idealized as a 'rough steel' surface. The coefficient of friction was then calculated as:

$$\mu = \tan(0.8*25°) = 0.36 \tag{3-14}$$

Thus, a coefficient of static friction equal to 0.36 was used for the tangential contact formulation, acting in both the circumferential and longitudinal directions along the pipe surface. The normal contact direction was defined as a "hard" contact. Hard contact definition is an idealized contact formulation, assuming zero penetration, while separation of the two surfaces is still permitted as the system deforms. The contact methodology is shown schematically in Figure 3-15.

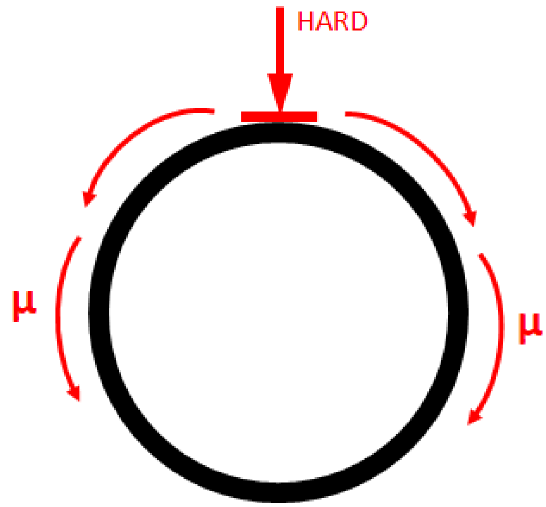

Figure 3-15: Contact between soil and pipe

Surface-to-surface contact was required in this application due to the choice of the solid elements used for the soil block. One drawback of using C3D10 tetrahedral solid elements was when applying uniform pressure to the faces of these elements, the elements produce zero nodal forces at the corner nodes (Optimec, 2014). Therefore, these elements could not be used in node-to-surface contact simulations as the contact force would decrease to zero in such circumstances, permitting penetration of the surfaces. However, the surface-to-surface contact employs the contact algorithm across the entire element surface (as opposed to nodes only) eliminating the possibility of nodal penetration into one surface. C3D10 elements are recommended for use in surface-to-surface contact simulations when used with the penalty enforcement method (Dassault Systemes, 2014).

3.7 Load Definition

Buried pipelines are subjected to two primary basic load cases: gravity loading and surface loading. Gravity loading includes the self-weight of the pipeline and the weight of the overburden soil. Surface loading can include a variety of loading sources including surface dead load, surface live load, snow load, etc. The most common and critical among these is vehicular traffic; particularly large farming equipment and industrial trucks. Therefore, the buried pipelines were analyzed for the combination of gravity loading and surface truck wheel loading. Additional loading may include groundwater (buoyancy), compaction, seismic, soil movement, etc.; however, the effects of these loads were not considered.

3.7.1 Gravity Loading

Gravity loading was applied automatically to the entire model in ABAQUS through the use of the gravity load case. Gravity load was applied based on the density of each material used, specifying the expected gravitation acceleration value. A gravitational acceleration of -9.81m/s^2 in the vertical direction was used for the analyses. The load application dialog is shown in Figure 3-16.

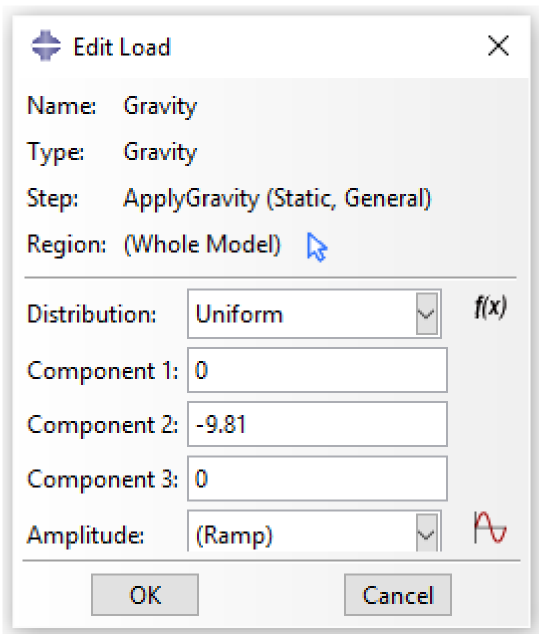

Figure 3-16: Gravity load input

3.7.2 Surface Load Application

The surface live load considered consisted of the weight of vehicular traffic. Depending on the geological location of the buried pipeline, the magnitude of surface live load can vary drastically between pedestrian traffic, large truck traffic, farm equipment, and construction traffic. For the purposes of these analyses, surface live load was assumed to be the maximum axle loads of a CL-800 truck, acting over the wheel contact area. Loading was taken from the Canadian Highway Bridge Design Code S6-14, utilizing the appropriate dynamic load allowance (DLA factor) (Canadian Standards Association, 2014). The Canadian S6-14 code was used as it is applicable for buried arch-type structures, of which a decommissioned pipeline is considered. There is limited guidance offered by the Canadian pipeline codes regarding consideration for surface loading, with no specific method of analysis required (Warman et al., 2006). The CSA Z662-19 Canadian Oil and Gas Pipeline Systems code specifies surface traffic loading as an 'additional load' left to the designer for calculation and inclusion (Canadian Standards Association, 2019). Therefore, the Canadian S6-14 code was adopted for this purpose. For buried arch-type structures, the DLA factor is defined as:

$$DLA = 0.4(1 - 0.5D_E) \tag{3-15}$$

where the DLA is related to the burial depth, D_E, in m. This DLA factor is not considered less than 0.1, corresponding to a burial depth equal to 1.5 m. Therefore, all burial depths 1.5 m and deeper has the same 0.1 DLA factor applied. As the burial depth decreases less than 1.5 m, the DLA increases.

The axle loads of the CL-800 truck travelling perpendicular to the pipe axis were applied in ABAQUS as pressure loads acting over their respective wheel contact areas. The truck was positioned such that the maximum axle load was placed such that the center of the wheel contact area is on the vertical centroidal axis of the pipe cross-section. The axle layout, loading, and wheel contact areas are shown in Figure 3-17 (Canadian Standards Association, 2014).

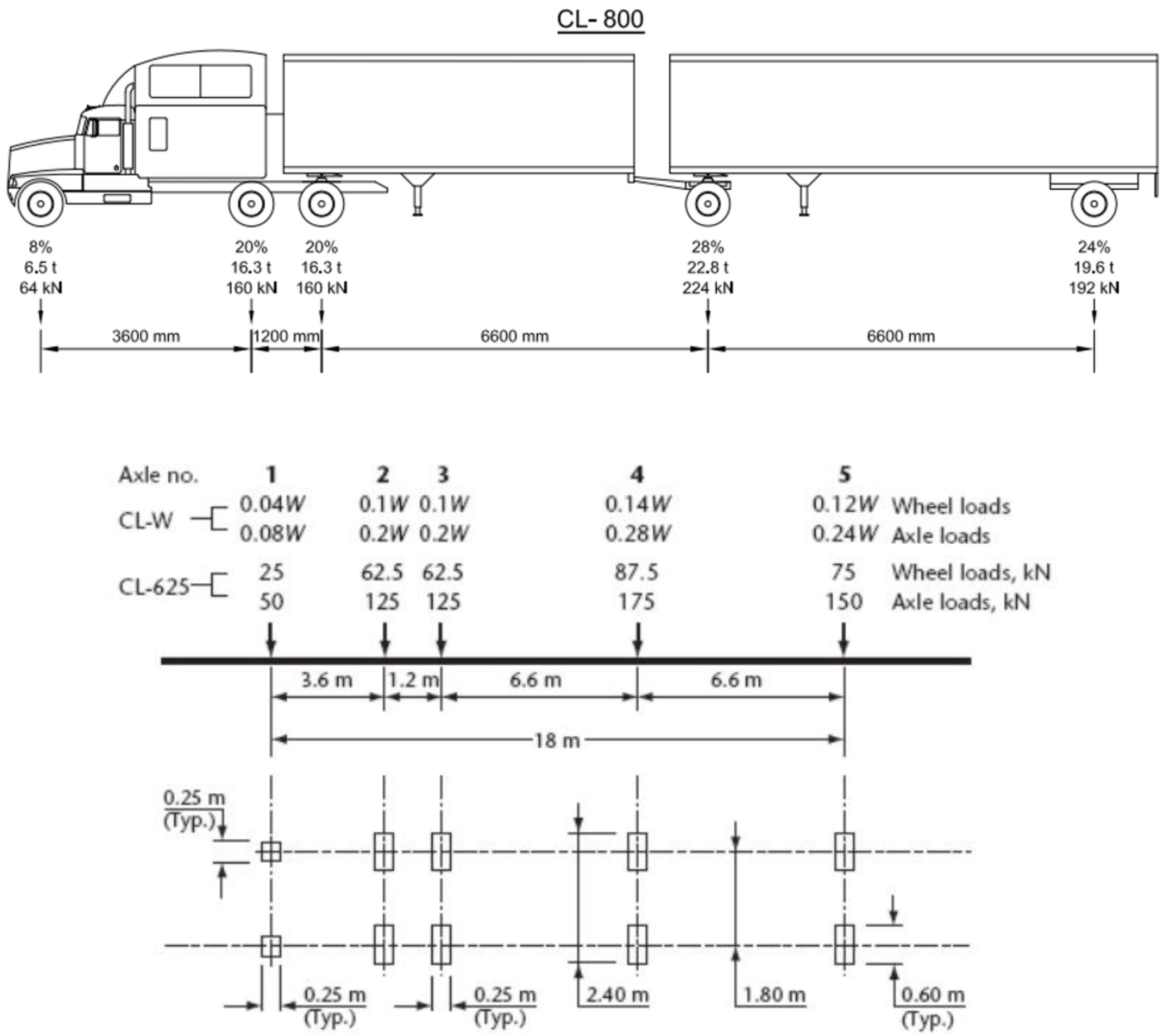

Figure 3-17: CL-800 loading (Canadian Standards Association, 2014)

The loading geometry applied in the models is shown in Figure 3-18. For the cases using heavier farming/construction equipment with varying contact areas, the same load application method applied and will be explained in further detail hereafter.

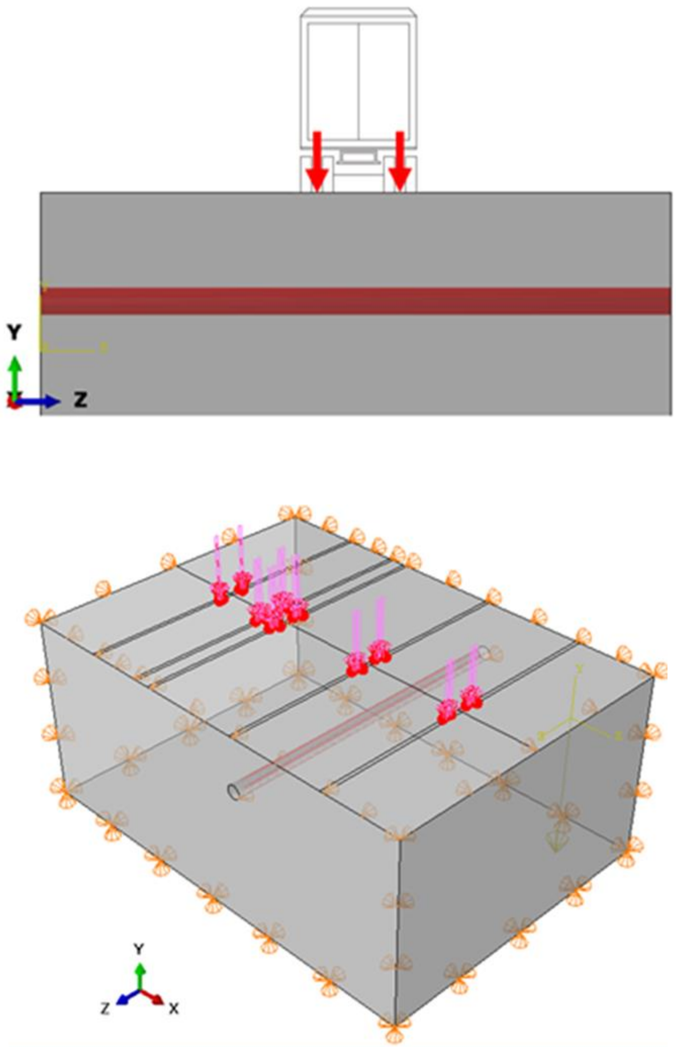

Figure 3-18: Surface live load input

3.7.3 Load Steps

The analysis was divided into three separate loading steps: one initial step and two load application steps. Each load application step (steps 2 and 3) was applied in a minimum of 10 increments. The purpose of applying the load in small increments was to improve the accuracy, reduce the potential for element distortion, and aid in obtaining an equilibrium solution. If the load was applied in too few increments (e.g. all the load at once), the elements may distort and deform excessively and the analysis may not converge, negatively impacting the accuracy of the resulting stresses and strains. The load steps were run using the non-linear geometric solution option, Nlgeom. This option is used to account for geometric non-linearities of the system (Dassault Systemes, 2014). Both the geometry and material properties of the analysis are non-linear in nature and at shallow burial depths, local deformations become significant. Thus, non-linear analysis was justified. When using the non-linear option, the system stiffness matrix is updated after each step, accounting for the deformation effects of the previous step. As a result, more accurate results were obtained. The methodology used in each load step is described below:

i. ***Step 1: Establishment of boundary conditions and contact definition:*** The initial step was used to establish the model boundary conditions and to generate the frictional contact between the pipe and surrounding soil. No load was applied during this step. Defining the boundary conditions and contact prior to the application of the load ensured stability of the model during initial definition. The boundary conditions and contact definition remained unchanged throughout the remaining steps of the analysis.

ii. ***Step 2: Application of gravity load:*** Gravity loading was the first load to be applied to the system. The weight of the pipe and overburden soil is a constant load over the life of the pipeline and applying this load as a separate case allows for a "zero-load" stress state baseline to be obtained prior to application of the surface live load. The independent effects of overburden and surface live load could then be isolated.

Depending on the burial depth, the stresses induced by the overburden were significant and must not be ignored. Due to the non-linear geometric deformations, deformations and stresses due to the overburden influenced the resulting stress state due to the concentrated surface load.

iii. ***Step 3: Application of surface live load:*** The final step involved the application of the surface live load. The primary purpose of the analysis was to obtain the static response of the buried decommissioned pipeline due to the applied surface loading. Through comparing the stress state before and after live load application, the increase in stress and deflections was obtained.

3.8 Limitations

A comprehensive parametric investigation of the static response of decommissioned pipelines subjected to surface live loading was conducted. Although effort was made to develop a thorough and all-inclusive investigation, the following limitations of the presented study apply:

i. The investigation is focused towards downstream, transmission pipelines and therefore is not directly applicable to upstream pipelines;

ii. The models developed do not incorporate pipe section irregularities and imperfection such as surface defects, girth welds, pipe section misalignment, non-circular pipe cross-sections, local corrosion, and post-operation residual stresses and strains;

iii. Although the soil material model developed is sufficiently adequate to achieve an accurate transfer of stresses from the soil surface to the pipe section, the model is simplified and should not be used for definite soil behaviour beyond the overall behaviour presented herein;

3.9 Summary of Parametric Study

A total of six parametric studies were conducted, consisting of over 100 finite elements models developed. The parametric study was conducted as two distinct investigations. The first investigation focused on the effects of load transfer and pipe and soil stiffness. The second investigation focused on the effects of surface load magnitude, geometry, and orientation. The initial models developed studied the effects of burial depth on the resulting static behavior of decommissioned pipelines. From this initial study, a critical burial depth was selected to be used in all subsequent investigations. The general synopsis of each parameter considered is briefly described below. A more detailed description of the parameters and the effect on the static response of decommissioned pipelines is presented in Chapter 4. In all cases, four different large bore pipe diameters were analyzed, allowing the simultaneous analysis of the effect of pipe diameter.

3.9.1 Burial Depth

The initial parameter investigated was the burial depth, also referred to as depth of soil cover. The burial depth was measured from the soil surface to the pipe crown. The burial depth can vary significantly between pipelines due to numerous factors including contents being transported, soil conditions, surface constraints, and depth of frost penetration if applicable. The burial depth affects the resulting confining pressure, soil stiffness, weight of overburden, and more importantly, the load transfer path. As the burial depth decreases, the load path of the surface loading to the pipe section becomes shorter and more direct. Intuitively, shallow burial depths results in greater load attraction, stress magnitude, and stress concentration. Based on the results from the burial depth analysis, a critical burial depth was selected for use in all subsequent investigations.

3.9.2 Pipe Wall Thickness

It is common for pipelines within the petrochemical and fluid transportation industry to use standard wall thicknesses as defined by ASME/ANSI B36.10/19. Standard wall thicknesses are economical as they are commonly stocked by fabricators and thicker walled sections result in greater thermal expansion and stresses. Once decommissioned, pipelines begin to degrade at a higher rate than during operation as the corrosion protection methods are no longer present or maintained. The increase in corrosion acts to reduce the effective wall thickness of the pipe section. Therefore, the effect of wall thickness was analyzed. The full spectrum of wall thickness was addressed, including wall thickness greater than the standard thickness to very thin wall thickness prior to the onset of perforation. Through using different pipe diameters for the same wall thickness, the influence of the local stiffness and diameter-to-thickness ratio of the wall section was also analyzed.

3.9.3 Soil Stiffness

The interaction between buried structures and the surrounding soil matrix significantly influences the structural behavior of the system. The surrounding soil acts as the load transfer continuum while also providing confining pressure acting to resist deformation and stiffen the system. Through incorporating a realistic frictional soil-pipe contact definition, the influence of the surrounding soil on the structural behavior of the decommissioned pipeline was fully realized. The most significant material property affecting the system behavior was the soil stiffness. As the stiffness of the soil decreases, the soil deforms a greater amount and transfer additional load to the stiff pipe section. Soil material type and inherent stiffness are highly variable between two pipe systems and even along a single system. Therefore, examining the effect of soil stiffness on the static behavior of the pipeline was imperative, although the soil was still considered homogenous within a single model.

3.9.4 Surface Loading Magnitude and Geometric Orientation

The second portion of the parametric investigation studying the behavior of decommissioned pipelines subjected to surface live loading focused on the influence of varying the surface load magnitude, location, and orientation.

3.9.4.1 Construction Loading

Depending on the location of the buried pipeline, the surface load magnitude can vary between pedestrian traffic, the CL-800 truck already considered, construction equipment, and large farming equipment. To study the influence of varying the magnitude of the surface live load, a typical construction earth moving truck was considered. Varying the surface vehicle resulted in the simultaneous change in the loading magnitude, wheel location, and effective bearing area. Therefore, the effect of using the construction equipment on the resulting structural behavior was not intuitive.

3.9.4.2 Surface Load Orientation and Multiple Lane Loading

The analyses described above all considered a single surface load travelling perpendicular to the pipe section, with the maximum axle load placed directly above the pipe crown. However, there are numerous other combinations of surface load orientation, location, and number of parallel loads which are practically possible. For the purposes of this parametric investigation, two such additional combinations were considered – a single surface load travelling parallel with the pipe section and multiple surface loads travelling perpendicular to the section. The scenario of a surface load travelling parallel with the pipe section was further divided into the axle load centered over the pipe, with wheel loading on either side of the pipe; and the axle load offset from the pipe, with one wheel line placed directly over the pipe crown. Multiple parallel loads travelling perpendicular to the pipe section was also considered through modelling three parallel CL-800 trucks, spaced at standard highway lane spacing.

3.9.5 Ultimate Limit States Loading

The final scenario analyzed considered the effects of using Ultimate Limit State (ULS) load and material factors for analysis. The investigations described above all consider actual loading and resulting working stress. However, the Canadian design codes typically call for design to be conducted using ULS analysis and associated partial factors. The partial factors act to increase the magnitude of the imposed load and decrease the material resistance. Therefore, although the working stresses remained within the usable range (i.e. below yield stresses), the application of the load factors posed the possibility to result in critical cases that exceed the material strength.

Chapter 4

Parametric Investigation Results and Discussion

In order to develop a comprehensive understanding of the structural response and behaviour of buried decommissioned and abandoned pipelines, a parametric study was conducted to investigate the effects of various parameters including burial depth, pipe wall thickness, pipe diameter, diameter-to-thickness ratio, soil stiffness, surface load magnitude, surface load orientation, multiple surface loads, and ultimate limit state analysis.

4.1 Key Results of Interest

For each of the parametric analyses conducted and described below, the primary results of interest included the pipe section ovalization and resulting normal stresses: longitudinal stresses along the pipe axis arising from longitudinal bending and circumferential hoop stresses arising from the external pressure differential and transverse soil friction. The pipe section ovalization was defined using the Modified Iowa Equation as the vertical change in pipe diameter divided by the pipe external diameter (American Lifelines Alliance, 2001). The key stresses of interest were the normal stresses as opposed to the typical von Mises stress used in steel design. Similar to the research reviewed in the literature, pipeline stresses are commonly divided into the normal stresses along the length of the pipe in the longitudinal direction and circumferentially around the pipe section. The von Mises stress criteria is defined as:

$$\sigma_{VM}=\sqrt{\frac{(\sigma_{11}-\sigma_{22})^2+(\sigma_{22}-\sigma_{33})^2+(\sigma_{33}-\sigma_{11})^2+6\left(\sigma_{12}^2+\sigma_{23}^2+\sigma_{31}^2\right)}{2}} \tag{4-1}$$

where σ_{VM} is the von Mises stress; in MPa, σ_{ii} is the normal stress in direction i, in MPa; and σ_{ij} is the shear stress in direction ij, in MPa. As can be seen, the von Mises stress is merely a combination of the normal and shear stresses in all orthogonal directions. As a result, the underlying behaviour of the pipe section is lost when looking solely at the von Mises stress. In order to gain a fundamental understanding of the static behaviour of the decommissioned pipelines, it was far more advantageous to look specifically at the two primary normal stresses. Analyzing the normal stresses provided a clear insight into the longitudinal bending behaviour, circumferential deformation and soil slippage, and local stress concentrations due to the imposed surface live loads. The governing stress can be identified, indicating the potential failure modes, critical loading geometry, and overall static response. Therefore, for the majority of the discussion to follow, only the normal stresses are thoroughly analyzed and discussed. The von Mises stresses are still provided in the data to capture the complete data set and were used for ease of geometric and mesh convergence analysis. The von Mises stress also proved useful for visualization of stress concentration locations. Von Mises stress is typically used as a generally accepted failure envelope when considering yielding of steel. However, the stresses obtained through each analysis were well below the pipe yield stress. As a result, discussion of the von Mises stresses proved to be of little benefit in understanding the static response of the decommissioned pipelines.

The stresses obtained were located directly below the point of load application at the pipe crown, invert, and springline of the cross section (top-most, bottom-most, and mid-height, respectively). For the majority of the analyses, the maximum stresses occurred at the pipe crown. This is consistent with the conclusions presented in the literature review by numerous investigations conducted by others (Arockiasamy et al., 2006; Kabir, 2006; Noor & Dhar, 2003; Scott, 2015).

Therefore, only stresses found at the pipe crown are presented herein, with stresses from other locations selectively noted as required for further discussion on the structural behaviour.

4.2 Effect of Burial Depth

The initial models explored the effects of burial depth on the static response of a buried decommissioned pipeline subjected to surface live load. In total, 28 separate models were developed based on the modelling methodology and techniques previously described in Chapter 3. For each pipe diameter, seven models were developed with depths of soil cover equal to 3.0 m, 2.5 m, 2.0 m, 1.5 m, 1.0 m, 0.5 m, 0.25 m, as show in Figure 4-1. The depth of soil cover was measured from the soil surface to the pipe crown. The pipe sections considered had standard wall thickness equal to 9.5 mm and the soil was considered as soft clay with a homogenous elastic modulus equal to 25 MPa. The purpose of this investigation was to establish the baseline models from which all subsequent models would be compared.

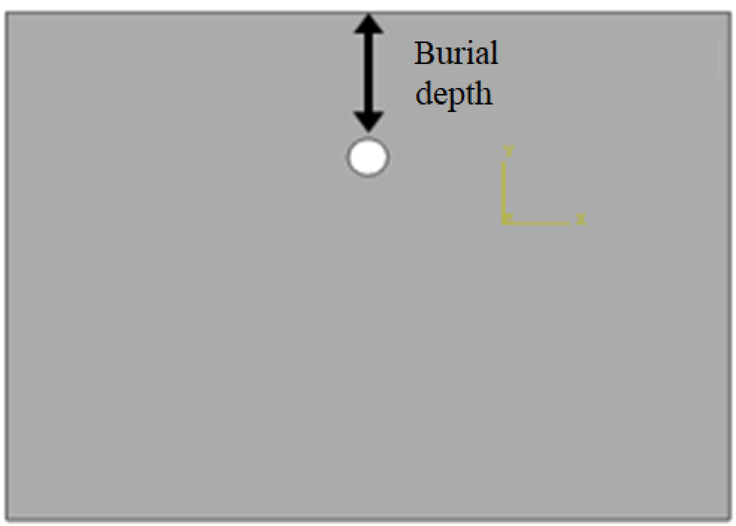

Figure 4-1: Burial depth schematic

In general, the buried pipe section deformed as expected for a hollow structural beam with a uniformly distributed support. Under the action of overburden only, the pipe underwent uniform vertical deflection while remaining straight. The pipe section ovalized symmetrically and stress concentrations were present at the extremities of the ovalized section. Under the effects of surface live load, the pipe deformed similar to a beam subjected to a concentrated load. The largest localized deflection was realized directly below the point of load application. As the burial depth was decreased, the resulting stresses and deformations increased. The ovalized cross section of the standard 34” pipe at a burial depth equal to 1.0 m is shown in Figure 4-2 and Figure 4-3 as reference. The deformed shape under the combination of soil overburden and surface live loading was not uniform and the maximum lateral deformation was skewed towards the top half of the section. The bottom of the section remained oval, supported by the surrounding soil. The top of the pipe section deformed into a flattened shape, with minimum curvature observed at the pipe crown. The increased deformation of the pipe crown was due to the combination of a localized wheel load and the bending moment. The induced positive bending moment acted to flatten the pipe crown and invert, while widening the springline of the section. The additional concentrated surface loading further enhanced the flattening of the pipe crown while having minimal influence on the pipe invert, shifting the ovalized springline up along the cross-section.

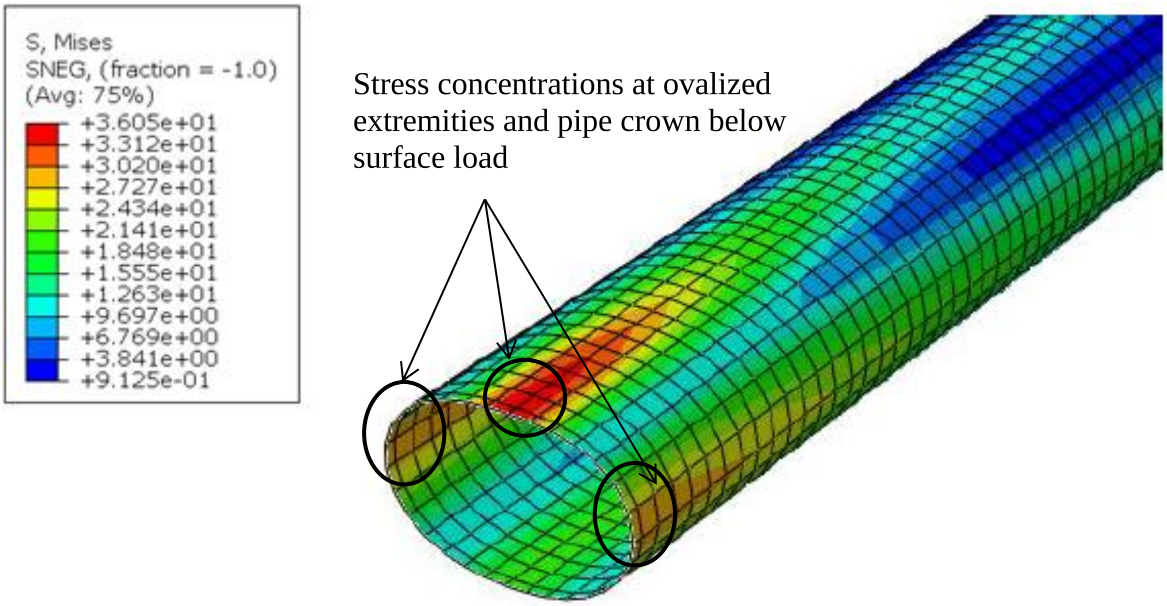

Figure 4-2: Typical stress concentration and ovalization of buried pipe - 34" pipe von Mises stress shown for reference

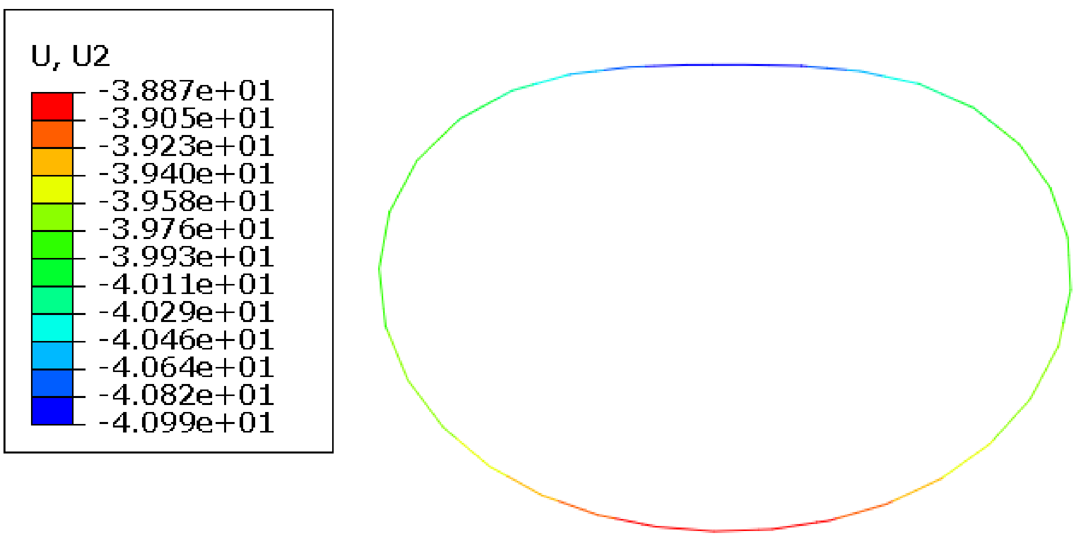

Figure 4-3: Typical deformed shape of ovalized pipe cross section - 34" pipe vertical displacement (U2) shown as reference

As the burial depth decreased, the live load path from the soil surface to the pipe section became shorter and more direct. The pipe section has a much higher relative stiffness compared with the surrounding soil matrix. Therefore, as the burial depth decreased, the soil deformed a greater amount and the pipe section attracted more load, resulting in a significant stress increase. The maximum stresses were located at the pipe crown in all cases and were compressive stresses. The compressive stresses were a result of both the global and local bending of the section. The top crown surface of the pipe section is considered to be the extreme compressive fiber in both the global and local bending cases. Therefore, the stresses resulting from these two cases were additive. It can be seen in Table 4-1 and Figure 4-4 that both the longitudinal and hoop stresses increased in magnitude with decreasing burial depth. This increase is non-linear, representative of a natural logarithmic curve, indicating that the burial depth is a significant factor affecting the resulting stress state.

Table 4-1: Effects of burial depth on maximum normal stresses at the pipe crown due to soil overburden and surface live load

			Maximum Stresses at Pipe Crown [MPa]		
Model ID	Pipe Diameter [inch]	Depth of Soil Cover [m]	Hoop S11	Longitudinal S22	Von Mises VM
1	34	3.00	-21.94	-11.02	19.81
2	34	2.50	-20.91	-12.31	17.87
3	34	2.00	-20.83	-14.47	18.29
4	34	1.50	-22.84	-18.42	20.95
5	34	1.00	-32.95	-28.63	30.96
6	34	0.50	-69.18	-55.56	64.23
7	34	0.25	-176.76	-116.97	156.52
8	28	3.00	-23.80	-11.37	20.58
9	28	2.50	-22.62	-12.60	19.64
10	28	2.00	-22.46	-14.74	19.78
11	28	1.50	-24.39	-18.63	22.09
12	28	1.00	-34.33	-28.94	31.93
13	28	0.50	-69.46	-55.89	63.37
14	28	0.25	-161.39	-109.69	141.89
15	24	3.00	-24.76	-11.38	21.46
16	24	2.50	-23.52	-12.55	20.38
17	24	2.00	-23.30	-14.67	20.36
18	24	1.50	-25.18	-18.57	22.63
19	24	1.00	-34.99	-28.94	34.21
20	24	0.50	-68.51	-55.62	63.73
21	24	0.25	-152.44	-106.76	136.38
22	20	3.00	-24.89	-11.04	21.59
23	20	2.50	-23.64	-12.17	20.47
24	20	2.00	-23.37	-14.25	20.37
25	20	1.50	-25.21	-18.15	22.55
26	20	1.00	-34.85	-28.56	32.16
27	20	0.50	-66.41	-54.88	61.28
28	20	0.25	-142.63	-102.68	126.86

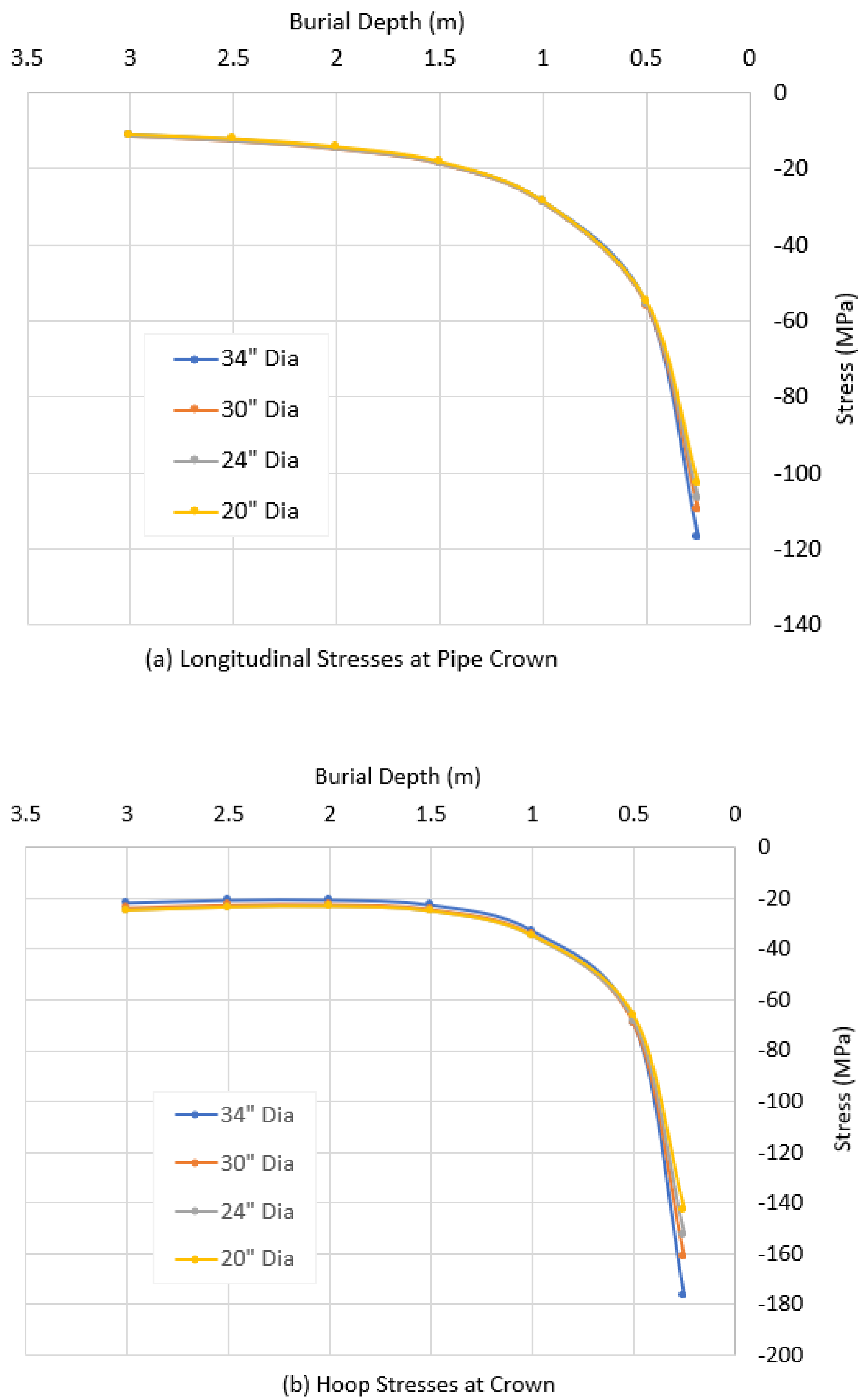

Figure 4-4: Effect of burial depth on principal normal stresses at pipe crown due to soil overburden and surface live load

At deep burial depths, there was minimal increase in stresses and the graphs plateau until the burial depth reaches approximately 1.5 m. At burial depths equal to or shallower than 1.0 m, the resulting stresses began to increase rapidly with a significant change in the slope of the curve at this point. Further, the stress concentrations became more localized at the crown of the pipe section, indicating that the surface load began to act more similarly to a point load compared to a uniform load as would be prescribed by the Boussinesq's theory. Figure 4-5 compares the longitudinal stresses of the 34" pipe section at 3.0 m and at 0.25 m. The stress concentrating effect is clearly shown, which confirms that at shallow burial depths the entire three-dimensional stress state must be considered. The circumferential hoop stresses and other pipe diameters followed the same visual representation. The 1.0 m threshold was interpreted visually from the graphs shown above. At burial depths less than 1.5 m, the DLA factor increases with decreasing the depth of soil cover, further amplifying the resulting stresses and strains. Therefore, the step change in the stress behavior around the 1.0 m depth of soil cover interval was a combination of the increased dynamic loading factors, the concentration of the surface applied loading, and fundamental soil arching effects. Based on this observation, all subsequent analyses were conducted assuming a depth of soil cover equal to 1.0 m. This depth was considered both practical in terms of typical pipeline installation and critical in terms of the resulting three-dimensional stress state.

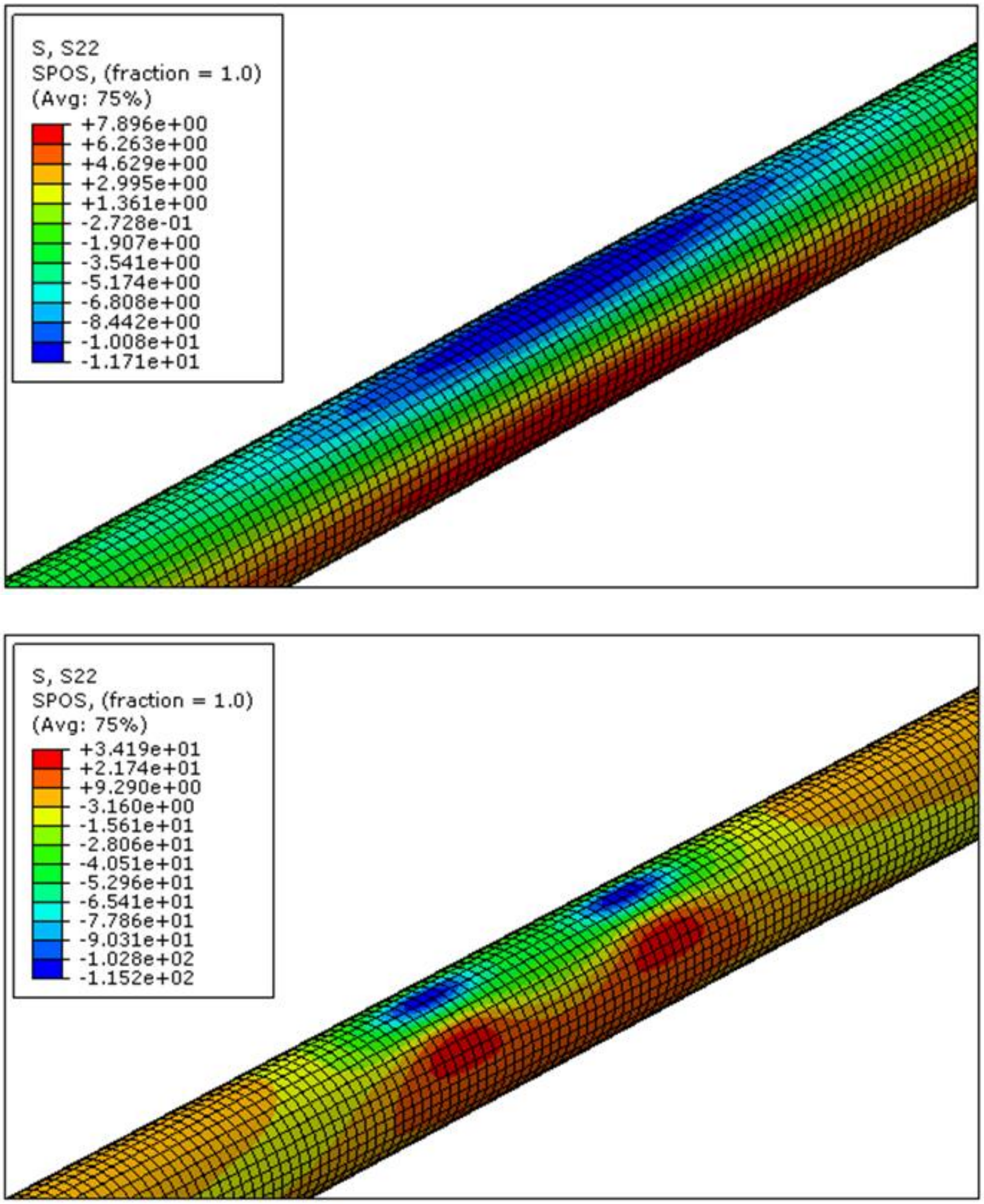

Figure 4-5: Burial depth - 34" dia. pipe: Longitudinal stresses for 3.0 m (top) and 0.25 m (bot)

Further, it was observed that at deeper burial depths, the smaller diameter pipes experienced larger stresses compared with the larger diameter pipes. As the diameter decreases, the pipe section's moment of inertia and resulting stiffness decrease accordingly. Therefore, under the same applied surface loading, the pipe stresses due to global bending of the section increase. At deep burial depths, the surface applied load acted similar to a uniformly distributed load on the pipe surface. However, as the burial depth continued to decrease, there existed a shift and the smaller diameter pipes began to experience lower stresses compared to the larger diameter pipes. This transition from smaller to larger diameter pipes governing the stress state occurred at an approximate depth of 0.5 m soil cover. At these shallow burial depths, the surface load acted similar to a concentrated force, as described above. As a result, the local bending stresses of the pipe surface began to govern the stress state. By maintaining a constant wall thickness between diameters, the smaller pipe diameters possess larger local wall stiffness due to the increased local curvature of the surface. For the smaller diameter pipes, the increase in stresses due to the reduction in global moment of inertia was more than offset by the simultaneous reduction in diameter-to-thickness ratio and subsequent decrease in local bending stresses due to the higher local stiffness of the section. This observation regarding diameter-to-thickness ratio and local stiffness of the section was further confirmed in the wall thickness study presented below in Section 4.3.

The resulting pipeline stresses were a combination of the effects from the soil overburden and the surface applied live load. If the previously plotted stresses are separated into stresses caused by live load and soil overburden, the influence of the two loadings is clearly shown. The resulting von Mises stress (combination of both principal stresses) acting on the 34” pipe section is shown in Figure 4-6 as the representative influence of the two loading cases. At shallow burial depths, the primary stress acting on the pipe section was due to the surface live load. However, at deeper burial depths, the stresses resulting from soil overburden cannot be ignored and eventually became the governing load case.

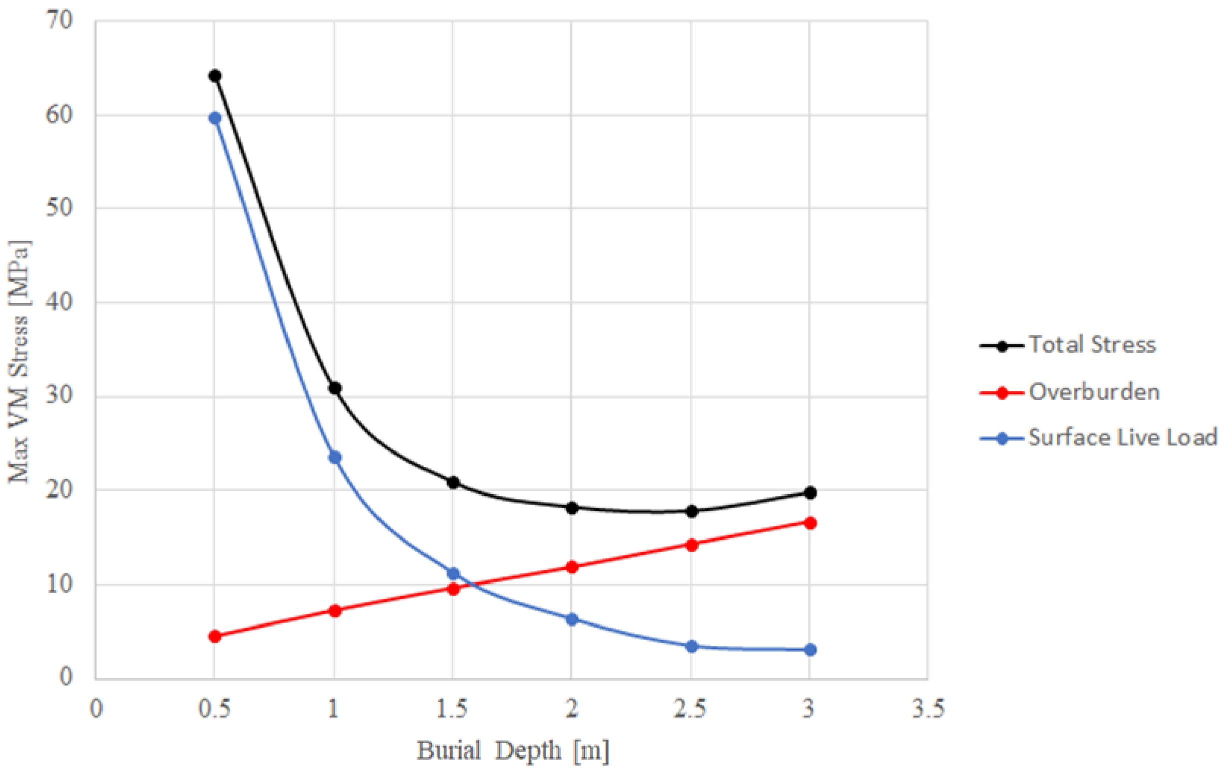

Figure 4-6: Maximum von Mises stress at pipe crown due to separate load effects - 34" pipe section

As can be seen, at deep burial depths, the stresses due to overburden exceeded the stresses due to the surface live load. There existed a transition depth in which the stress caused by the soil overburden was equal to the stress caused by the surface live load. When located below this transition depth, the stress due to overburden became the critical stress. When located above this transition depth, the stress due to the surface live load became the critical stress. In this analysis, this transition depth was located in the vicinity of 1.5 m. This transition depth correlated well with the previously determined critical depth of 1.0 m and the corresponding step change in the slope of the curves resulting from local bending and an increased dynamic loading factor.

In addition to the maximum stresses, the pipe ovalization also increased as the burial depth decreased, as shown in Figure 4-7. Similar to the stresses described above, as the burial depth decreased the pipe section attracted a larger portion of the load, thus, increasing ovalization of the section. As the pipe diameter decreased, smaller pipe sections experienced smaller ovalization while the increasing trends shown in the graphs were nearly identical. Smaller pipe sections have inherently smaller absolute dimensions and increased local wall stiffness. These two effects contributed to the smaller magnitude in ovalization as described by the Modified Iowa Equation.

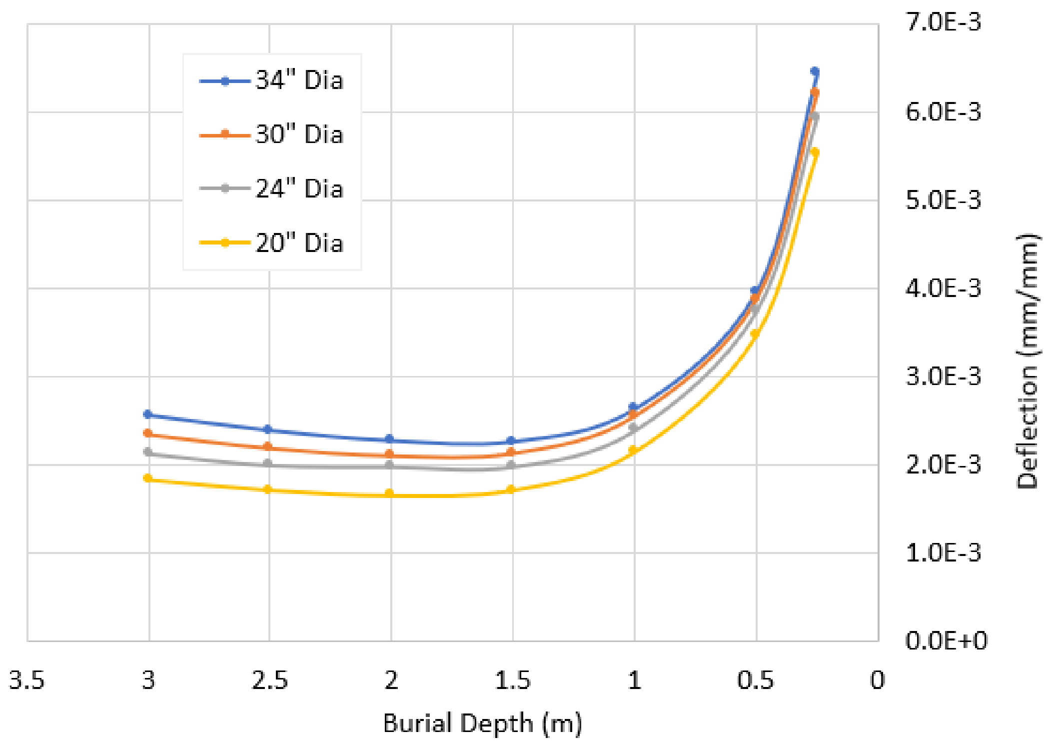

Figure 4-7: Effect of burial depth on vertical ovalization

At shallow burial depths, the load began to act similar to a concentrated load and local deformations began to govern. This resulted in the aforementioned flattening of the pipe crown and increase in the height of the maximum horizontal bulge location. However, the Modified Iowa Equation does not differentiate between local deformations, only the relative difference between the pipe crown and the invert. Therefore, the steep slope shown at shallow burial depths also includes local deformation of the pipe crown, not typically noted when describing pipe ovalization. Further, it was observed that at burial depths deeper than approximately 1.5 m, the degree of ovalization began to increase relative to the valley experienced at 1.5 m. This increase was a direct result of the phenomena described above, where the stress state due to soil overburden became critical compared with the surface live load and continued to increase with depth. This observation further validated the transition point noted at approximately 1.5 m.

Finally, it was observed that at the 0.25 m minimum depth considered, the maximum normal stress experienced by the 34” pipe section was 178 MPa. This stress value is still well below the pipe steel yield stress of 415 MPa. Although still below the yield stress, these stresses are considered significant and will further increase as the pipe wall thins over time due to global corrosion. In addition, this stress begins to approach 50% of the tensile strength of the material. It is within this range that fatigue loading of the pipe section becomes detrimental. It is to be noted that fatigue loading was not considered in this analysis.

4.3 Effect of Wall Thickness

As described above, through the burial depth analysis, a depth of soil cover equal to 1.0 m was determined as a realistic critical value for the pipeline stress state. Therefore, the effect of wall thickness on the resulting behavior of buried decommissioned pipelines subjected to surface live load was analyzed using the critical 1.0 m burial depth. The baseline wall thickness assumed for all pipeline analyses was the standard pipe wall thickness of 3/8” (9.5 mm). To understand the influence of the pipe section wall thickness on the resulting stress state, the wall thickness was varied between a maximum thickness of 5/8” (15.875 mm, equivalent to a 34” schedule 30 section) and a minimum thickness of 1/16” (1.5875 mm) at the extreme end of the study, as shown in Figure 4-8. Typical pipe section fabrication tables for the diameters considered have a common minimum wall thickness of 1/4" or 6.35 mm. Therefore, a wall thickness less than 1/4" can be considered a direct result of uniform global corrosion around the pipe section. For each pipe diameter, six wall thicknesses were considered between the two extremes in 1/8" increments, totaling 24 finite element models. The wall thickness was reduced from the outside of the section, representative of external global corrosion. Therefore, within each model, the actual diameter of the pipe section was slightly modified, although the nominal diameter is listed for all models in the data presented below.

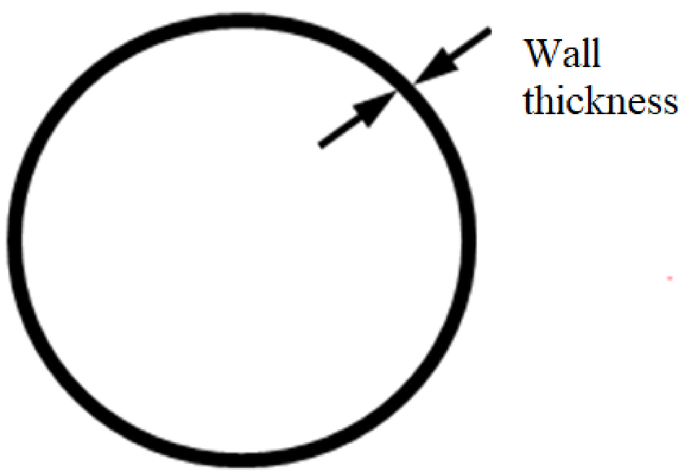

Figure 4-8: Pipe section variable wall thickness

As the wall thickness was reduced, both the longitudinal and hoop stresses at the pipe crown increased as shown in Table 4-2 and Figure 4-9. However, the hoop stresses increased to a maximum value and then began to decrease while the longitudinal stresses continued to increase in magnitude. The increase in longitudinal stresses was again due to the reduction in the section's global and local moment of inertia, increasing both the global and local bending stresses. The moment of inertia of the pipe section is proportional to the wall thickness squared. Therefore, as the wall thickness was reduced, the moment of inertia was also significantly reduced.

Table 4-2: Effect of wall thickness on the maximum normal stresses at the pipe crown due to soil overburden and surface live load

			Maximum Stress at Pipe Crown [MPa]		
ID	Pipe Diameter [inch]	Wall Thickness [inch]	Hoop S11	Longitudinal S22	Von Mises VM
1	34	5/8	-31.63	-23.46	28.40
2	34	1/2	-33.38	-26.06	30.35
3	34	3/8	-32.95	-28.63	30.96
4	34	1/4	-29.48	-31.29	30.47
5	34	1/8	-23.88	-35.51	31.27
6	34	1/16	-25.07	-40.94	35.61
7	28	5/8	-29.77	-22.81	26.98
8	28	1/2	-33.23	-25.89	30.25
9	28	3/8	-34.33	-28.94	31.93
10	28	1/4	-31.36	-31.76	31.60
11	28	1/8	-24.20	-35.47	31.33
12	28	1/16	-23.04	-39.79	34.62
13	24	5/8	-27.21	-22.01	25.04
14	24	1/2	-32.10	-25.41	29.27
15	24	3/8	-34.99	-28.94	34.21
16	24	1/4	-33.13	-32.07	32.65
17	24	1/8	-25.09	-35.24	31.44
18	24	1/16	-22.09	-38.89	34.09
19	20	5/8	-23.34	-20.91	22.21
20	20	1/2	-29.48	-24.48	27.32
21	20	3/8	-34.85	-28.56	32.16
22	20	1/4	-35.33	-32.26	33.89
23	20	1/8	-26.85	-35.07	31.75
24	20	1/16	-21.63	-37.70	32.78

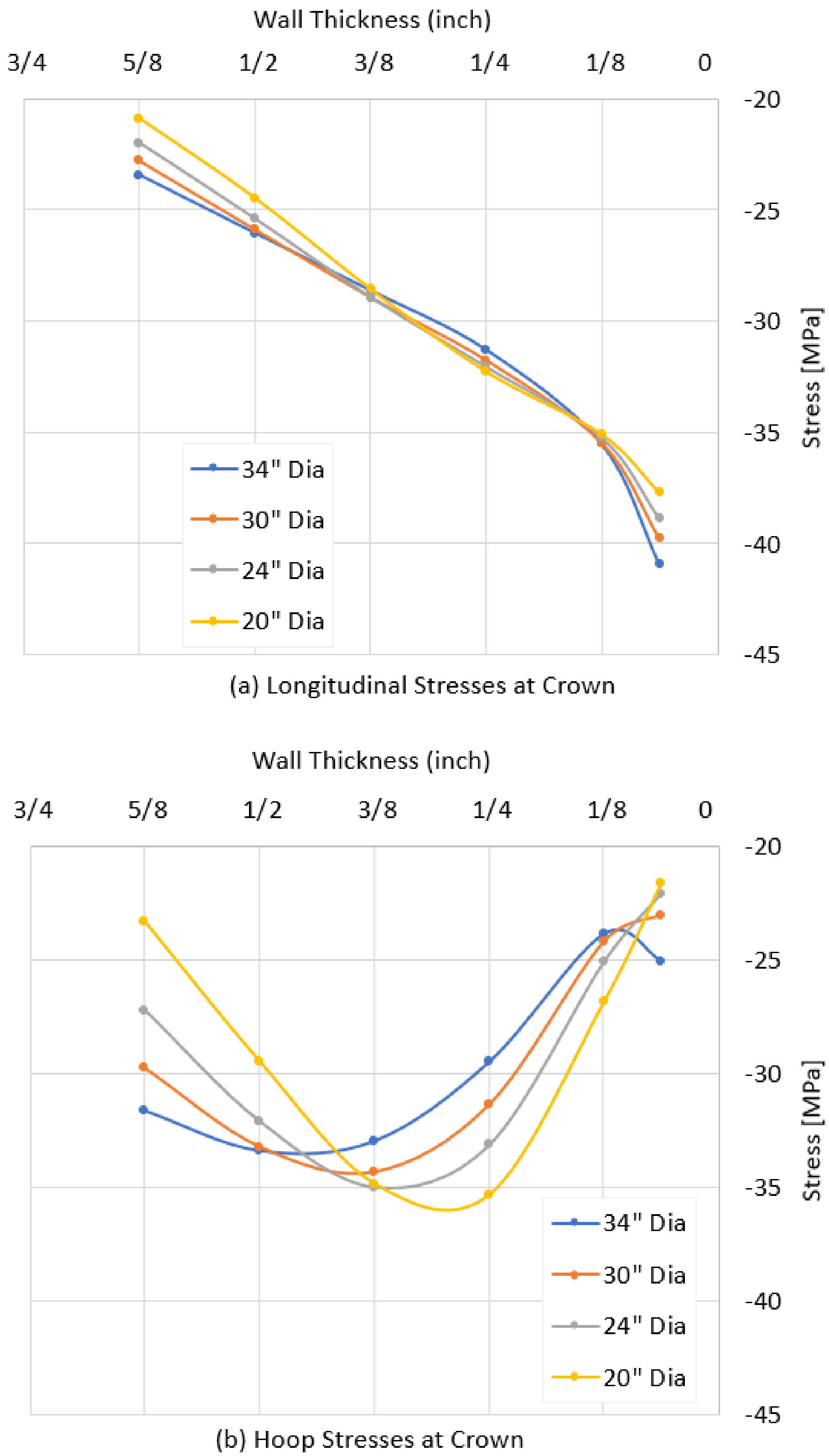

Figure 4-9: Effect of wall thickness on normal stresses at pipe crown due to soil overburden and surface live load

The circumferential hoop stresses also began to initially increase as the local wall thickness of the section was reduced. However, as the wall thickness continued to decrease, the corresponding hoop stresses plateaued and then also began to decrease. This subsequent reduction in the hoop stresses was due to both the localized effects of the load and the reduction in the section's relative stiffness. Firstly, as the wall thickness was reduced, the load effects became more localized at the location directly beneath the wheel loads. With a thick pipe wall, the stiffness of the pipe was large enough that the surface loads tend to interact with each other and produced a more uniform load on the pipe surface. As the stiffness of the pipe was reduced due to the reduction in wall thickness, the local deformations of the section increased and the surface loads began to act independently of one another. This localization of the surface load is shown as stress localizations as seen in Figure 4-10.

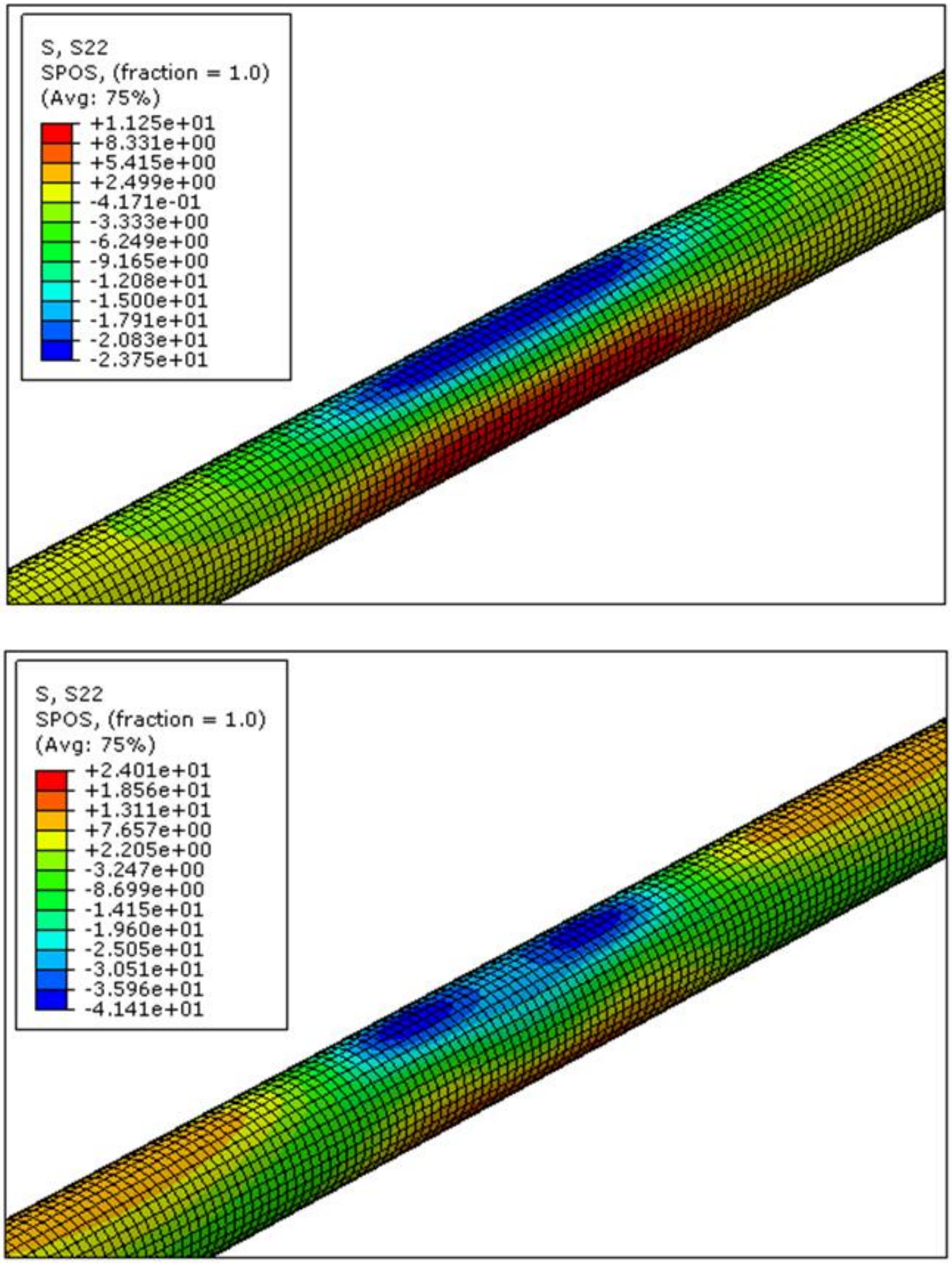

Figure 4-10: Effect of wall thickness - 34" dia. pipe: Longitudinal stresses for 5/8" (top) and 1/16" (bot) wall thickness

Secondly, the stiffness of the pipe section also decreased relative to the surrounding soil as the wall thickness was reduced. Due to soil arching effects, as the relative stiffness of the pipe section decreased, the pipe attracted less load and the soil attracted more load. This phenomenon is clearly shown through plotting the contact pressure for the 34” pipe section. As can be seen in Figure 4-11, the normal contact pressure acting on the pipe crown decreased as the pipe wall thickness was reduced. There existed a 40% reduction in the contact pressure between the 5/8” and 1/16” wall thickness. This relationship is nearly linearly proportional and indicates that the pipe was subjected to less load and the soil resisted a larger portion of the load. As the soil attracted a larger portion of the load, the amount of soil slippage increased, starting from the pipe crown and flowing around the circumference of the section. This increase in frictional forces around the circumference induced a tensile hoop stress at the pipe crown, reducing the compressive stress. It is this reduction in compressive stresses that appears to be a reduction in total stress.

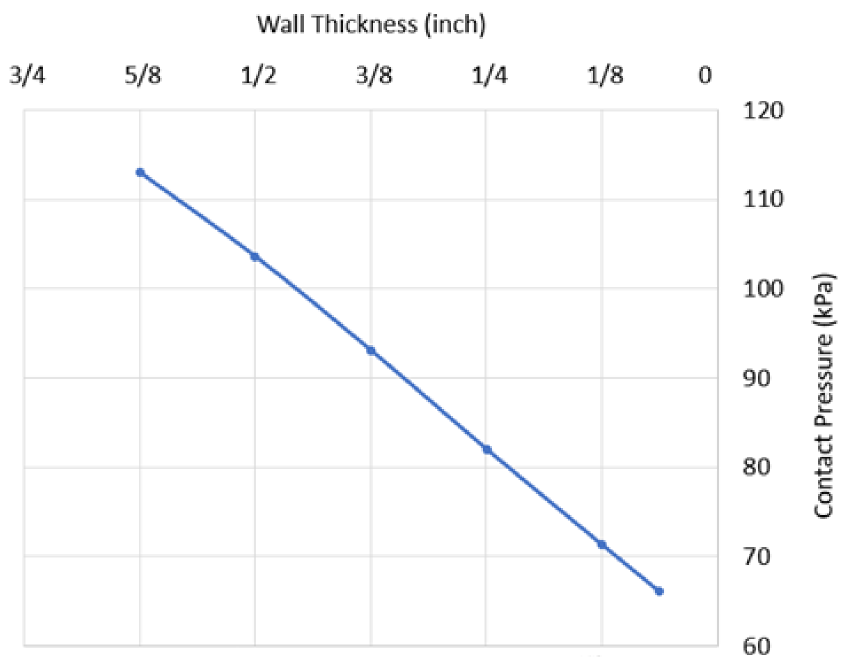

Figure 4-11: Effect of wall thickness on the contact pressure acting on 34" pipe crown

The variation in the resulting normal stresses compared with the diameter-to-thickness, D/t, ratio is shown in Figure 4-12. As can be seen, there exists a rapid change in the longitudinal and hoop stresses with changes in the D/t ratio in the vicinity of 100. As the D/t ratio begins to exceed 100, the slope of the stress increase curve reduces significantly. The D/t ratio was approximately 90 for the standard 34" pipe and 53 for the standard 20" pipe. As a result, the initial conclusions described in the burial depth analysis regarding increased local stiffness offsetting the increase in stresses of smaller diameter pipes are confirmed. A smaller D/t ratio corresponded to a larger local wall stiffness and lower corresponding stresses. Due to the much higher local stiffness of the smaller diameter pipe, as the burial depth decreased and the load became more concentrated, the larger diameter pipes experienced greater local bending stresses.

Finally, the effect of wall thickness on the resulting pipe section ovalization was investigated and is shown in Figure 4-13. It was observed that as the wall thickness was reduced the pipe ovalization increased, as was intuitively expected. The reduction in the section global and local stiffness allowed the cross section to deform more easily under the same applied load. The increase in ovalization was nearly linear up until a very thin wall thickness, at which point the increase began to plateau. This plateau and reduction in slope was again due to increased soil slippage and the reduction in load attracted by the pipe section.

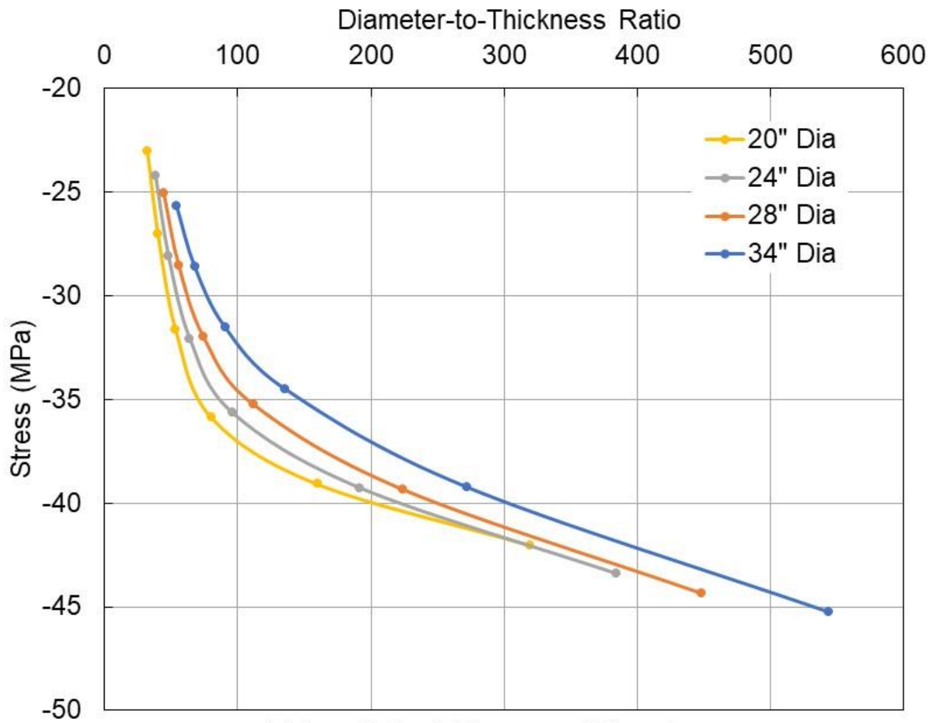

(a) Longitudinal Stresses at Pipe Crown

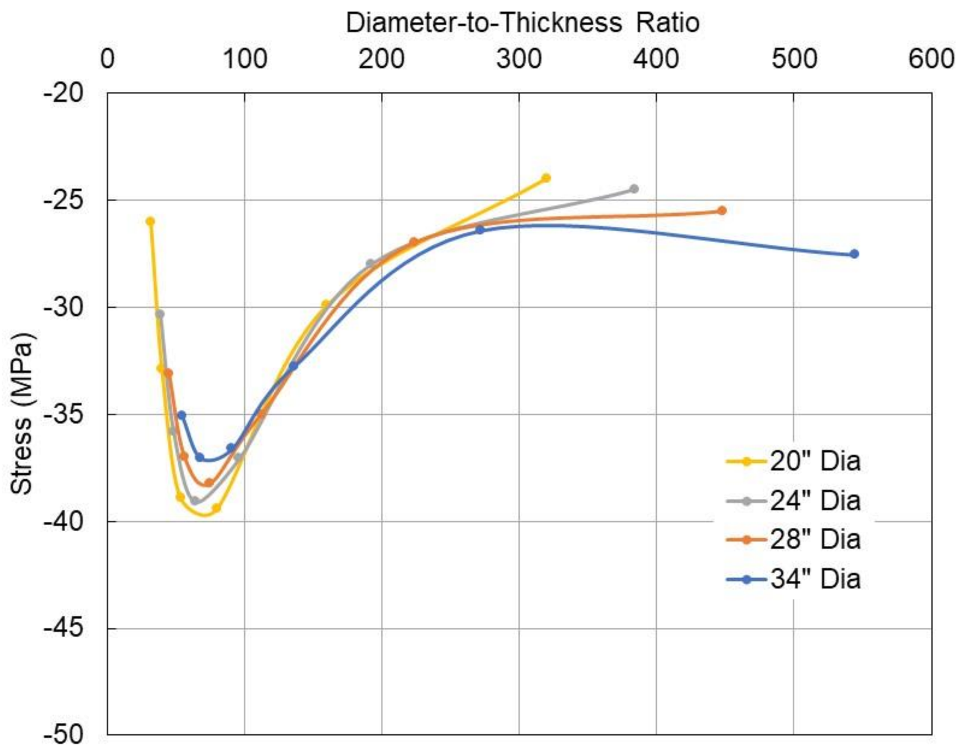

(b) Hoop Stresses at Pipe Crown

Figure 4-12: Effect of diameter-to-thickness ratio on the stresses at the pipe crown subjected to soil overburden and surface live load

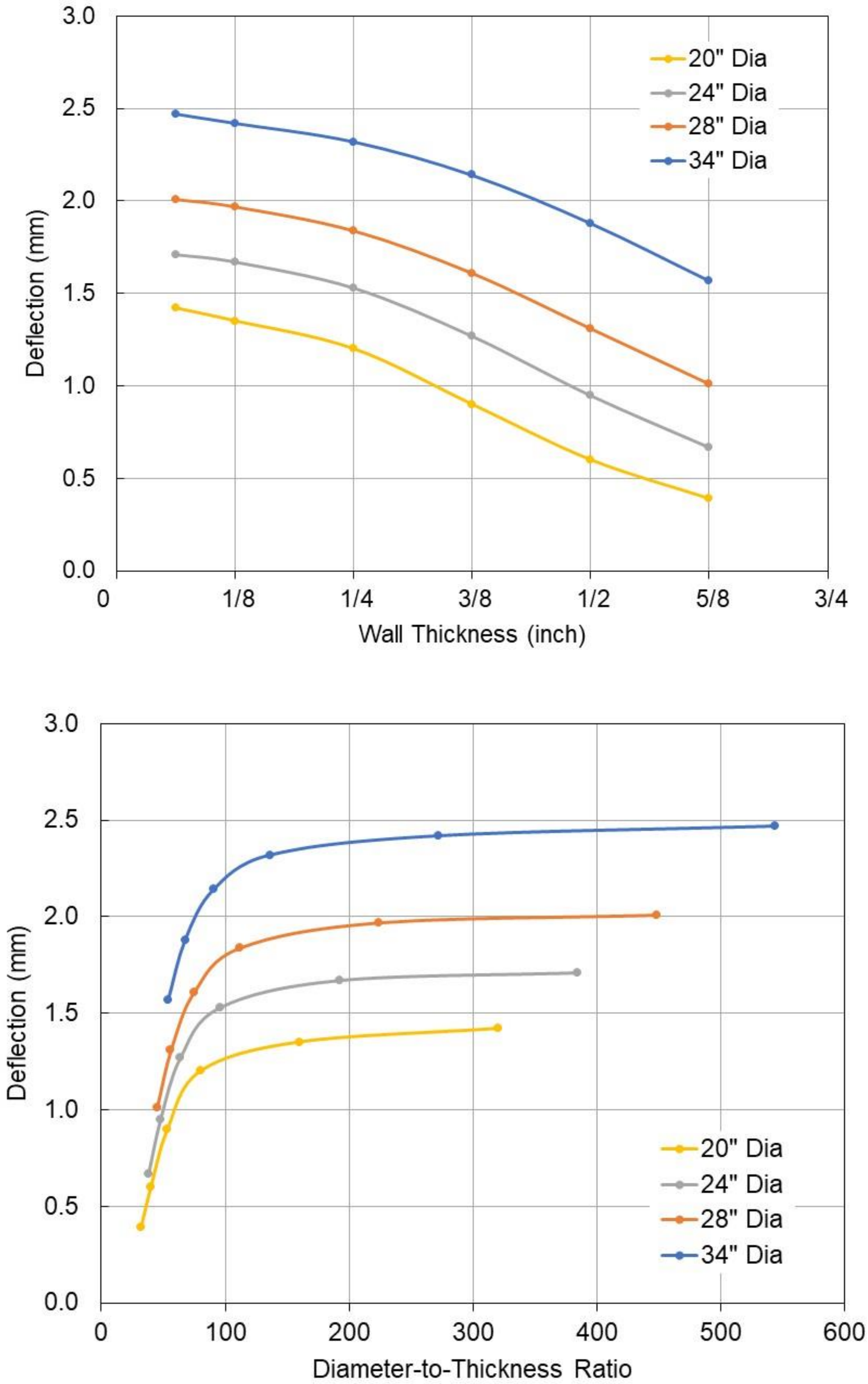

Figure 4-13: Vertical ovalization: effect of wall thickness (top) and diameter-to-thickness ratio (bot)

In the models analyzed, no initial imperfections were considered. The pipe section was modelled as a perfectly round, uniform, homogenous structure. The presence of initial imperfections in the pipe cross-section would have the potential to greatly influence the global and local behavior of the pipeline. As seen throughout the literature review, local imperfections can greatly reduce the load bearing capacity of the section and initiate locations of local buckling. Therefore, with the extremely thin wall thickness considered above, it must be noted that the results presented do not include the effect of imperfections. At this thin wall thickness, local imperfections such as dents, grooves, and perforations would significantly alter the results and may lead to local buckling which was not captured here.

In addition, the soil structure was also considered to be a uniform homogenous matrix. Compared with field studies, soil consists of variably sized particles, including large aggregates. Considering the possibility that a large aggregate be in contact with the pipe section at the maximum load locations, this local stress riser would also considerably increase the potential for local buckling of the cross section. As a result, care must be taken when examining the results of the pipeline with extremely small wall thicknesses as presented above.

4.4 Effect of Soil Stiffness

The static response of a buried pipeline subjected to the applied surface loading was significantly influenced by the surrounding soil. The surrounding soil is responsible for transferring external loading to the pipe section, resisting pipe ovalization and bending, and is the underlying cause of pipeline corrosion. The most significant influencing material property of the soil matrix is the soil elastic stiffness. As previously discussed, the soil arching effects and subsequent load transfer from the soil surface to the pipe section is dependent on the relative stiffness between the two materials. Considering pipelines can be installed within a variety of soil types, it was imperative to understand the effects of soil stiffness on the static behavior of buried pipelines subjected to surface live loads. The elastic modulus of the soil (Figure 4-14) was varied between 5 MPa and 250 MPa. These elastic moduli were representative of very soft clay and dense sand/gravel, respectively (Subramanian, 2010). This range covered a wide spectrum of possible backfill soils and compaction levels, while soils with stiffness greater than 250 MPa were intuitively deemed non-critical for the pipe stress state. The soil matrix was assumed to be homogenous, ignoring the effects of possible soil layers. Similar to the investigation regarding the effects of pipe wall thickness, the soil stiffness analysis was conducted using the previously determined critical depth of 1.0 m soil cover.

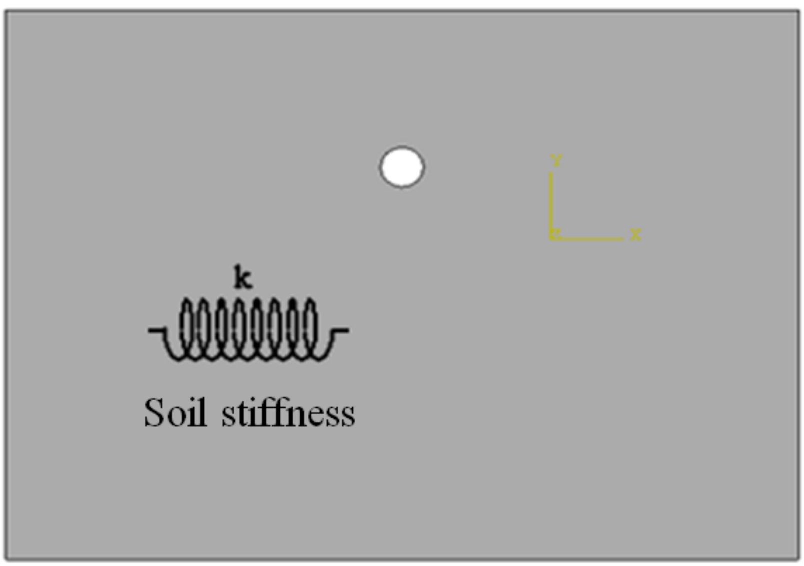

Figure 4-14: Variable soil stiffness

The models with variable soil stiffness were run in the same fashion as the previous analyses and the resulting stress state is shown in Table 4-3 and Figure 4-15.

Table 4-3: Effect of soil stiffness on the maximum normal stresses at the pipe crown due to soil overburden and surface live load

			Maximum Principal Stresses at Pipe Crown [MPa]		
ID	Pipe Diameter [inch]	Soil Elastic Modulus [MPa]	Hoop S11	Longitudinal S22	Von Mises VM
1	34	250	-8.09	-6.61	7.43
2	34	100	-14.02	-12.40	13.24
3	34	50	-21.56	-19.17	20.42
4	34	25	-32.95	-28.63	30.96
5	34	15	-44.73	-37.82	41.53
6	34	10	-56.26	-46.56	52.01
7	34	5	-79.24	-64.01	72.72
8	28	250	-8.11	-6.53	7.46
9	28	100	-14.54	-12.38	13.61
10	28	50	-22.59	-19.29	21.15
11	28	25	-34.33	-28.94	31.93
12	28	15	-45.79	-38.09	42.49
13	28	10	-56.33	-46.55	52.16
14	28	5	-75.16	-62.76	69.83
15	24	250	-8.30	-6.48	7.56
16	24	100	-15.12	-12.35	13.94
17	24	50	-23.43	-19.29	21.68
18	24	25	-34.99	-28.94	34.21
19	24	15	-45.52	-37.92	42.25
20	24	10	-54.56	-46.03	50.84
21	24	5	-69.03	-61.16	65.46
22	20	250	-8.67	-6.43	7.79
23	20	100	-15.91	-12.27	14.43
24	20	50	-24.24	-19.13	22.12
25	20	25	-34.85	-28.56	32.16
26	20	15	-43.48	-37.17	40.69
27	20	10	-50.09	-44.83	47.68
28	20	5	-59.25	-59.12	59.19

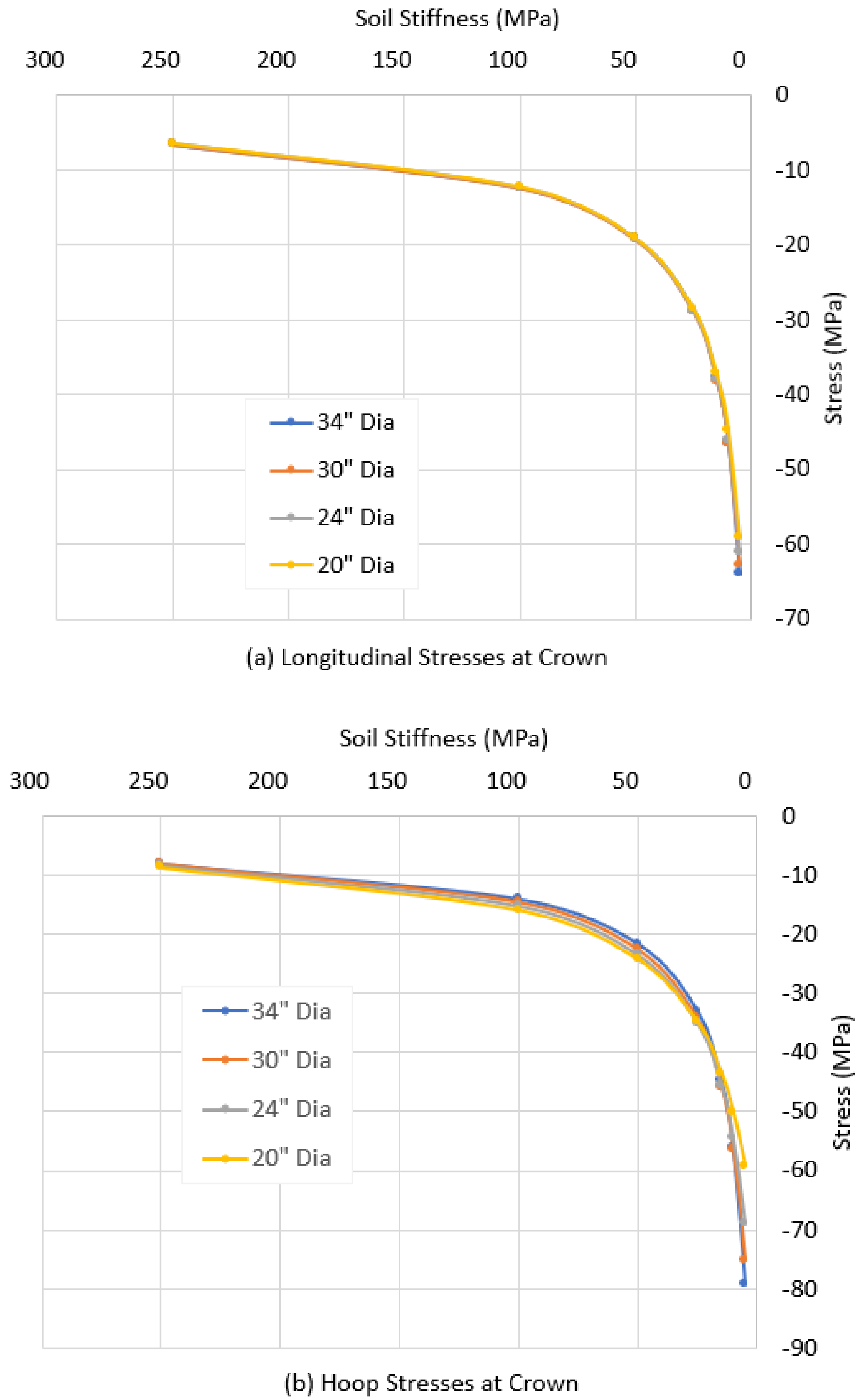

Figure 4-15: Effect of soil stiffness on normal stresses at pipe crown due to soil overburden and surface live load

As can be seen in the plots, as the soil stiffness was reduced, both the longitudinal and circumferential normal stresses at the pipe crown increased, following a natural logarithmic curve. This increase in stresses was a direct result of the soil arching effects. As the soil stiffness decreased relative to the pipe section, the pipe attracted a greater percentage of the surface load and the resulting stress state increased. This additional loading increased both the global and local bending stresses.

Similar to the previous analyses, smaller pipe diameters generally experienced larger stresses at reasonable values of soil stiffness. However, as the soil stiffness began to decrease below 25 MPa, there existed a shift and the larger pipes experienced larger stresses. With a very low soil stiffness, similar to very soft clay, the surface live load resembled that of a concentrated point load applied directly to the pipe crown. The soil resisted very little of the total load and the surface load is transferred near directly to the pipe crown. Due to the same increase in local wall thickness as described above, the smaller diameter pipes experienced lower local bending stresses. Further, the soil provided less confining pressure, increasing the pipe section deformation and corresponding local bending stresses. This localization effect is shown below in Figure 4-16. Due to the inherently lower local stiffness of the wall section, the local stresses experienced by the larger pipe sections lead to an overall increase on the global stress state of the section.

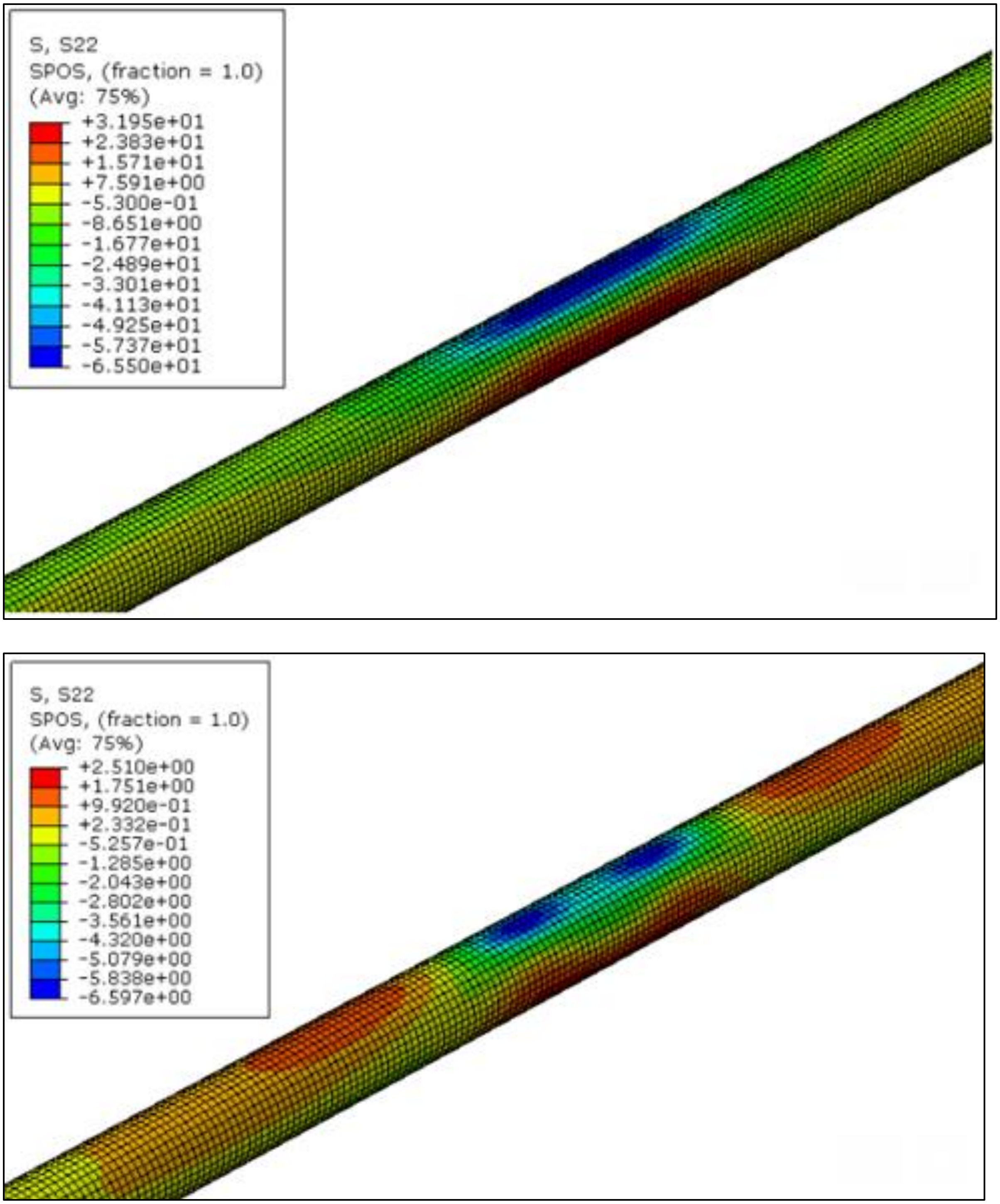

Figure 4-16: Effect of soil stiffness - 34" dia. pipe: Longitudinal stresses for 250 MPa (top) and 5 MPa (bot) soil elastic modulus

The degree of vertical ovalization as defined by the Modified Iowa Equation also increased as the soil stiffness was reduced, as shown in Figure 4-17. The increase in ovalization followed a similar natural logarithmic curve as did the normal principal stresses. This increase was a result of both the soil arching effects and the reduced passive confining pressure of the surrounding soil. As the stiffness of the soil decreased, the pipe attracted a larger portion of the load and this intuitively lead to greater deformation and ovalization of the cross-section. In addition, as the soil stiffness decreased so did the corresponding confining resistance. The pipe section was able to mobilize the surrounding soil a greater amount, leading to an increased ovalization and resulting stress state. With a very high soil stiffness, both the stress state and the ovalization of the pipe section became negligible. The stiff surrounding soil supported the majority of the surface live load and effectively restrained the pipe section from deforming.

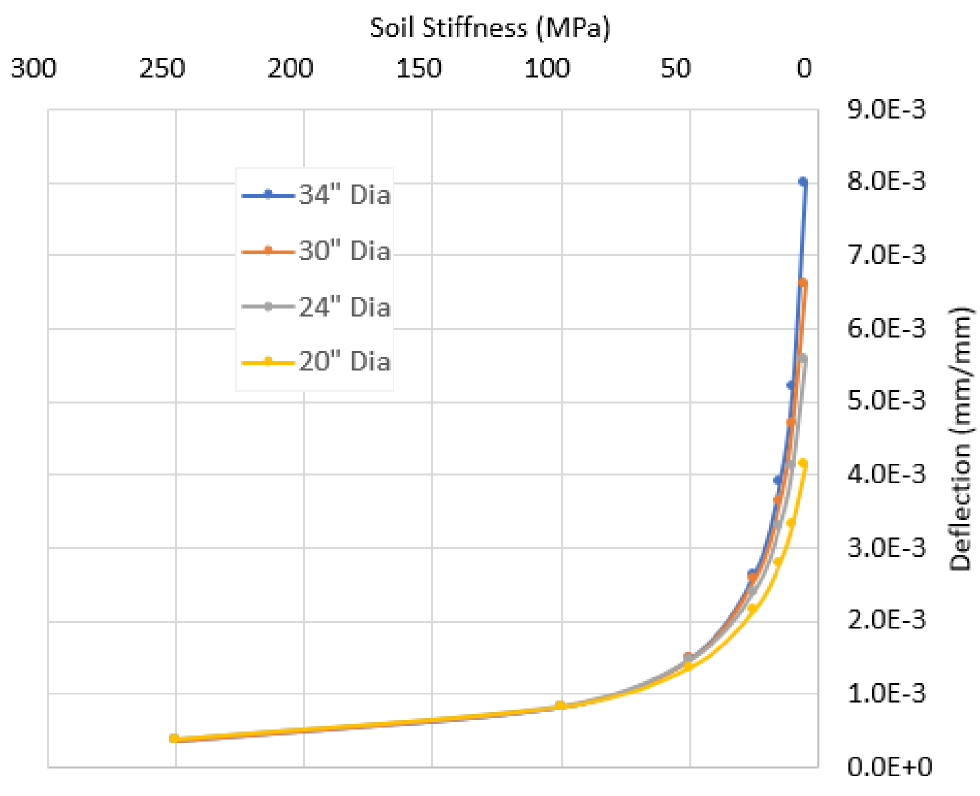

Figure 4-17: Effect of soil stiffness on vertical ovalization

4.5 Effect of Surface Load Variation

All of the analyses completed above assumed the surface live load to be a CL-800 truck positioned with the maximum axle load directly above the pipe section. This loading was selected as defined by various design codes including the Canadian Highway Bridge Design Code S6-14, and is commonly considered as a maximum surface design load throughout the structural engineering industry (Canadian Standards Association, 2014). However, there are other various loading types and configurations that have the potential to be more critical than the loading considered above. The vehicle load type, the number of vehicle loads, and the direction of load travel all result in reasonable load cases that differ significantly from the loading previously considered. Therefore, it was warranted that these additional loading conditions be investigated to observe the various impacts they may have on the static behavior of a buried decommissioned pipeline subjected to surface live loading.

4.5.1 Construction Vehicles

The loading considered in the previous analyses is that of a CL-800 truck. This truck is typically considered as a conservative vehicle load for design of roads, highways, bridges, concrete slabs on grade, etc. However, given the location of pipelines in often remote and secluded locations, buried pipelines can be subjected to various other vehicle loads with axle loading exceeding the CL-800 truck. Vehicles such as farming combines, track or mobile cranes, and other large construction equipment often have very large wheel bearing pressures. Therefore, it was deemed necessary to consider the effects of other vehicle loads on the static response of buried pipelines. Although the axle loading may be larger, the wheel contact area also tends to be larger, increasing the loading area and resulting zone of influence. As a result, the increase and/or decrease in stress state was not intuitively obvious.

For the purposes of this analysis, a typical large earth moving dump truck was considered as shown in Figure 4-18. As can be seen, the maximum axle load of the construction equipment was 567 kN, compared to the maximum axle load of 224 kN for the CL-800 truck. The construction equipment was approximately 2.5 times heavier than the loading considered thus far. However, the wheel contact area was also four times larger and the wheel spacing was 60% larger compared with the CL-800 truck. Therefore, it was not intuitive that the resulting stress state should simply be linearly increased by the increase in axle loading.

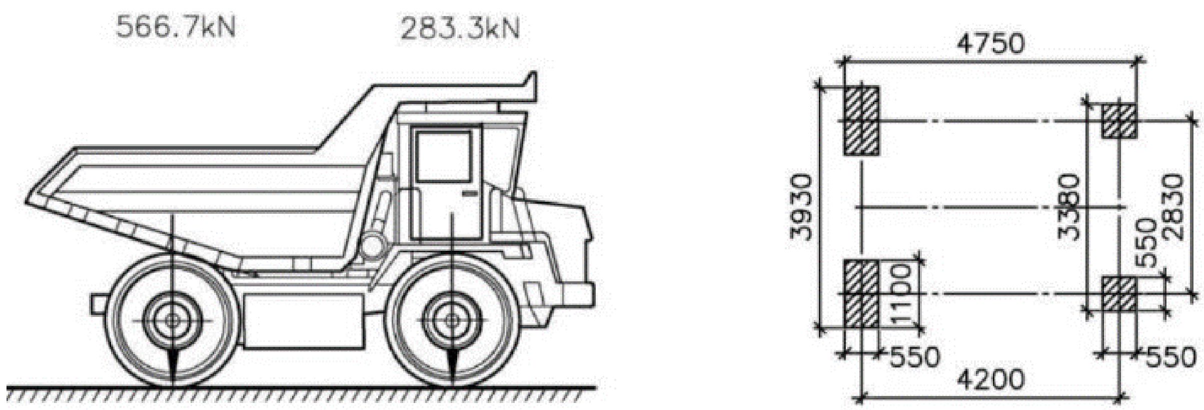

Figure 4-18: Earth moving truck wheel loading

The construction equipment loading was applied as a pressure load in the same manner as the previous CL-800 truck. The same dynamic load allowance factor was applied, corresponding with the modelled critical depth of 1.0 m. The non-linear analysis was performed for each of the pipe diameters and the resulting increase in longitudinal and circumferential stress at the pipe crown is shown in Table 4-4, and increase in von Mises stress as shown in Table 4-5.

Table 4-4: Pipe crown normal stresses due to construction equipment surface live loading and soil overburden

			Pipe Crown Stress [MPa]		% Increase	
Pipe Diameter [inch]	Surface Load	Burial Depth [m]	Hoop S11	Longitudinal S22	Hoop S11	Longitudinal S22
34"	CL-800	1.0	-32.95	-28.63	105%	113%
34"	Construction Equip.	1.0	-67.59	-61.10		
28"	CL-800	1.0	-34.33	-28.94	83%	93%
28"	Construction Equip.	1.0	-69.98	-61.75		
24"	CL-800	1.0	-34.99	-28.94	82%	91%
24"	Construction Equip.	1.0	-70.93	-61.24		
20"	CL-800	1.0	-34.85	-28.56	80%	91%
20"	Construction Equip.	1.0	-70.13	-60.30		

Table 4-5: Pipe crown von Mises stress due to construction equipment surface live loading and soil overburden

			Pipe Crown Stress [MPa]	% Increase
Pipe Diameter [inch]	Surface Load	Burial Depth [m]	Von Mises VM	Von Mises VM
34"	CL-800	1.0	30.96	107%
34"	Construction Equip.	1.0	64.18	
28"	CL-800	1.0	31.93	87%
28"	Construction Equip.	1.0	59.58	
24"	CL-800	1.0	34.21	84%
24"	Construction Equip.	1.0	62.91	
20"	CL-800	1.0	32.16	84%
20"	Construction Equip.	1.0	59.27	

As can be seen, both the longitudinal and circumferential stresses increased under the application of the construction equipment loading as compared with the CL-800 truck. However, the increase was not simply linear with the increase in the magnitude of the surface load. The surface load magnitude was approximately 2.5 times the standard loading, while the increase in stresses was only close to double, with circumferential hoop stresses increasing approximately 80-105% and longitudinal stresses increasing approximately 90-110%. The difference between the magnitude and resulting stress increase was due to the larger wheel bearing area and spacing of the wheels. Having a larger wheel bearing area engaged a larger area of soil, increasing the zone of influence. As a result, the load transfer cone extended further outside of the pipe section and the pipe attracted an overall smaller portion of the surface load. Based on these results, it would be feasible to develop a correlation between the pipeline stresses and surface load vehicle, categorized by magnitude, wheel bearing area, and wheel spacing.

It is also seen that the smaller pipe diameters experienced a slightly smaller stress increase with the applied construction loading. The smaller pipe sections had an inherently smaller projected cross-section and a larger local stiffness as previously described. With a larger wheel bearing area, the resulting load transfer cone extended further outside the smaller cross-section compared with the larger diameter pipes. Therefore, the smaller pipes carried a proportionately smaller amount of the surface applied load, with the soil carrying a greater amount. Further, the local wall stiffness of the smaller pipe section was stiffer for the reasons previously described. The smaller pipe sections subsequently experienced a smaller increase in local bending stresses as compared with the larger pipe diameters. As a result, the increase in the overall stress state of the smaller pipe diameter pipe sections was nominally smaller.

4.5.2 Surface Load Orientation and Multiple Lane Loads

In addition to the possible types of surface loading a buried pipeline may be subjected to, the geometry of the surface loading can also vary significantly. The models analyzed thus far examined the effects of a single surface load travelling perpendicular to the pipe axis. It is reasonable to imagine two additional scenarios with a single surface vehicle travelling parallel to the pipe axis or multiple surface vehicles travelling perpendicular to the pipe axis. These two investigations are presented hereafter. Multiple surface vehicles travelling parallel to the pipe axis was not considered as it was expected that the vehicle spacing would be too large to have a significant influence on the stress state of the buried decommissioned pipeline. The adjacent vehicles would fall well outside of the pipeline location, and with only a 1.0 m burial depth, the pipeline would carry negligible additional load.

4.5.2.1 Load Travelling Parallel to Pipe Section

The current models analyzed considered the load travelling perpendicular to the pipe axis as it was expected that the stress state would be maximum by positioning the maximum axle load closest to the center of the pipe span. This positioning maximized both the local and global bending stresses. However, it was also practical to assume that the surface loading was travelling parallel to the pipe axis. Positioning the loading in this orientation subjected the pipeline to multiple surface loads along the length of the pipe. Two loading cases were considered for this orientation – one with the axle line centered with the pipe section (one-wheel line on either side of the pipe) and one with a single wheel line centered over the pipe section (the axle line offset from the pipe section) as shown in Figure 4-19 and Figure 4-20. These diagrams are schematic representations only and the total length of the soil block was adequately adjusted as to eliminate the influence of the boundary conditions.

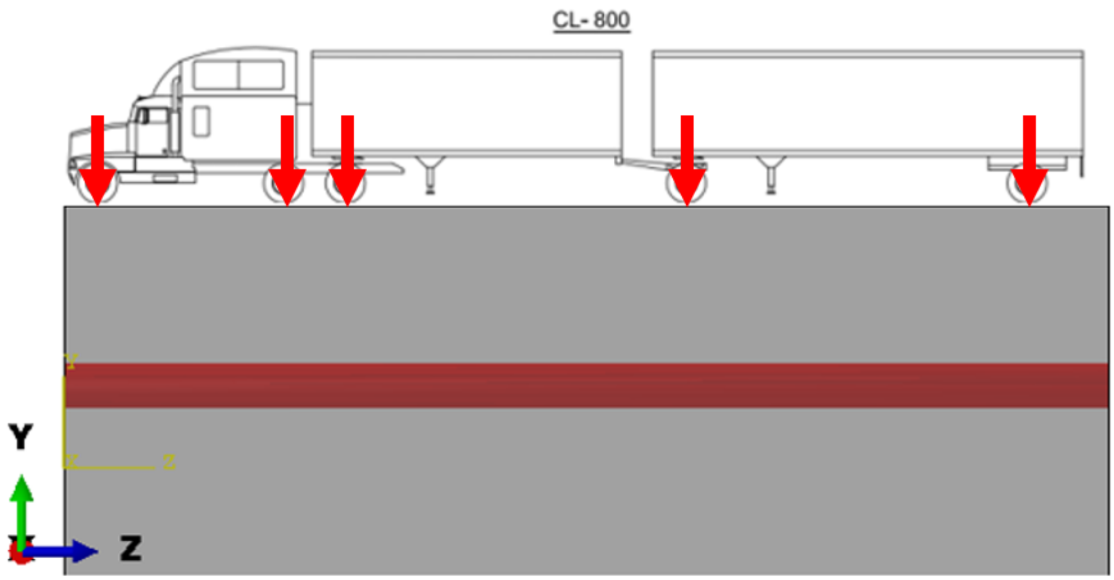

Figure 4-19: CL-800 truck travelling parallel to pipe axis

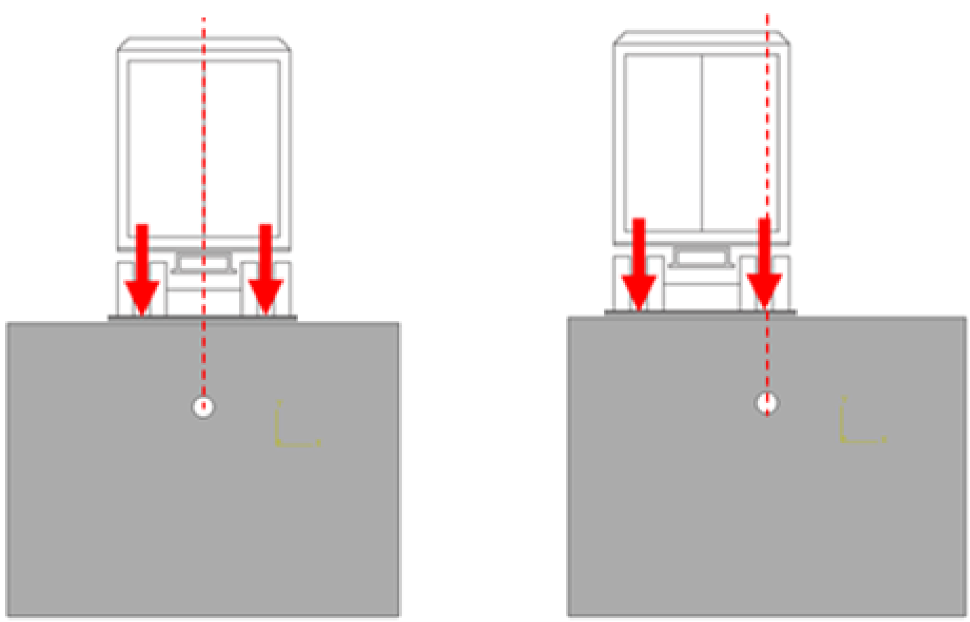

Figure 4-20: Axle centric with pipe (left) and axle offset with pipe (right)

The resulting normal stresses in the circumferential and longitudinal direction for each loading scenario are shown in Table 4-6. As can be seen, the critical case for the two scenarios occurred when one wheel line was located directly over the pipe section (axle offset), with stresses nearly double that of the concentric axle load case. This increase in stresses was due to both soil arching effects and the critical burial depth used. This study clearly showcased the importance of the proximity of the load to the pipe axis. The burial depth was taken as 1.0 m and the wheel spacing was 1.8 m for the CL-800 truck. Therefore, with the axle centered over the pipe axis, the direct load path was at nearly a 45° angle. It is common industry practice to assume a soil load transfer slope of 1H:2V, or 26°. It is clear that in this case, much less load was attracted to the pipe section and the majority of the load was resisted by the soil only.

Table 4-6: Pipe crown normal and von Mises stresses due to soil overburden and CL-800 truck travelling parallel to pipe

			Pipe Crown Stress [MPa]		
Pipe Diameter [inch]	Axle Location	Burial Depth [m]	Hoop S11	Longitudinal S22	Von Mises VM
34"	Perpendicular	1.0	-32.95	-28.63	30.96
34"	Concentric	1.0	-11.53	-11.87	13.91
34"	Offset	1.0	-29.28	-23.14	25.56
28"	Perpendicular	1.0	-34.33	-28.94	31.93
28"	Concentric	1.0	-11.85	-11.84	13.87
28"	Offset	1.0	-30.21	-24.96	26.21
24"	Perpendicular	1.0	-34.99	-28.94	34.21
24"	Concentric	1.0	-11.72	-11.54	13.74
24"	Offset	1.0	-30.48	-24.69	29.54
20"	Perpendicular	1.0	-34.85	-28.56	32.16
20"	Concentric	1.0	-11.27	-11.08	13.26
20"	Offset	1.0	-29.93	-24.06	27.33

As can be seen in Table 4-6, each of the load cases with the CL-800 truck travelling parallel to the pipe section resulted in stresses lower than the baseline case with the CL-800 truck travelling perpendicular to the pipe section. With the wheel line centered over the pipe axis or offset, the opposite wheel line load which was positioned away from the pipe section increased the confining pressure provided by the soil. Although the wheel line was located far away from the pipe section and had little contribution to the overall stresses, it did displace the soil towards to the pipe section, providing an additional active confining pressure. Further, the parallel truck case incorporated either only one wheel load of the critical axle directly over the pipe with the adjacent wheel load positioned 1.8 m away or with two adjacent wheel loads each positioned at 0.9 m on either side of the pipe section. In the case of a truck travelling perpendicular to the pipe, both wheel loads of the maximum axle were positioned over the pipe, resulting in a larger load imposed on the pipe section.

Finally, the stress visualization of the load scenarios was also observed. Figure 4-21 shows the longitudinal stresses of the CL-800 truck travelling parallel to the 34” pipe section, with the axles positioned both concentric and offset from the pipe centerline. Distinct compressive bending stresses at the top extreme compression fiber at the locations of the wheel loads were clearly observed. In between the axle locations, negative bending moments were observed resulting in net tensile stresses at the extreme top fiber of the pipe section. The negative bending moments also acted to reduce the net positive bending moments and resulting compressive stresses. Based on the presence of negative bending moments along the pipe section, it was further concluded that the pipe would undergo stress and strain reversals throughout its loading history.

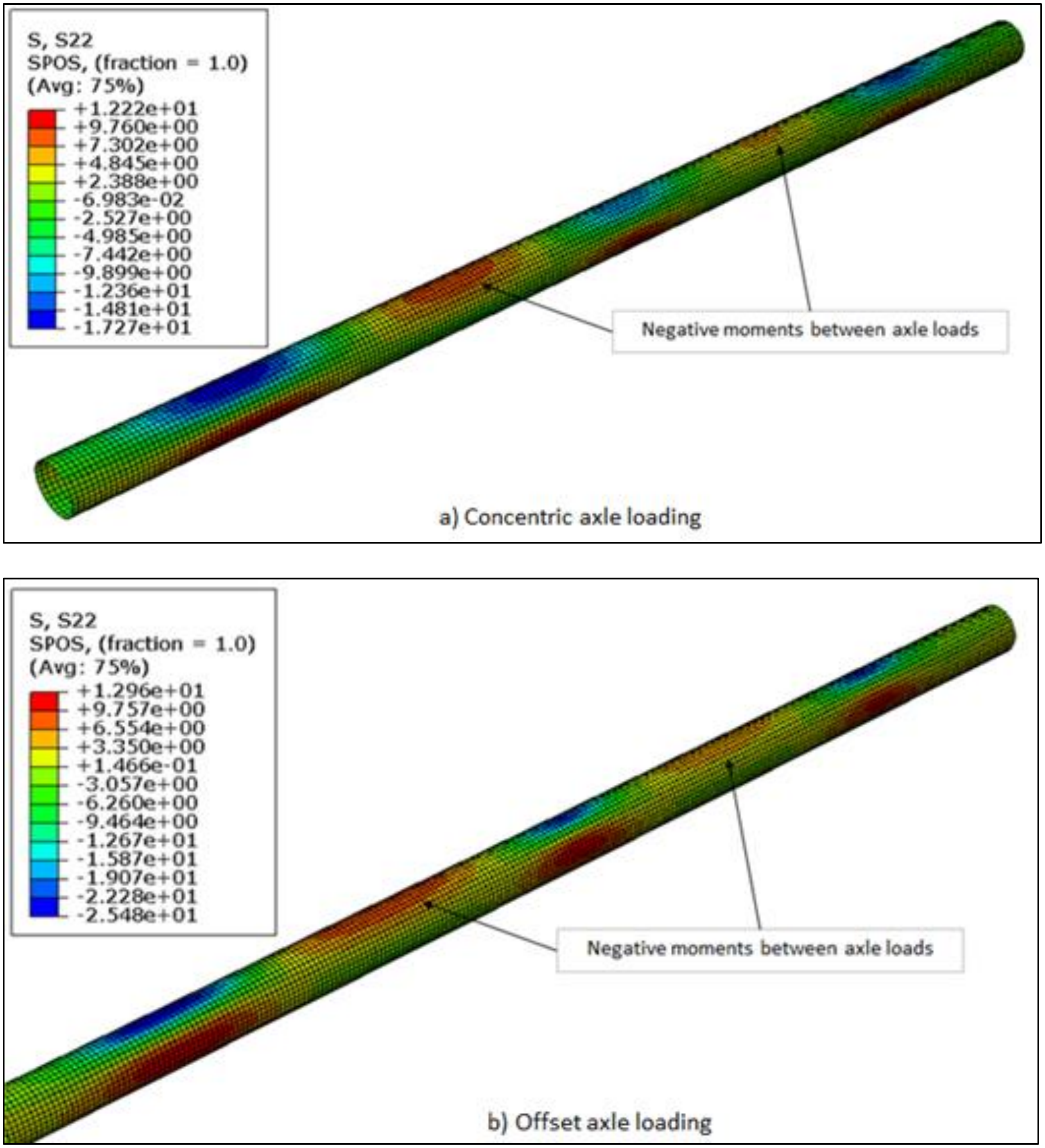

Figure 4-21: Longitudinal stress visualization of CL-800 truck travelling parallel to 34" diameter pipe

4.5.2.2 Multiple Trucks Travelling Perpendicular to Pipe Section

In addition to the single surface load, the presence of multiple surface loads was also considered. Within congested construction sites or farm fields, it is practical to envision multiple trucks travelling parallel to each other, perpendicular to the pipe axis. In the analysis considered, three parallel trucks were modelled assuming typical 3.0 m clearance envelope as per S6-14 and shown in Figure 4-22 (Canadian Standards Association, 2014). Three trucks were considered a practical maximum assumption and allowed for accurate modelling without updating the model geometry beyond the previous analysis. The resulting maximum stresses under the central truck were obtained and compared to the baseline case of a single truck in Table 4-7 and Table 4-8.

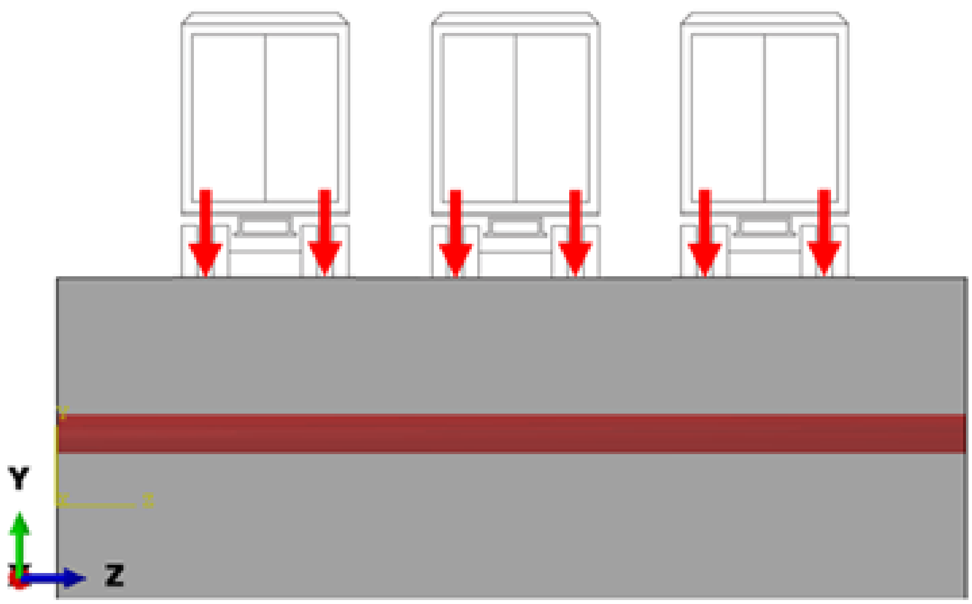

Figure 4-22: Multiple parallel CL-800 trucks travelling perpendicular to pipe

Table 4-7: Pipe crown normal stresses due to soil overburden and multiple surface loads

Pipe Diameter [inch]	Surface Loading	Burial Depth [m]	Pipe Crown Stress [MPa] Hoop S11	Pipe Crown Stress [MPa] Longitudinal S22	% Change Hoop S11	% Change Longitudinal S22
34"	Single CL-800 Truck	1.0	-32.95	-28.63	27%	-16%
34"	3 - CL-800 Trucks	1.0	-41.96	-24.15		
28"	Single CL-800 Truck	1.0	-34.33	-28.94	27%	-14%
28"	3 - CL-800 Trucks	1.0	-43.60	-24.96		
24"	Single CL-800 Truck	1.0	-34.99	-28.94	27%	-12%
24"	3 - CL-800 Trucks	1.0	-44.55	-25.33		
20"	Single CL-800 Truck	1.0	-34.85	-28.56	26%	-12%
20"	3 - CL-800 Trucks	1.0	-43.93	-25.01		

Table 4-8: Pipe crown von Mises stress due to soil overburden and multiple surface loads

Pipe Diameter [inch]	Surface Loading	Burial Depth [m]	Pipe Crown Stress [MPa] Von Mises VM	% Increase Von Mises VM
34"	Single CL-800 Truck	1.0	30.96	24%
34"	3 - CL-800 Trucks	1.0	38.42	
28"	Single CL-800 Truck	1.0	31.93	25%
28"	3 - CL-800 Trucks	1.0	40.01	
24"	Single CL-800 Truck	1.0	34.21	24%
24"	3 - CL-800 Trucks	1.0	42.56	
20"	Single CL-800 Truck	1.0	32.16	24%
20"	3 - CL-800 Trucks	1.0	38.76	

As can be seen, the circumferential hoop stresses increased slightly compared with the single surface load case, while the longitudinal bending stresses actually marginally decreased. The increase in circumferential stresses was due to greater mobilization of the surrounding soil and ovalization of the section. The longitudinal stresses decreased due to the section being continuously supported by the soil. The soil acted similar to a continuous spring and the pipe similar to a continuously supported beam. Therefore, by applying additional surface loads away from the midpoint of the section, the additional loading induced a negative moment at the midpoint, reducing the net positive moment.

The visual representation of the resulting stress state for the 34” diameter pipe section is show in Figure 4-23. As can be seen, there exist three distinct stress concentration pairs, representing the wheel load application points of each surface load. In addition, there exist negative bending moments adjacent to the surface load points. This again exhibits the possibility of stress and strain reversals experienced by the buried decommissioned pipeline throughout its life cycle.

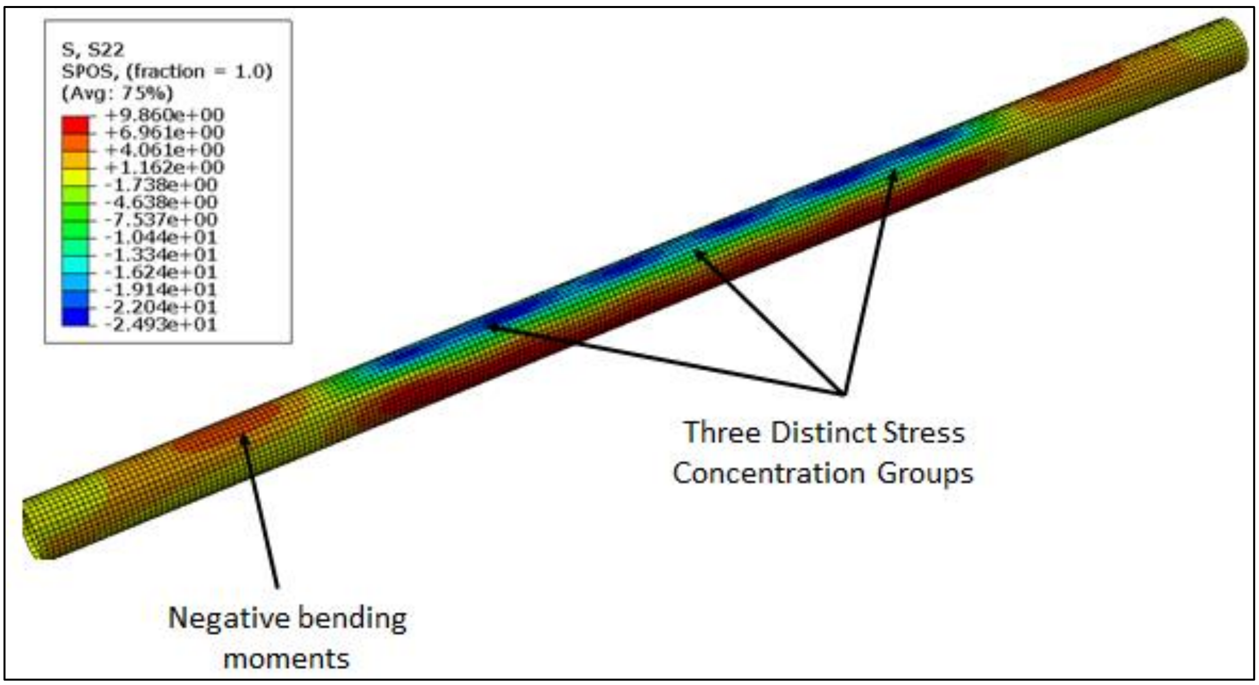

Figure 4-23: Visualization of longitudinal stresses due to multiple surface loads on the 34” diameter pipe

4.6 Ultimate Limit States Condition

For each of the parameters investigated thus far, service level loads were used in order to obtain an accurate representation of the stresses and strains to be expected under the considered loading. However, it is industry practice and generally accepted (commonly required) throughout the structural engineering industry that structures be designed for the ultimate limit state (ULS) in addition to the service loading. The ULS design methodology in Canada employs partial load and resistance factors to both the load cases and the material properties in order to obtain a satisfactory safety factor and/or probability of failure. Therefore, ULS combinations as specified by the Canadian Bridge Code S6-14, were applied (Canadian Standards Association, 2014):

$$\mathrm{ULS{:}}\ 1.25\mathrm{DL} + 1.7\mathrm{LL}(1 + \mathrm{DLA}) \tag{4-2}$$

Using the specified load factors for the dead load (*DL*), live load (*LL*), and dynamic load allowance factor (*DLA*), the baseline model loading was updated and the resulting stresses were obtained as per Table 4-9 and Table 4-10.

Table 4-9: Ultimate Limit State analysis - Pipe crown normal stresses due to soil overburden and surface live load

Pipe Diameter [inch]	Limit State	Burial Depth [m]	Pipe Crown Stress [MPa] Hoop S11	Pipe Crown Stress [MPa] Longitudinal S22	% Change Hoop S11	% Change Longitudinal S22
34"	Service	1.0	-32.95	-28.63		
34"	Ultimate	1.0	-49.23	-44.47	49%	55%
28"	Service	1.0	-34.33	-28.94		
28"	Ultimate	1.0	-52.01	-45.11	52%	56%
24"	Service	1.0	-34.99	-28.94		
24"	Ultimate	1.0	-52.99	-45.79	51%	58%
20"	Service	1.0	-34.85	-28.56		
20"	Ultimate	1.0	-53.41	-45.33	53%	59%

Table 4-10: Ultimate Limit State analysis - Pipe crown von Mises stress due to soil overburden and surface live load

Pipe Diameter [inch]	Limit State	Burial Depth [m]	Pipe Crown Stress [MPa] Von Mises VM	% Change Von Mises VM
34"	Service	1.0	30.96	
34"	Ultimate	1.0	47.53	54%
28"	Service	1.0	31.93	
28"	Ultimate	1.0	49.38	55%
24"	Service	1.0	34.21	
24"	Ultimate	1.0	53.13	55%
20"	Service	1.0	32.16	
20"	Ultimate	1.0	50.23	56%

The resulting stresses increased by approximately 50 to 60%, which is similar to the average of the 1.25 and 1.7 factor. Since the pipe stresses remained within the elastic range and the geometric constraints of the surface load remain unchanged, increasing the load by a linear factor results in a near linear increase in the resulting stresses. These ULS stresses should then be compared to the yield stress, reduced by an applicable material resistance factor. Assuming a material resistance factor of 0.9 for ductile steel, the stress still remained well below the reduced yield of 373 MPa. Therefore, even under the application of ultimate limit states, the intact pipelines were at little risk of failure.

4.7 Overview of Soil Behaviour

The analysis of soil behaviour lies outside the primary scope of the research presented within this thesis. Within the scope of this thesis, the soil acted as a medium through which the live load was transferred from the surface of the soil block to the pipe section. Based on this fundamental purpose, the soil material properties, element type, mesh configuration, and contact algorithm was selected as to achieve an accurate transfer of load applied to the pipe surface. The methodology for the selection of these parameters was previously described in detail in Chapter 3. The detailed behaviour of the soil is the key objective of the research conducted by another party, focusing on the resulting soil subsidence should a pipeline collapse occur. However, there is still value is describing the general soil transfer mechanisms that occurred within this parametric study.

As previously described, the soil acted as a solid continuum, transferring the surface load to the pipe section through a process known as soil arching. Terzaghi (1974) soil arching theory describes the process through which an unstable soil mass transfers load to an adjacent rigid body. The pipe section was much stiffer than the surrounding soil. Therefore, as the soil underwent large deformations and mobilized shear stresses, stress redistribution occurred and the load was transferred towards the pipe section. Subsequently, the pipe was subjected to higher pressure loads. As the relative stiffness of the pipe section increased, the contract pressure also increased, as described in section 4.3. This effect was prevalent during both the effect of wall thickness and the effect of soil stiffness investigations. The load transfer and stress distribution is further shown in Figure 4-24 below, outlining the maximum principal stresses in the soil in relation to the soil-pipe relative stiffness. To remain concise, only the figures regarding the effects of soil stiffness are shown. The stress redistributions were similar for a reduced wall thickness.

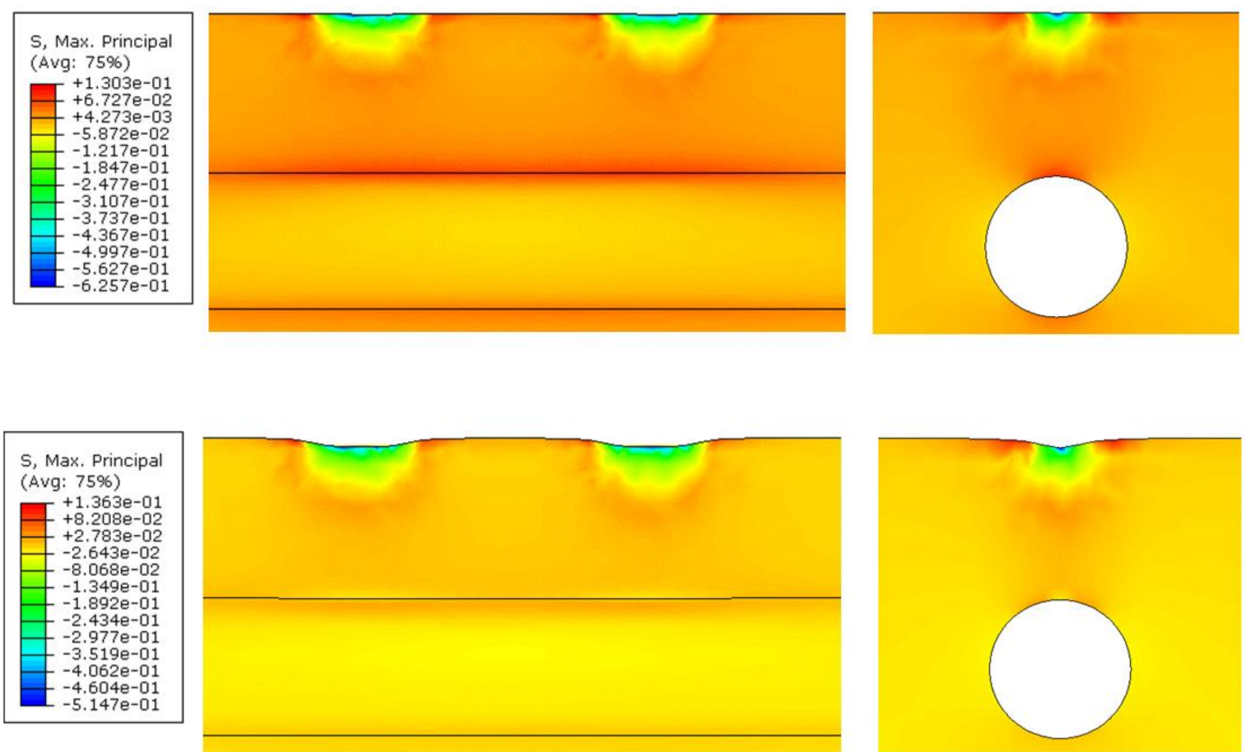

Figure 4-24: Soil maximum principal stress: Soil elastic modulus 100 MPa (top) and 5 MPa (bottom)

The compressive load path is clearly shown from the soil surface to the pipe section. Maximum compressive stresses were present at the centroid of the surface applied pressure load and are transversely distributed as the load transfers through the soil. Minor tensile stresses were observed at the pipe surface as the soil slips along the interface. The soil at the edges of the wheel bearing area also experienced tensile stresses as the deformation of the load is resisted by the surrounding soil on the surface. This action was similar to a plate subjected to a point load. Comparing the soils with 100 MPa and 5 MPa elastic moduli, it was observed that the load transfer path was much more direct and localized in the less stiff soil. The relative stiffness of the pipe section increased with decreasing soil stiffness, attracting a majority of the surface applied load. The 100 MPa stiff soil in the vicinity of the pipe section experienced much higher stresses as compared to the 5 MPa stiff soil, indicating that the soil supported a larger percentage of the load. This stress concentration can be clearly observed at the pipe crown, with the principal stresses much higher in the stiffer soil. This observation is similar to the conclusions outlined by Kabir (2003).

Further, the difference in contact pressure acting on the pipe surface between the 100 MPa and 5 MPa soil is shown in Figure 4-25. As the soil stiffness decreased and the relative stiffness of the pipe increased, the contact pressure at the pipe crown also increased and became more localized. The contact pressure in the 100 MPa soil is distributed over the top hemisphere of the pipe section, with the maximum pressures still concentrated at the pipe crown. However, for the 5 MPa soil, a very pronounced contact pressure concentration was observed at the pipe crown and the pressure quickly dissipated over the circumference of the section. Therefore, it was concluded that as the soil stiffness was reduced, the soil displaced a greater amount and the surface load acted similar to a concentrated load applied directly to the pipe crown. This observation is further shown by observing the amount of soil slip across the interface, as shown in Figure 4-26. As the soil stiffness decreased, the soil slipped a greater amount across the surface of the pipe. The surface applied load was able to mobilize the less stiff soil a greater amount, resulting in stress redistribution from the displaced soil to the stiff pipe section; a direct result of the soil arching effects described above. This increased mobilization is clearly observed by examining the deformed shape of the soil surface in Figure 4-25 and Figure 4-26. The less stiff soil experienced significantly greater local deformation at the points of surface load application.

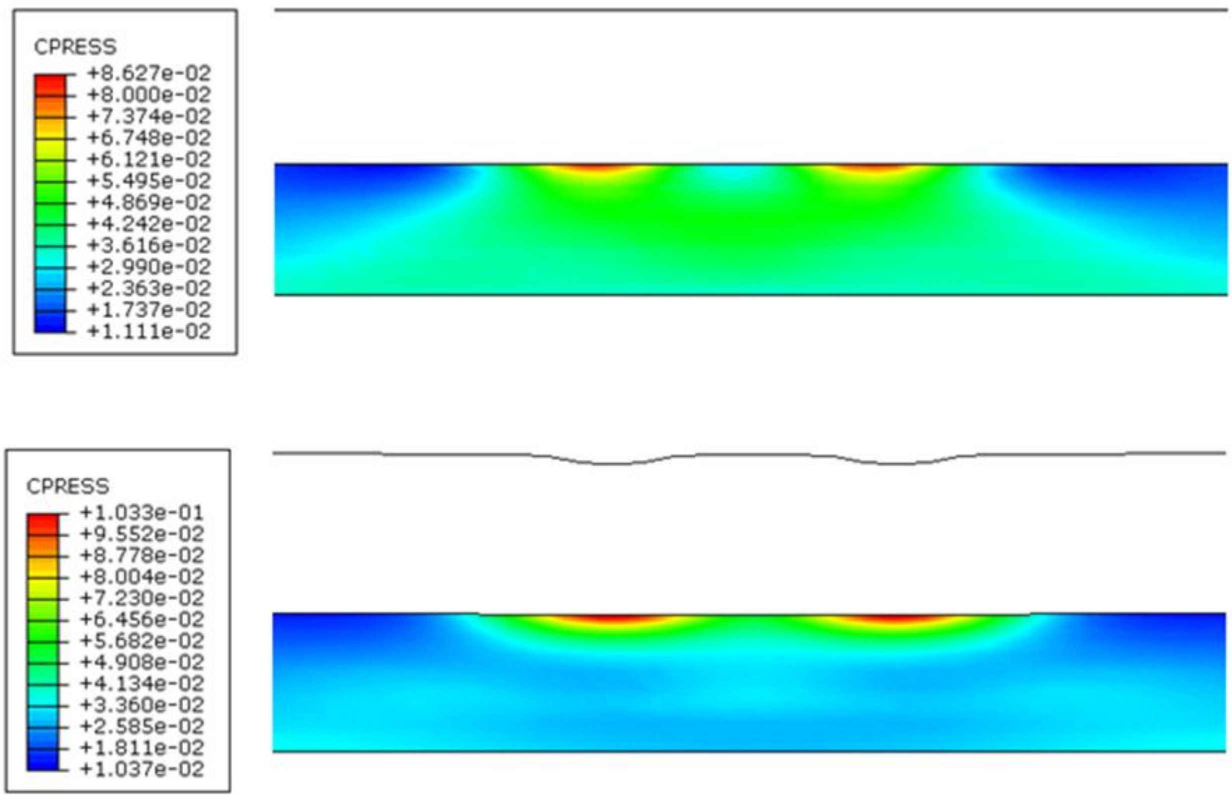

Figure 4-25: Contact pressure on pipe surface for soil elastic modulus of 100 MPa (top) and 5 MPa (bottom)

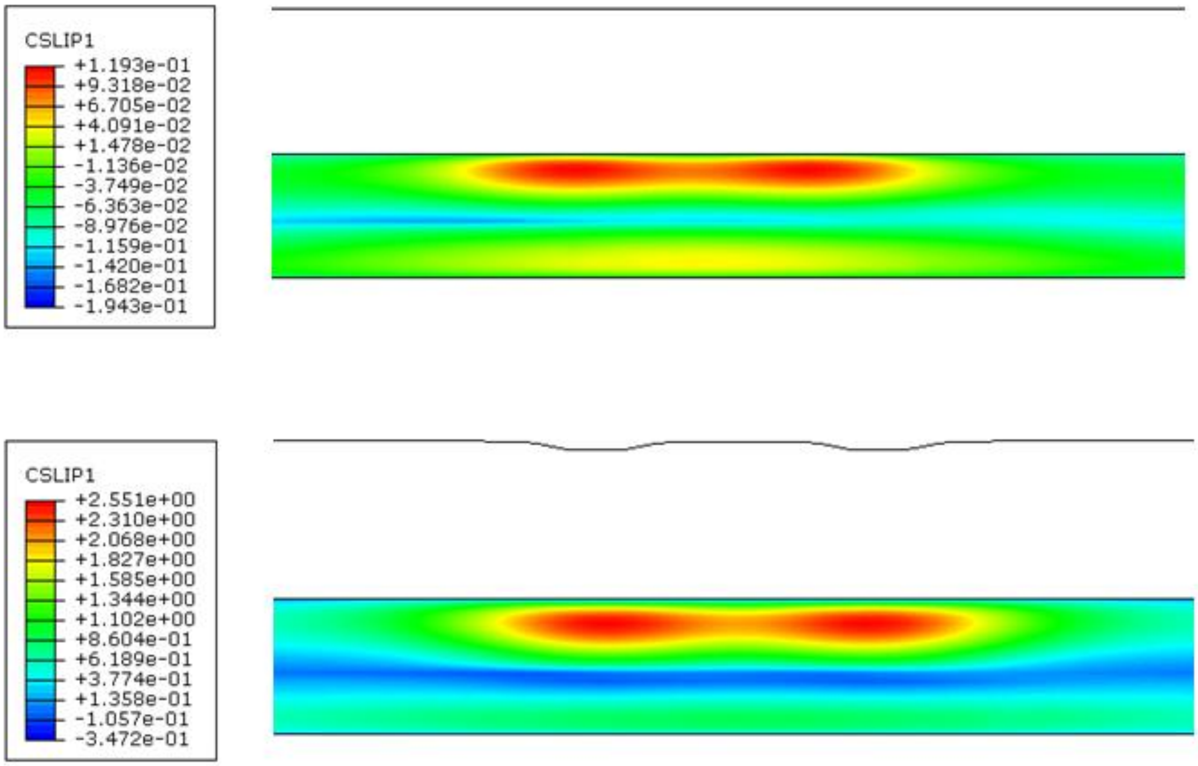

Figure 4-26: Vertical soil slippage across the pipe surface for soil elastic modulus of 100 MPa (top) and 5 MPa (bottom)

Chapter 5

Summary, Conclusions and Future Works

5.1 Summary

Buried steel pipelines serve as the primary means of transportation of oil and gas industry related products. However, buried pipelines also pose significant environmental and public safety risks, even long after decommissioning and abandonment. Decommissioned pipes are subjected to corrosion which decreases the structural integrity and load carrying capacity of the section. Consequently, corroded pipelines may no longer be capable of bearing the imposed loads due to soil overburden and surface live load. The initial step in determining structural integrity of decommissioned and abandoned pipelines was determining the baseline stress state of the pipeline immediately after decommissioning, subjected to surface live load. Using the finite element software ABAQUS, finite element models were developed and a parametric analysis was performed to determine the stress state of decommissioned pipelines. A buried pipeline was modelled within a uniform soil block, utilizing a frictional contact definition between the two. A surface live load consisting of the axle loads of a CL-800 truck travelling perpendicular to the pipe section was applied and the resulting pipeline stresses and deformations were obtained. A variety of variables influencing the stress state of buried pipelines were parametrically analyzed. The variables considered included burial depth, pipe section wall thickness, pipe diameter, diameter-to-thickness ratio, soil elastic stiffness, surface loading type, surface load orientation and position, multiple parallel live loads, and ultimate limit states analysis. A significant influencing variable was the burial depth. Depending on pipeline requirements and soil conditions, pipeline burial depth can vary drastically. Therefore, the first analysis concerned the effects of burial depth on the static response of decommissioned pipelines subjected to surface live load. Based on the results from the burial depth analysis, a reasonable critical burial depth of 1.0 m was chosen and used for all subsequent parametric studies.

5.2 Conclusions

Based on the finite element analyses and parametric investigation, the following conclusions were observed. The stress states mentioned below are located at the pipe crown, the location of maximum normal stress in all models.

1. As the burial depth decreases, the resulting longitudinal and circumferential hoop stresses tend to increase. The increase in stress state follows a natural logarithmic curve, indicating that the burial depth is a critical parameter.
2. The stress state of the pipe becomes significant and critical at a depth of soil cover equal to approximately 1.0 m. As the burial depth decreases relative to this depth, the stress state increases rapidly. As the burial depth increases, the stresses due to surface live load become less influential. At a burial depth less than 1.5 m, the dynamic allowance factor significantly increases, enhancing the effects of the surface live load.
3. As the pipe section wall thickness decreases, both the longitudinal and circumferential stresses tend to increase. Reducing the wall thickness of the pipe acts to reduce the pipe section’s moment of inertia, increasing the longitudinal bending stresses and ovalization. The circumferential stresses initially increase and then begin to decrease as a result of localization of the load, increase in soil slippage, and a reduced relative stiffness causing the pipe to attract less load due to soil arching effects.
4. As the soil stiffness decreases, the resulting stress state of the pipe increases, following a natural logarithmic curve. A reduced soil stiffness increases the relative stiffness of the pipe section causing the pipe to attract more load due to soil arching effects.
5. As the pipe diameter decreases, the resulting stresses typically increase. However, there exists a transition depth of approximately 0.5 m, at which the larger pipe sections

experience larger stresses due to a reduced local wall stiffness and increased local stresses and deformation.

6. Pipe ovalization tends to increase with decreasing burial depths, wall thickness, and soil stiffness.
7. Applying a higher magnitude surface load tends to increase the resulting stress state. The increase in stresses is not directly proportional as larger vehicles tend to have larger wheel bearing areas and spacing. Both of these variables act to increase the load influence cone, resulting in the load spreading further outside of the pipe section.
8. Surface vehicles travelling parallel to the pipe axis result in lower overall stresses compared with perpendicular travel. However, parallel loading induces stresses along the entire length of the pipe. Parallel loading positioned offset from the pipe such that one wheel line is located directly above the pipe produce stresses greater than those produced if the axle is centered.
9. Multiple parallel surface loads travelling perpendicular to the pipe axis induce additional stress concentrations along the length of the pipe and increase the resulting stress state of the section.
10. Both parallel and multiple surface loads induce negative bending moments along the pipe section. These negative bending moments result in stress and strain reversals in the pipeline over its decommissioned lifecycle. The negative bending moments also reduce the net positive moments and corresponding stresses.
11. Ultimate limit state analysis proportionally increases the resulting stresses.

Based on the analyses conducted, each of the parameters and scenarios investigated significantly influence the resulting stress state of the decommissioned pipeline. However, even as the burial depth, wall thickness, and soil stiffness was reduced, the stress state of the pipeline remained well below yield. Therefore, for the load cases and parameters considered, decommissioned pipeline pose little risk of collapse.

5.3 Future Work

The analysis conducted showcased the behaviour of decommissioned pipelines. Of importance, the pipe sections experienced stress concentrations and stress/strain reversals under typical surface loading. Therefore, it is imperative to extend the scope of the current investigation to include:

1. Local corrosion – extreme local corrosion at the locations of maximum stress concentrations has the potential to result in section buckling well below the pipeline yield strength. There exist locations along the pipeline where the maximum stresses are in either the longitudinal direction or the circumferential direction. Therefore, the effects of local corrosion depth and dimensions should be investigated. Similar research was noted in the literature review; however, these experimental and numerical investigations are typically conducted on isolated pipe sections neglecting the influence of soil-structure interaction. Further, most local corrosion experiments subjected the pipe section to axial force and/or bending. The localized effect of a concentrated surface load has not been investigated. The concentration of the surface load is of primary concern at very shallow burial depths.
2. Inclusion and influence of pre-decommissioning critical irregularities and imperfections including surface defects, girth welds, pipeline misalignment, and post-

operation residual stresses and strains – the presence of such irregulars have the potential to increase the critical local stress concentrations.

3. Low-cycle fatigue – since the pipeline experiences stress/strain reversal, the section is susceptible to fatigue loading effects. Strain reversals are caused from loading and unloading, with the pipe section experiencing stress amplifications from zero stress to tensile or compressive stresses of various magnitudes around the circumference of the section. When subjected to multiple surface loading or surface vehicles travelling parallel to the pipe section, the section experienced negative and positive bending moments, resulting in stress hysteresis loops between tension and compression under each vehicle pass. Models can be developed to represent both experimental and in-*situ* fatigue loading.
4. Post-fatigue behavior – through the initial fatigue analysis, diagrams for stress amplitude (s) versus number of cycles (N) (i.e. S-N curves) for the fatigue life of corroded decommissioned pipelines can be developed. Post-fatigue static loading analyses can then be performed to determine the residual stiffness and strength of the pipe section.
5. Full-scale experimental testing – although the parametric investigation performed was validated through geometric and mesh convergence, and comparison with values and results found within the literature, it is recommended that the baseline analyses conducted be replicated though full-scale experimental testing. Once validated, an analytical model can be developed for use in decommissioned and abandoned pipeline design and assessment.

References

AASHTO. (1998). *LFRD Bridge Design Specifications - 2nd Edition.* Washington, DC: American Associateion of State Highway and Transportation Officials.

Alberta Energy Regulator. (2013). *Report 2013-B: Pipeline Performance in Alberta, 1990-2012.* Calgary: Alberta Energy Regulator.

American Lifelines Alliance. (2001). Appendix B: Soil Spring Representation. In *Guidelines for the Design of Buried Steel Pipe* (pp. 68-69). ALA.

Arockiasamy, M., Chaallal, O., & Limpeteeprakarn, T. (2006, February). Full-Scale Field Tests on Flexible Pipes under Live Load Application. *Journal of Performace of Constructed Facilities, 20*(1), 21-27.

BGC Engineering Inc. (2017). *Assessment of Soil Spring Parameters for Overbends in Soil Types K, L, and M.* Calgary.

Brachman, R., Moore, I., & Rowe, R. (2000). The design of a laboratory facility for evaluating the structural response of small-diameter buried pipes. *Canadain Geotechnical Journal, 37*, 281-295.

Canadian Association of Petroleum Producers. (2019). *Oil and Natural Gas Pipelines.* Retrieved from CAPP - Canada's Oil & Natural Gas Producers: https://www.capp.ca/explore/oil-and-natural-gas-pipelines/

Canadian Standards Association. (2014). *CSA S6-14: Canadian Highway Bridge Design Code* (11 ed.). Mississauga, Ontario: CSA Group.

Canadian Standards Association. (2019). *CSA Z662-19: Oil & Gas Pipeline Systmes.* Toronto: CSA Group.

Cheng, Y. F. (2013). *Stress Corrosion Cracking of Pipelines.* Hoboken, NJ, USA: John Wiley Publishing.

Das, S., Ahmed, A., & Cheng, J. R. (2010, February). Numerical Investigation of Tearing Fracture of Wrinkled Pipe. *Journal of Offshore Mechanics, 132*, 1-10.

Das, S., Cheng, J., & Murray, D. W. (2007). Prediction of the fracture life of a wrinked steel pipe subject to low cycle fatgue. *Canadian Journal of Civil Engineering, 34*(9), 1131-1139.

Dassault Systemes. (2014, April 23). *Abaqus Analysis User's Guide.* Retrieved Decemeber 31, 2017, from http://abaqus.software.polimi.it/v6.14/books/usb/default.htm

Dewanbabee, H. (2009). *Behaviour of Corroded X46 Steel Pipe under Internal Pressure and Axial Load.* Windsor: University of Windsor.

Ghazijahani, T. G., & Showkati, H. (2013). Experiments on cylindrical shells under pure bending and external pressure. *Journal of Constructional Steel Research*, 109-122.

Grigory, S., & Smith, M. (1996). Residual strength of 48-inch diameter corroded pipe determined by full scale combined loading experiments. *International Pipeline Conference* (pp. 377-386). ASME.

Jeglic, F. (2004). *Analysis of Ruptures and Trends on Major Canadian Pipeline Systems.* Calgary, AB: National Energy Board.

Kabir, A. (2006). *Soil-Structure Interaction Analyses of Buried Rigid Pipes under Surface Loads.* Dhaka: Bangladesh University of Engineering & Technology.

Kelly, P. (2015, April 28). *8.3 Yield Criteria in Three Dimensional Plasticity.* Retrieved from Mechanics Lecture Notes: An introduction to Solid Mechanics: http://homepages.engineering.auckland.ac.nz/~pkel015/SolidMechanicsBooks/Part_II/08_Plasticity/08_Plasticity_03_YieldCriteria.pdf8_Plasticity_03_YieldCriteria.pdf

Lawrence Berkley National Laboratory. (2017). *Engineering Division*. (University of California) Retrieved December 19, 2017, from http://www-eng.lbl.gov/~shuman/NEXT/CURRENT_DESIGN/PV/movesa/PipeSize(B36.10_19).pdf

Lee, H. (2010). *Finite element analysis of a buried pipeline.* Manchester: University of Manchester.

Limam, A., Lee, L.-H., & Kyriakides, S. (2012). On the collapse of dented tubes under combined bending and internal pressure. *International Journal of Mechanical Sciences, 15*, 1-12.

Liu, H., & Cheng, Y. (2020). Corrosion of initial pits on abandoned X52 pipeline steel in a simulated soil solution containing sulfate-reducing bacteria. *Journal of Materials Science & Technology, 9*, 7180-7189.

Massachussets Institute of Technology. (2017). *Three-dimensional solid element library*. Retrieved 2019, from https://abaqus-docs.mit.edu/2017/English/SIMACAEELMRefMap/simaelm-r-3delem.htm

Massachussets Institute of Techonology. (2017). *Three-dimensional conventional shell element library*. Retrieved 2019, from https://abaqus-docs.mit.edu/2017/English/SIMACAEKEYRefMap/simakey-r-shellsection.htm#simakey-r-shellsection

Mohareb, M., Kulak, G., & Murray, D. (2001). Testing and Analysis of Steel Pipe Segments. *Journal of Transportation Engineering, 127*(5), 408-417.

Nazemi, N., & Das, S. (2010). Beahviour of X60 Line Pipe Subjected to Axial and Lateral Deformations. *Journal of Pressure Vessel Technology, 132*(3), 7.

Neya, B., Ardeshir, M., Delavar, A., & Bakhsh, M. (2017). Three-Dimensional Analysis of Buried Pipes Under Moving Loads. *Open Journal of Geology, 7*, 1-11.

Noor, M., & Dhar, A. (2003). Three-Dimensional Response of Buried Pipe under Vehicle Loads. *ASCE International Conference on Pipeline Engineering and Construction* (pp. 658-665). Baltimore: ASCE.

Optimec. (2014). *Tetrahedral elements available in ABAQUS for structural analysis? When to use what?* Retrieved December 12, 2017, from http://optimec.ca/news/tetrahedral-elements-available-abaqus-structural-analysis-use/

Ozkan, I. F., & Mohareb, M. (2009). Testing and Analysis of Steel Pipes under Bending, Tension, and Internal Pressure. *Journal of Structural Engineering, 132*(2), 187-189.

PM Internation Suppliers. (2017). *API 5L X Grades*. Retrieved from PM International Suppliers, LLC: http://www.api5lx.com/api5lx-grades/

Poulos, H. (1974). Analysis of longitudinal behaviour of buried pipes. *Proceedings of Conference on Analysis and Design in Geotechincal Engineering,* (pp. 189-223). Austin, Texas.

Prewitt, T., Kaufman, J., & Finneran, S. (2017). Long Term Structural Integrity Considerations for Abandoned Pipelines. *NACE International Corrosion Conference.* Houston, Texas.

Roy, K., Hawlader, B., Kenny, S., & Moore, I. (2016). Finite element modeling of lateral pipeline-soil interactions in dense sand. *Canadian Geotechnical Journal, 53*(3), 490-504.

Sadowski, A. (2013). Solid or shell finite elements to model thick cylindrical tubes and shells under global bending. *Internation Journal of Mechanical Sciences, 74*, 143-153.

Scott, C. (2015). *Understanding the Mechanisms of Corrosion and their Effects on Abandoned Pipelines.* Dublin, Ohio: Det Norske Veritas.

Subramanian, N. (2010). Appendix C - Properties of Soils. In *Design of Steel Structures* (pp. 1396-1400). Oxford, UK: Oxford University Press.

Terzaghi, K. (1943). Arching in Ideal Soils. In *Theoretical Soil Mechanics* (pp. 66-76). New York: John Wiley & Sons.

Trickey, S., & Moore, I. (2007). Three-Dimensional Response of Buried Pipes under Circular Surface Loading. *Journal of Geotechnical and Geoenvironmental Engineering, 133*(2), 219-223.

Trifonov, O. (2015). Numerical stress-strain analysis of buried steel pipelines crossing active strike-slip faults with an emphasis on fault modeling aspects. *Journal of Pipeline Systems Engineering and Practice, 6*(1).

Verruijt, A. (2018). *An Introduction to Soil Mechanics.* Cham, Switzerland: Springer International Publishing.

Warman, D., Chorney, J., Reed, M., & Hart, J. (2006). Development of a Pipeline Surface Loading Screening Process. *Proceedings of IPC2006 6th International Pipeline Conference* (pp. 1-12). Calgary: ASME.

Xu, L. Y., & Cheng, Y. F. (2012). An experimental investigation of corrosion of X100 pipeline steel under uniaxial elastic stress in near-neutral pH solution. *Corrosion Science*, *59*, 103-109.

Yeom, K. J., Lee, Y.-K., Oh, K. H., & Kim, W. S. (2015). Integrity assessment of corroded API X70 pipe with a single defect by burst pressure analysis. *Engineering Failure Analysis, 57*, 553-561.